NIR imaging of vascular endothelial cells using Cy5.5-lectin conjugates

by

Cecilia Nguyen

A Thesis submitted to the Faculty of Graduate Studies of

The University of Manitoba

in partial fulfillment of the requirements of the degree of:

MASTER OF SCIENCE

Department of Oral Biology

University of Manitoba

Winnipeg, Manitoba

Abstract

The objective of this study was to develop a fluorescent near-infrared endothelial cell binding conjugate using *Lycopersicon esculentum* lectin and Cy5.5 N-hydroxysuccinimide ester for the purpose of imaging the microvascular network in mouse hearts under *in vivo* and *ex vivo* conditions. Cy5.5-lectin conjugate was synthesized with a dye/protein ratio of 2.90 ± 1.54 (n=6). Mouse hearts were successfully labelled in both *in vivo* and *ex vivo* and showed similar labelling patterns. Cy5.5-lectin labelling patterns and that of ICAM2 and FITC-lectin co-localized, indicating binding to endothelial cells. Finally, it was shown that Cy5.5-lectin is capable of visualizing, in real-time, areas of normal and abnormal heart perfusion at resolutions of 76.8 pixels/mm. Areas of the heart that were not perfused post-ligation displayed no Cy5.5 staining on histological sections and during real-time cardiac imaging of intact hearts showed minimal fluorescent signal (~35 a.u.) compared to areas where normal perfusion occurred (~150 a.u.).

Acknowledgements

I can never adequately express my gratitude in the form of words towards the people who helped me accomplish this task. The first person I would like to thank is my supervisor, Dr. Olga Jilkina, who gave me the opportunity to do this project and patiently mentored me throughout the learning process and experiments involved. Secondly, I would like to thank Bozena Kuzio, Saro Bascaramurty and Lori Gregorash for their technical support. Without Bozena's expertise in the various experimental protocols, especially mouse heart perfusion, the *ex vivo* experiments would have been very difficult if not impossible. Thank you to Saro for all her help and guidance in regards to the vast amount of histological preparations and slides that were needed in this project. Thank you to Lori for all her help and amazingly steady hands that were needed for the tail-vein injections. I would also like to thank Dr. Eugene Gussakovsky for designing and providing various technological tools, especially the real-time imaging system. Overall, I would like to thank the various people at the Institute for Biodiagnostics – National Research Council of Canada who welcomed me into their workplace and provided a fantastic environment. I am grateful to the University of Manitoba and the Province of Manitoba for the financial support they provided through the form of the Manitoba Graduate Scholarship.

Table of Contents

List of Tables

Chapter 1 – Literature Review

Chapter 2 – Materials and Methods

Chapter 3 – Results

List of Figures

Chapter 1 – Literature Review

Chapter 2 – Materials and Methods

Chapter 3 – Results

Commonly Used Abbreviations

2D – 2-dimensional

3D – 3-dimensional

BSA – Bovine serum albumin

CT – Computed tomography

D/P – Dye/Protein (ratio in moles)

ECG – Electrocardiogram

FITC – Fluorescein isothiocyanate

ICAM2 – Intercellular adhesion molecule 2

KHB – Krebs-Henseleit buffer

LAD – Left anterior descending artery

LEA – Lycopersicon esculentum

LV – Left ventricle

MRI – Magnetic resonance imaging

NADH – Nicotinamide adenine dinucleotide

NHS - N-hydroxysuccinimide

NIR – Near-infrared

PET – Positron emission tomography

POD – Pseudo-optical density

PRP – Pressure rate product

ROI – Region of interest

RV – Right ventricle

Chapter 1 – Literature Review

1.1. Introduction

In cardiovascular research, near-infrared (NIR) fluorescence imaging has emerged as a new imaging modality (McVeigh 2006). There are many advantages to imaging within the NIR spectral range (650 - 900 nm) which include minimal interference from endogenous fluorescent chromophores and low tissue absorption by haemoglobin and myoglobin (Kovar *et al.* 2007; Nighswander-Rempel *et al.* 2005). These characteristics are desirable in the imaging of endothelial cells and the endothelial network within intact organs. Many cardiovascular diseases such as hypertension and atherosclerosis are associated with endothelial dysfunction (Ross 1999; Steinberg *et al.* 1996). Endothelial dysfunction also has been shown to be an indirect complication associated with other non-cardiovascular diseases such as diabetes mellitus (Hoenig *et al.* 2008). Development of a tool that can visualize the normal and disease conditions within the cardiovascular system would improve the ability to understand, monitor and diagnose variety of diseases.

In this study, endothelial cell-binding fluorescent conjugate using tomato lectin and Cy5.5 N-hydroxysuccinimide (NHS) ester was synthesized. The binding of the conjugate to endothelial cells in mouse models using both *in vivo* and *ex vivo* infusion methods was evaluated. Intracellular adhesion molecule 2 (ICAM2) and fluorescein isothiocyanate (FITC)-lectin staining patterns were compared to Cy5.5-lectin labelling patterns and co-localization was seen. Currently there is no readily available optical probe capable of imaging endothelial cells in the NIR range under *in vivo* conditions. Most available current imaging modalities as well as histological techniques are also unable to monitor micro-vascular networks well due to limits in spatial resolution and

image contrast. Histological techniques are further limited by the short mean free path of visible light in tissue caused by strong absorption therefore limiting imaging to only a few microns in thickness. Finally, it was proposed that Cy5.5-lectin conjugate, used as a deposition flow tracer, could aid in real-time imaging of normal and abnormal heart perfusion. The results of this thesis can be applied to many different scenarios involving simulated cardiovascular conditions and perhaps used in different animal models. The following literature review will survey current cardiovascular imaging modalities, review the usefulness of NIR imaging and highlight the different components of the Cy5.5-lectin conjugate imaging method.

1.2. The heart

For imaging studies, the heart is a very useful model because it is one of the few organs in which techniques have been developed that allows for both *ex vivo* and *in vivo* imaging experiments. The heart is also a well studied organ and it is understood that the heart is a multi-chamber muscular organ responsible for the circulation of blood cells and plasma throughout the body (Vishy 2008). Structurally, the wall of the heart is composed of a layer of simple squamous endothelial cells, called the endocardium (Brutsaert 1989). The myocardium of the heart is the thick layer of specialized cardiac muscle cells called cardiomyocytes that comprise the majority (approximately 80% of total cellular protein content and roughly 25% of total cell number) of the heart (Van Der Laarse *et al.* 1989). Between the endocardium and the myocardium is the sub-endocardial layer, which contains small nerves and the Purkinje fibres. Purkinje fibres are responsible for conducting the electrical impulses responsible for maintaining coordinated cardiac contractions even in the absence of a complete nervous system (Thornell and Eriksson

1981). This is one of the many features of the heart that allows it to be an excellent model in *ex vivo* experiments. The outermost layer of the heart, called the pericardium, is a thick layer of fibrous tissue that protects the heart (Vishy 2008). An important microvascular network that originates from the large and small coronary arteries and veins exists throughout the heart (Robert H. 2010). The perfusion of this microvascular network of the heart begins at the aorta, which is a large and accessible vessel; however, the perfusion is heterogeneous. The heart has the ability to adjust perfusion based on workloads (Austin *et al.* 1990). The specific cellular responses that include the endothelial cells that line every blood vessel and signalling pathways involved in changing the perfusion patterns of hearts are discussed later. In terms of a model for testing imaging, the heterogeneous perfusion in hearts allows for dynamic imaging sessions, such as stress tests, that are not as easily monitored in other organs. Due to these overall characteristics, the heart is an excellent model for testing a new probe for NIR imaging.

1.3. Current cardiovascular imaging modalities

Cardiac imaging can provide very useful information on cardiac structure, metabolism, perfusion and oxygenation which are all functions critical in the understanding of the normal heart as well as in disease situations. Over the last century, many different cardiac imaging techniques have been developed but all strive for the same result which is to provide minimally invasive yet detailed anatomical and physiological data of the heart in real time. An important part of real time imaging is the ability to record the dynamic physiological changes that occur within the heart. To this end, techniques that combine imaging technology with chemical blood flow tracers have

been developed. These tracers can be classified as deposition tracers or first-pass tracers. As the name implies, deposition flow tracers, such as microspheres, are deposited into the intravascular space of the tissue of interest proportional to the blood flow and often will remain bound for the imaging period (Prinzen and Bassingthwaighte 2000). Deposition flow tracers can also bind intracellular targets such as mitochondria (e.g. Rhodamine 800) (Munch *et al.* 2011). Paired with an imaging technique that is capable of following the deposition of these tracers, a qualitative description of myocardial perfusion can be attained. Deposition flow tracers could also be extracted post-imaging from the tissue and the value measured should therefore provide a quantitative estimate of blood flow. However, this method of extraction is mostly limited to research settings as the tissue or organ has to be heavily processed and therefore no longer viable. The most common deposition flow tracers are microspheres that are available in a range of sizes (Prinzen and Bassingthwaighte 2000). In contrast, first-pass tracers do not bind or remain in the tissue. A benefit of first-pass tracers is that they are often smaller in size and therefore have a lower chance of obstructing blood flow (Prinzen and Bassingthwaighte 2000). Disadvantages of first-pass tracers are that kinetic measurements must be very fast in order to avoid overestimation due to recirculation of the tracer and that complex computer reconstruction, dependent on image quality and stability of the signal, is needed to determine flow (Petrella and Provenzale 2000). Both types of tracers are used today in conjunction with different imaging techniques. The following sections highlight current cardiac imaging technologies and the corresponding use of tracers.

1.3.2. Echocardiography

Echocardiography, a version of ultrasound technology that is specifically applied to the heart, is capable of providing detailed imaging of moving anatomical structures such as heart valves as well as heart function via ejection fraction (Sugeng *et al.* 2008). Procedures are simple and non-invasive. Echocardiography has the added benefit of being one of the cheapest current cardiac imaging tools therefore it is readily available in hospitals and small clinics as well as in the research setting. The technology is based on the propagation and reflection of sound waves, produced by vibrating quartz crystals, through different tissues (Hauff *et al.* 2008). Data is then collected in equally spaced lines that are approximately 10 – 20 μm apart and depending on the frequency range of the scanner, maximum tissue depth is between 5 – 15 mm (McVeigh 2006). With recent advances in computer processing capabilities, echocardiography scans have become faster, more accurate, which has allowed for real-time, 3-dimensional scans (Burri *et al.* 2012). Spatial resolutions achieved by new real-time, 3-dimensional echocardiography systems have been reported to be approximately 0.7 × 0.7 × 0.5 mm to 1.2 × 1.2 × 0.8 mm (Lu *et al.* 2008). Echocardiography is also capable of imaging blood flow in microvascular networks with a minimum of 1 mm/s blood velocity using the Doppler processing technique (McVeigh 2006). In order to acquire higher resolution images, several studies have attempted to design contrast agents that react to the ultrasound waves. These include encapsulated micro-bubbles, liposomes and perfluorocarbon nano-particles that are conjugated to specific binding proteins such as intercellular adhesion molecule-1 (ICAM1) (Dayton and Ferrara 2002). However, it has been found that the larger size of these molecular probes (>250 nm) limit their applications due to inefficient binding to

targeted tissues especially in the microcirculation (Jaffer and Weissleder 2004). In terms of accuracy, echocardiography has also been found to underestimate volume and function measurements (Gardner *et al.* 2009).

1.3.3. Magnetic resonance imaging

Magnetic resonance imaging (MRI) is a non-invasive imaging tool capable of imaging cardiac structures, function and blood perfusion in real time. MRI technology depends on the distribution and concentration of specific atoms throughout the body. Atoms that have an odd number of protons or neutrons, such as hydrogen, possess the ability to have magnetic moments and these moments can be aligned when a very strong magnetic field, such as that found in a MRI scanner, is applied (Rodgers and Robson 2011). Ninety degree shifts in these moments can be caused by applying specific radiofrequency energy pulses which for hydrogen is 63.75 MHz in a 1.5 Tesla (T) MRI system (Geuns *et al.* 1999; Rodgers and Robson 2011). After the energy pulse, these atoms must return to equilibrium, however the time required for these atoms to return to equilibrium differs in various tissues (Geuns *et al.* 1999). Atoms can also return to equilibrium via two different processes known as longitudinal relaxation, which is characterized by T_1 relaxation time, and transverse relaxation, which is characterized by T_2 relaxation time (Geuns *et al.* 1999). T_1 and T_2 relaxation times can be used to visualize and contrast different tissues (Geuns *et al.* 1999). To generate an image, the MRI system applies a magnetic gradient, in which only a narrow band will be affected by the corresponding radiofrequency energy pulse. Within in these slices, temporary gradients, signals, and short changes in the magnetic field are applied and the resulting changes in the atoms are recorded and then further processed into an image (Geuns *et al.*

1999). The signal from atoms such as hydrogen in a typical 1.5 T clinical MRI system is fairly weak therefore contrast agents for MRI have been developed in order to improve the image quality (Edelman 2004). Using multiple contrast agents, MRI scans can achieve spatial resolutions of 1 mm x 1 mm x 2 mm^3 (Li *et al.* 2011). These agents are mostly based on superparamagnetic iron oxide nano-particles or gadolinium chelates (Jaffer and Weissleder 2004). Using gadolinium chelates, a first-pass tracer, MRI is capable of assessing the degree and location of myocardial infraction (Simonetti *et al.* 2001). Overall, MRI is capable of imaging vessel perfusion, assess cardiac function, as well as diagnose and monitor arterial diseases such as arteriosclerosis (Bandettini and Arai 2008). Newer MRI systems using stronger magnets ($\geq$ 3T) are capable of performing MR angiography without the usage of contrast agents (Miyazaki and Akahane 2012). These systems, gated by electrocardiogram (ECG) measurements, depend on the signal differences between systolic and diastolic triggered data acquisitions to generate an image (Miyazaki and Akahane 2012). MRI does have disadvantages in that it cannot be used on patients with ferromagnetic implants and even MRI-compatible pacemakers should be subjected to MRI scans with caution. The scanner is also limited by size and can be claustrophobic to the patient, which can cause stress and anxiety (Thorpe *et al.* 2008). MRI scan procedures are often long and therefore can add even more stress for the subject. Unlike echocardiograph systems, MRI is not portable and also requires a high level of maintenance due to the constant use of cryogens such as liquid nitrogen and liquid helium that is needed to keep the superconducting magnets cool (Fletcher *et al.* 1999).

1.3.4. Positron emission tomography

Positron emission tomography (PET) is an imaging modality based on tracking the distribution of injected radiolabeled metabolic tracers, such as 18 F-2-deoxy-2-fluoro-glucose, by the positrons they release and therefore is excellent at imaging chemical processes that occur within the heart. PET scans will record instances where two gamma rays, generated by the annihilation a positron with an electron, simultaneously trigger the detectors located on the opposite sides of the subject (McVeigh 2006). These tracers often have specific targets such as endothelial cells and can also target cellular processes such as apoptosis and gene expression (Blankenberg and Strauss 2002). The most common and versatile radionuclides used in PET are carbon-11 and fluorine-18 (Ruth 2009). However, both carbon-11 and fluorine-18 have a very short half-life (approximately 20 minutes and 110 minutes respectively) and therefore must be produced nearby and used immediately. This limits the locations where PET scans can occur and increases the overall cost of using the PET scan therefore similar to MRI systems, PET scanners are often only available in major hospitals and clinics. Small scale or microPET scanners, designed for small animal studies, can achieve a spatial resolution of approximately 1.5 mm (Muehllehner and Karp 2006). Whole-body general scanners however, can only achieve spatial resolutions from 4.5 mm to 6 mm under ideal conditions (Muehllehner and Karp 2006). Compared to the previously described imaging modalities, PET scans currently have the worst spatial resolution therefore it is often used in combination with other imaging modalities.

1.3.5. Computed Tomography

Computed tomography (CT), also known as computerized axial tomography (CAT), is an imaging modality that uses externally applied x-rays to generate an image (Buzug 2012). Unlike conventional x-ray techniques, CT is able to take image slices through the subject and then render the stacked images into 3D structures. This is done by rotating the x-ray beam around the subject, which located at the center of a stationary detector ring (Buzug 2012). Recent developments in CT have given rise to multi-row detector CT systems capable of rapid and detailed scans of the cardiovascular system. The advantage of these CT scans is that a full data set can be acquired in 5 – 10 seconds and the spatial resolution of the images is approximately 0.5 to 0.75 mm (Cademartiri *et al.* 2004; Schroeder *et al.* 2008). Unfortunately there are disadvantages to CT scans, which include longer post-imaging processing times due to the large volume of image slices, especially with the multi-row detectors and the high radiation dosage to patients (Buzug 2012). CT, with the usage of non-radioactive iodine-based contrast agents such as iomeprol 400, is capable of providing structural data and some limited perfusion data (Cademartiri *et al.* 2006). This limits the clinical applications of CT in cardiovascular imaging to assessing calcification of the coronary arteries as well as the supra-aortic trunks and identification of any major vessel stenosis (Buzug 2012; Schroeder *et al.* 2008).

1.3.6. Single Photon Emission Tomography

Single photon emission tomography (SPECT) scans are very similar to PET scans however the gamma rays emitted by tracers used in SPECT scans are only detected in one direction at a time (McVeigh 2006). Also unlike PET scans, the gamma radiation in

SPECT scans are detected directly because it is produced by radionuclide tracers injected into the subject (McVeigh 2006). The most common radionuclide used in SPECT scans is technetium-99m, an isotope that is readily available, cheap, and has a 6 hour half-life (Bartholoma *et al.* 2010). Imaging with technetium-99m results in images with a spatial resolution around 3.5 – 4 mm (Holly *et al.* 2010). In cardiac SPECT imaging, 99mTc-sestamibi, a lipophilic cationic deposition tracer that accumulates in mitochondria, is commonly used (Carvalho *et al.* 1992). In general, SPECT is capable of providing functional information regarding the perfusion and metabolic processes that are occurring within the imaged tissue (Gullberg *et al.* 2010). SPECT scans have been used to evaluate the left ventricular ejection fraction as well as study fatty acid metabolism in patients with hypertrophic cardiomyopathy (DePuey *et al.* 1993; Okizaki *et al.* 2007). Unfortunately, the radiation dosage received from SPECT is of concern, with the average radiation dosage in a cardiac scan averaging around 6 mSv (Husmann *et al.* 2009).

Table 1-1: Summary of current common cardiac imaging techniques.

Imaging modality	Spatial Resolution	Average Effective Radiation Dose* (millisieverts)	Time	Cost^
Echocardiography°	~1mm^3	n/a	Short	$
MRI	1mm^3	n/a	Long	$$$$
PET	4.5-6mm	5-7‡	Long	$$$
CT	0.5-0.75mm	7‡	Medium	$$$
SPECT	3.5-4mm	6#	Medium	$$

°Spatial resolution is based on new real-time, 3D scanners
*Average natural background radiation in North America is approximately 3mSv‡
^Cost takes into account maintenance and scan with $ = low and $$$$ = high
‡Based on data from (Fazel *et al.* 2009)
#Based on data from (Husmann *et al.* 2009)

1.4. Optical Imaging

1.4.1. Absorbance Imaging

Absorbance imaging is based on the principle that light, as it passes through a medium is affected by that medium because some wavelengths can be absorbed while others are scattered or reflected. In the simplest situation, the amount of light absorbed is related to the distance the light must travel, the concentration of the medium and the natural absorptive characteristic of the medium also known as the extinction coefficient (Swinehart 1962). In solutions that do not scatter light, this is described by the Beer-Lambert Law:

$$A = \varepsilon lc \quad (1)$$

…where A, stands for absorbance, ε, the extinction coefficient, l, the pathlength and c, the concentration of the solution in question (Swinehart 1962). The extinction coefficient for many molecules is distinctly different from one another and the value is wavelength dependent. Knowing the extinction coefficients for the molecules in a sample at a particular wavelength allows spectral measurements to confirm and quantify the molecules in a non-scattering sample. Although this method works for solutions it must be modified when measuring absorbance in dense tissues such as the myocardium. Here, instead of measuring the amount of light that passes through a medium, the reflected and scattered light is detected; therefore, absorbance measured in this manner is often called pseudo-optical density measurements (POD) (Gussakovsky *et al.* 2012). The POD spectra of dense tissue can describe many tissue components (Malin *et al.* 1999). In *in vivo* cardiac imaging, POD spectra taken within the near-infrared range can provide information on the oxygenation of the tissue by virtue of the chemical changes that occur with haemoglobin and myoglobin. Both of these proteins are abundant in normally perfused hearts (haemoglobin within erythrocytes, which are found travelling through the blood vessels, and myoglobin within cardiomyocytes) and have an oxygenated form, which has a significantly different absorbance spectrum from the deoxygenated form (Faber *et al.* 2003; Millar *et al.* 1996). By acquiring spectra over a region of interest, an oxygenation map of the heart can be constructed and has been successfully demonstrated in pig hearts (Nighswander-Rempel *et al.* 2002). With current technology, image maps created by this method have pixel resolution around 1x1 mm^2, which is comparable to other imaging modalities (Kupriyanov *et al.* 2008). *In vivo* images have also been

successfully acquired for beating pig hearts undergoing surgery (Gussakovsky *et al.* 2012). However, absorbance imaging of the heart based on haemoglobin and myoglobin is limited by many factors. Firstly, the technique may provide good mapping of regional variations in tissue and blood oxygenation but lacks data regarding anatomical structures. Secondly, the spectral properties of myoglobin and haemoglobin are very similar therefore it is difficult to distinguish blood oxygenation from the oxygenation of muscle tissue (Arakaki *et al.* 2010). *Ex vivo* techniques are able to monitor oxygenation of only muscle tissue since the heart can be perfused with buffers instead of blood plasma, which eliminates the signal from haemoglobin (Nguyen *et al.* 2012). However, such an invasive technique would have limited applications. Thirdly, the POD data acquired is not absolute because the pathlength of the signal, unlike true absorbance measurements, can only be estimated. Instead POD data shows comparative oxygenation based on the reflectance/scatter reference used (e.g. a white polyurethane sponge) (Gussakovsky and Kupriyanov 2008). For these reasons, other optical imaging modalities are being developed.

1.4.2. Fluorescence Imaging

Excitation of a molecule, leading to the emission of light, often occurs via two possible processes: fluorescence and phosphorescence (Haugland 2002). Fluorescence can be simply defined as the emission of light of lower frequency nanoseconds after a molecule is illuminated by a higher frequency light (Croney *et al.* 2001). Phosphorescence occurs on a much longer time scale (micro to milliseconds) and, compared to fluorescence, involves less favourable electronic states (Lettinga *et al.* 2000). For both fluorescence and phosphorescence to occur, a molecule must absorb the energy

of a photon emitted by a light source such as a laser and must then move to a higher electronic state from the ground state (S_0) (Jameson *et al.* 2003). This stage is called the excitation or absorption stage. Often the spin of the electrons are unaffected therefore, after excitation, the molecules are usually left with two unpaired electrons and a total electron spin value of zero. All electronic states with a total electron spin value of zero are called singlet states and are denoted by the letter "S" (Jameson *et al.* 2003). After excitation to a higher electronic state such as S_1, it is also possible for the electrons to experience a spin reversal through a process known as intersystem crossing. Intersystem crossing would result in an electronic configuration that has a total electron spin value of 1 (Parker and Rees 1962). Electronic states with a total electron spin value of 1 are called triplet states and are denoted by the letter "T" (Jameson *et al.* 2003). The triplet state has a lower energy level than that of the S_1 state (Parker and Rees 1962). Because an excited molecule is unstable, the electrons will eventually return to the ground state and may release the energy in the form of a photon. Molecules capable of releasing energy in the form of a photon are called chromophores. The emission of light via the singlet state is called fluorescence whereas the emission of light via the triplet state is called phosphorescence. Since the triplet state has a lower energy level, the resulting photon is also of a lower energy and thus exhibits a longer wavelength (Parker and Rees 1962). Perrin-Jablonski energy diagrams illustrate this difference between fluorescence, phosphorescence as well as other competing non-radiative pathways (Figure 1-1). It is important to note that the release of energy can occur through a combination of different mechanisms. Non-radiative mechanisms include internal conversion and vibrational relaxation (Kasha 1950). Between the electronic states (S_o, S_1, S_2… T_1 etc.), there exists

multiple vibrational energy levels that electrons can be excited to. Internal conversion occurs when the molecule then undergoes a rapid transition from the lowest vibrational level of $S_{>0}$ to the upper vibrational levels electronic state below (Wagenknecht and Ford 2011). This process is not limited to the singlet states as internal conversion can also occur with the triplet states (Wagenknecht and Ford 2011). Vibrational relaxation, the result of collisions with other molecules in the solution, causes the further loss of vibrational energy that then reduces the energy of the electron to the lowest vibrational level of the electronic state (Wagenknecht and Ford 2011). From there, a variety of other mechanisms, such as the release of a photon, can occur. Intermolecular mechanisms for the release of energy and the subsequent return to ground state also exist. The best understood interaction that results in the emission of a photon is called Förster resonance energy transfer (FRET). Through dipole-dipole coupling between two chromophores, non-radiative energy is transferred from the donor molecule to the acceptor molecule (Clegg 1995). For the transfer to be successful, the fluorescence emission of the donor should overlap with the excitation spectra of the acceptor molecule (Clegg 1995). Because FRET requires the acceptor and donor molecule to be relatively close (10 - 100 Å), it has been used to study the complex interactions between various proteins, carbohydrates and nucleic acids (Clegg 1995; Selvin 2000).

Figure 1-1: A simplified Perrin-Jablonski diagram showing the different electronic states that are involved and a few different relaxation mechanisms. Relaxation mechanisms are not limited to only those shown. Dark lines show the different electronic states and thin lines show the vibrational levels. The divisions between different levels are not drawn to scale and for visual clarity, vibration levels are only shown with regards to vibrational relaxation (VR). S: Singlet states; T: Triplet states; IC: Internal conversion; VR: Vibrational relaxation; ISC: Intersystem crossing.

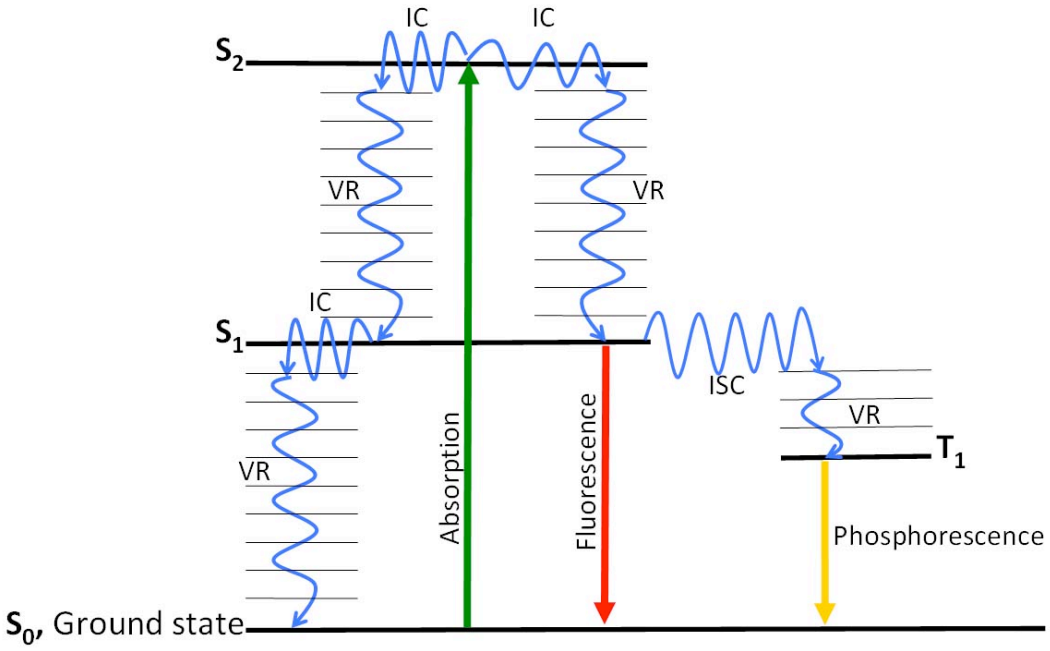

It is possible that through a combination of non-radiative processes, a complete loss of the energy absorbed occurs. Processes that follow this route are referred to as quenching. Aromatic molecules, which include many fluorescent molecules, can interact with other aromatic molecules through van der Waal forces and result in the formation of non-fluorescent complexes (Croney *et al.* 2001). These interactions cause noticeable changes to the absorbance spectrum. The most common changes include the presence of a higher energy (H-type aggregate) and/or lower energy (J-type aggregate) absorption

bands surrounding the absorption band from the free chromophore (Gruszecki 1991). H-type aggregates are generally highly quenched because the molecules are aligned parallel to each other, which increases the intermolecular forces that results in greater energy loss via non-radiative mechanisms (An *et al.* 2002). It is because of these competing mechanisms that the number of photons emitted does not equal the number of photons absorbed. The ratio of the number of photons emitted to the total number of photons absorbed is known as the quantum yield (Williams *et al.* 1983). The maximum ratio for any fluorescent molecule is equal to 1 however in practical applications this ratio rarely reaches the maximum value. In regards to fluorescence imaging, quantum yield and thus quenching is an important factor. Suitable dilutions of fluorescent solutions have been shown to reduce the amount of quenching that occurs and thus improve the fluorescence signal captured (Parker and Rees 1962). Other processes that reduce the amount of fluorescence signal produced by a chromophore include photobleaching, which differs from quenching processes because the effects of photobleaching are irreversible (Walker 2004). When a molecule is excited, the chemical reactivity of that molecule increases. Reactions include oxidative reactions as well as reactions between the chromophore and surrounding molecules, both of which result in the formation of non-fluorescent complexes (Chen *et al.* 2003). Photobleaching can be reduced by reducing exposure to oxygen, limiting the excitation wavelength to only what is required and keeping light exposure to a minimum (Stephens and Allan 2003).

1.4.3. NIR fluorescence imaging

The electromagnetic spectrum is an elegant way to describe different wavelengths of energy. The near-infrared (NIR) wavelengths are found ranging between 650 nm and

900 nm. There are many advantages to imaging within the NIR spectral range (650 - 900 nm). Firstly, at these wavelengths there is very little interference from endogenous fluorescent chromophores, such as NAD(P)H and flavins as well as very little interference from quenchers such as cytochromes, all of which mostly absorb and fluoresce in the spectral region between 359 - 650 nm (Kovar *et al.* 2007). Secondly, low tissue absorption by haemoglobin and myoglobin within the NIR range means that light penetration can be several millimetres (Nighswander-Rempel *et al.* 2005). One of the challenges with NIR imaging was the development of tools that could record these signals since NIR wavelengths are invisible to the human eye. The first NIR photographs were not taken until 1910 even though the camera obscura had been invented 100 years earlier (Wood 1910).

Figure 1-2: Schematic diagram illustrating the basic principles of three different NIR fluorescence imaging methods. Black arrows depict the excitation beam. Red arrows depict the fluorescence captured by detectors.

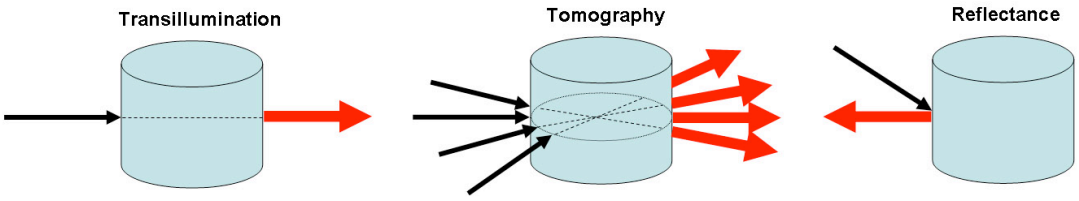

Advances in imaging techniques have now allowed for a variety of NIR imaging methods that can be divided into three classes: transillumination, tomography and reflectance (Figure 1-2). Transillumination fluorescence imaging uses an excitation beam to cause fluorescence, which then must propagate through the sample before it is

captured by a photodetector or camera. This usually means that the tissue scattering effect greatly affects the images produced in this method and thus also has poor spatial resolution (Vinegoni *et al.* 2009). To improve on transillumination fluorescence imaging, tomography systems have been developed. These systems use sequential excitation at different locations around a sample in order to reconstruct the fluorescence signals (Chang and Jaffer 2008). An advantage of this system is the ability to quantitatively measure the concentration of the fluorescent agent used (Ntziachristos *et al.* 2005). The spatial resolution achieved using this system in small animals is approximately 1 to 2 mm, which is comparable to other imaging modalities (Miller and Thrall 2004). Fluorescence tomography, however, does have a few disadvantages. Currently, dead and/or very transparent samples must be submerged in an appropriate solution or be in close contact with the excitation light sources in order to generate decent images (Chang and Jaffer 2008). This limits the size and shape of samples that can be imaged because the sample must be made very thin. It also means that often live samples are difficult to image. Attempts are being made to eliminate the need to submerge samples in solution and to couple the system with other imaging modalities such as MRI (Nuiachristos 2006). Fluorescence reflectance imaging (FRI) is an optical system that uses an excitation beam to cause fluorescence and through a series of filters, capture the reflected light. This system is simplest and most widely available fluorescence imaging modality. FRI has been demonstrated to successfully generate images of the vascular system under intra-operative conditions using the SPY™ imaging system (Novadaq Technologies Inc., Toronto, Canada), which is based on the fluorescence of indocyanine green (ICG) (Taggart *et al.* 2003). The SPY™ imaging system uses laser (806 nm) to excite ICG and

a charge-coupled device video camera equipped with the appropriate filters to capture the fluorescence (Takahashi *et al.* 2004). The FRI system also include fluorescence endoscopes, which detect the fluorescence of Cy5.5 and Cy7 in mouse models and intravascular fluorescence catheters that record the fluorescence of Cy5.5 and Alexa750 in order to monitor and characterize vascular plaque formation (Funovics *et al.* 2003; Zhu *et al.* 2005). Both the endoscope and the catheter use parallel fibre optic cables, one to transmit the excitation light from a laser source and the other to record the reflected light (Funovics *et al.* 2003; Zhu *et al.* 2005). NIR fluorescence catheters are capable of achieving spatial resolutions of approximately 1.0 mm when used intravascularly, which is comparable the other previously discussed imaging modalities (Jaffer *et al.* 2011). Recent advance have improved the spatial resolution of FRI endoscope systems allowing for *in vivo* confocal fluorescence microscopy. This new system has successfully imaged the microstructure of the bronchial wall in humans and is fairly non-invasive as the diameter of the probe is only 1 mm in diameter (Thiberville *et al.* 2007).

1.4.4. Fluorescent dyes used for imaging

Due to the numerous applications for fluorescence imaging systems, a multitude of NIR imaging agents have been developed. In general, fluorescence imaging agents, unlike radionuclides-based tracers, are long lasting and are capable of repeated excitation. The most common family of dyes or fluorophores used in fluorescence imaging are cyanine dyes. Cyanine dyes are a family of dyes whose structure contains two terminal nitrogen heterocyclic subunits linked by a polymethine bridge (Mojzych and Henary 2008). They characteristically have narrow absorption bands in the NIR range and extremely high extinction coefficients (Mojzych and Henary 2008). The different

cyanine dyes are named depending on the length of the polymethine bridge. Increasing the length of the polymethine bridge by one vinylene moiety (CH=CH) causes a bathochromic shift of about 100 nm (Mishra *et al.* 2000). Cyanine dyes with only one methine group show absorption in the visible spectral region whereas cyanine dyes with seven methine groups absorb in the 750 nm range. Studies have shown that the fluorescent quantum yield decreases as the polymethine bridge becomes longer (Haugland 2002). Cy5.5 *N*-hydroxysuccinimide (NHS) ester, with a polymethine bridge that is five carbons long, is a cyanine derivative that is excited in the NIR range at 675 nm and fluoresces at 694 nm (Figure 1-3A). It has an extinction coefficient of 250 000 M^{-1} cm^{-1} and a quantum yield of > 0.28 (Osborn 2002). Cy5.5-NHS ester exists in two varieties: a monofunctional dye and bisfunctional dye. As the name suggests, the two differ in the number of reactive NHS-ester groups (Figure 1-3B). The dye, in the NHS-esterified form, binds to the free amino groups of lysine residues as well as the N-terminal amino group of proteins such as lectin through an acylation reaction (Ko and Ma 2009). Free Cy5.5-NHS esters and endostatin-Cy5.5 conjugates have been used successfully in previous *in vivo* studies and no adverse or toxic effects have been reported (Bogdanov *et al.* 2007; Citrin *et al.* 2004).

Figure 1-3: Spectral and chemical structure of Cy5.5-NHS ester. A) Absorbance and fluorescence spectra of Cy5.5-NHS ester showing maximum absorbance at 675 nm and maximum emission at 694 nm. B) Chemical structure of monofunctional Cy5.5-NHS ester. C) Chemical structure of bisfunctional Cy5.5-NHS ester. D) Schematic diagram of the conjugation of monofunctional Cy5.5-NHS ester and a protein through acylation.

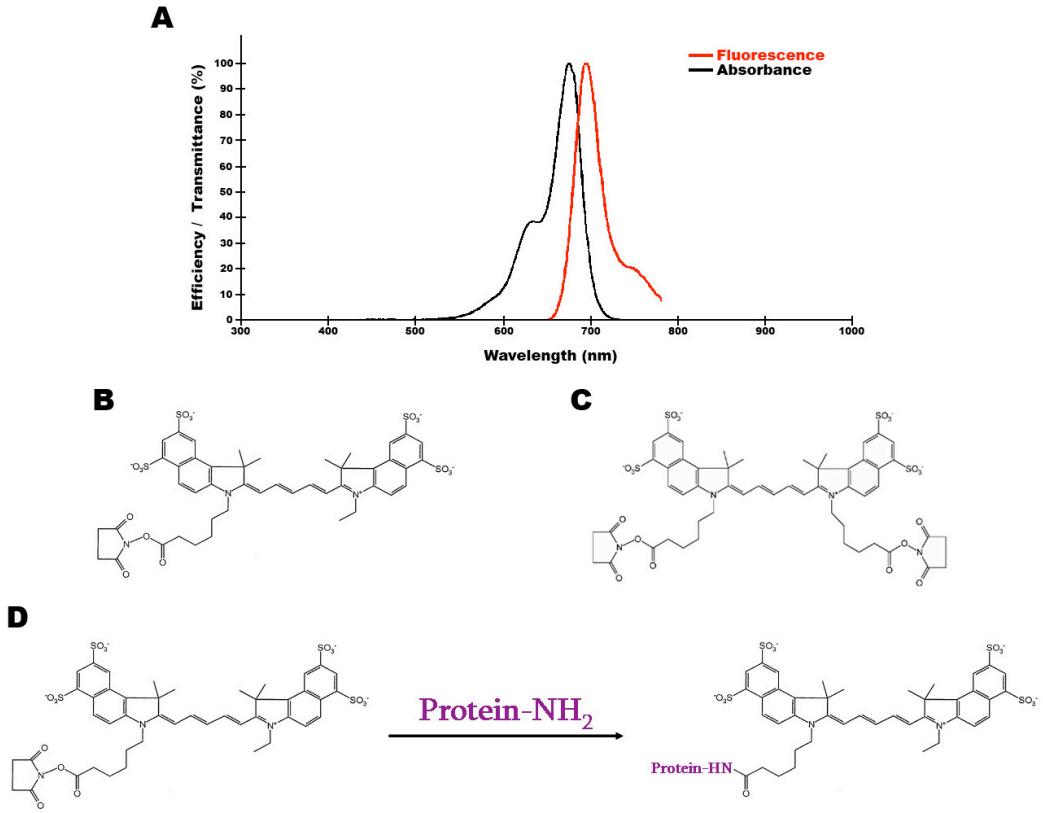

Fluorescence imaging agents can often be categorized into three groups: untargeted agents, targeted agents and agents that only fluoresce once activated. Untargeted agents, as the name implies, do not have any specific targets. The most well known untargeted fluorescent agent is indocyanine green (ICG), which has no functional groups that would allow for conjugation to other molecules (Marshall *et al.* 2010). ICG, a safe and FDA approved dye, has been used in both human and animal studies for over 50 years (Cherrick *et al.* 1960). Typically, the average dosage used for adults for the

purpose of cardiovascular function testing is 10 ml of ICG at a concentration 2.5 mg/ml (Marshall *et al.* 2010). Imaging systems based on ICG has been around for 30 years and have been used in ophthamology however systems based on ICG fluorescence have only recently been developed within the last decade (e.g. SPY™ imaging system by Novadaq Technologies Inc., Toronto, Canada as previously mentioned) (Desmettre *et al.* 2000). Unfortunately, ICG is fairly unstable once it is in solution (stable as a powder) compared to other fluorescent agents and therefore should be used within 10 hours after dilution (Marshall *et al.* 2010).

Unlike untargeted agents, targeted agents are often conjugates and have only been recently exploited. These conjugates are usually small-molecules, peptides, proteins and antibodies (Marshall *et al.* 2010). In cardiovascular studies the conjugates include peptides conjugated to fluorophores such as Cy7, VT680 and Alexa680 that target FXIIIa and fibrin in the thrombosis pathway (McCarthy *et al.* 2009; Tung *et al.* 2003). An antibody conjugate has also been developed for NIR fluorescence imaging of atherosclerosis. This antibody conjugated to Cy7 targets the extra-domain B of fibronectin, a well known marker for angiogenesis and vascular remodelling (Matter *et al.* 2004).

The last group of fluorescence imaging agents are molecules that can be activated. These agents, upon interaction with their target, undergo a chemical reaction that changes the molecule into a fluorescent state. Often the fluorophore is located closely to quencher molecules therefore very low to no fluorescence is seen. An example of this type of imaging agent is $(Cy5.5)_{11}$-PL-$MPEG_{92}$, which in its pre-cleaved state self-quenches and therefore produces very low fluorescence signal (Weissleder *et al.* 1999). However, upon

cleavage by specific lysosomal proteases found only in tumours, a 12-fold increase in signal occurs (Weissleder *et al.* 1999). In cardiovascular studies a few of these NIR agents that can be activated or unquenched have been developed. One is sulfonaphthoaminophenyl fluorescein, which in the presence of hypochlorous acid loses an aminobenzene ring (Shepherd *et al.* 2007). The resulting molecule is capable of producing a strong fluorescence signal when excited at 625 nm (Shepherd *et al.* 2007). Another example of these NIR agents used in cardiovascular studies is CatK-FITC-PGC-Cy5.5. The purpose of this conjugate is to evaluate cathepsin K activity because cathepsin K has been thought to be involved in the breakdown of atherosclerotic plaques (Jaffer *et al.* 2007).

Emerging types of fluorescent agents that are different from the three classes mentioned include luminescent semiconductor quantum dots. These particles are synthetic crystals that can be produced in various sizes (usually a few nanometres in diameter), which determines the spectral region where the molecule will fluoresce (Boeneman *et al.* 2012). For example 2 nm CdSe (cadmium-selenium) crystals fluoresce within the 495 to 519 nm range whereas 5 nm CdSe crystals fluoresce at the 605 to 630 nm range (Alivisatos *et al.* 2005). These have been shown to have high quantum yields, large Stokes shifts (i.e. the difference in wavelength between the maximum absorbance and the maximum emission) and are resistant to photobleaching (Boeneman *et al.* 2012). These characteristics make quantum dots a more ideal fluorescent agent compared to standard organic-based molecules such as the cyanine dyes. However, quantum dots do have a few characteristics that are undesirable. Quantum dots can randomly switch between emitting and non-emitting states which results in “blinking” signals that can

make quantifying fluorescence signals difficult (Alivisatos *et al.* 2005). Usage of quantum dots in biological imaging is also limited because the dots based on CdSe crystals are soluble in non-polar liquids (Alivisatos *et al.* 2005). Efforts have been made to coat the crystals with hydrophilic groups such as mercaptohydrocarbonic acids however these molecules are not stable (Aldana *et al.* 2001). Other coats make the crystals larger in size (>25 nm) which also limits biological applications (Mattoussi *et al.* 2001). Cadmium and selenium are also toxic chemicals which may also limit usage of these quantum dots.

Table 1-2: Excitation, emission wavelengths (nm) and extinction coefficients for common NIR fluorophores as provided by manufacturers.

Name	Excitation (nm)	Emission (nm)	Extinction coefficient ($M^{-1}cm^{-1}$)
‡Alexa660	663	691	132000
Alexa680	680	702	184000
Alexa700	696	719	192000
Alexa750	752	776	240000
Alexa790	784	814	260000
Allophycocyanin	650	660	700000
Cy5	650	670	250000
Cy5.5	675	694	250000
Cy7	743	767	250000
CyTE-777	777	812	130000
CyTE-783	783	814	174000
CyTE-807	807	839	120000
DyLight650	652	672	250000
DyLight680	682	712	140000
DyLight755	754	776	220000
DyLight800	777	794	270000
ICG	716-756	780-820	
IR125 (Tricarbocyanine)	795	833	
IRDye 800CW	774	789	240000
IRDye700DX	689	700	165000
Rhod800*	685	720	99000
Sulfonaphthofluorescein	614	676	
VT680	615-645	680-720	

‡Data for all "Alexa" dyes and allophycocyanin were provided by Invitrogen. Data for all "Cy" dyes were provided by GE Healthcare Life Sciences. Data for all "Dy Light" probes were provided by Thermo Scientific. Data on ICG was adapted from (Desmettre *et al.*2000). Data on IR125 was provided by Exciton (Dayton, Ohio, USA). Data on "IRDye" probes were provided by LI-COR Biosciences. Data on sulfonaphthofluorescein was adapted from (Shepherd *et al.* 2007). Data on VT680 was adapted from (McCarthy *et al.* 2009). *Data for Rhod800 was adapted from (Jilkina *et al.* 2006).

Table 1-3: Examples of targeted and activatable NIR conjugates used in cardiovascular research.

Targeted				
Fluorescent Dye	**Ligand**	**Target**	**Associated with**	**Reference**
Cy5.5	Peptide sequence	Thrombin	Thrombosis	Tung, CH. *et al.* 2002
Alexa680	Peptide sequence	FXIIIa	Thrombosis	Tung, CH. *et al.* 2003
Cy7, VT680, Alexa 680	Peptide sequence	Fibrin	Thrombosis	McCarthy, J.R. *et al.* 2009
Cy7	Antibody	Fibronectin	Angiogenesis	Matter, C.M. *et al*. 2004
Cy5.5	Peptide sequence	VCAM-1	Atherosclerosis	Kelly, K.A. *et al*. 2005
IRDye 800CW	Antibody	VEGF	Angiogenesis	Terwisscha van Scheltinga, A. *et al*. 2011
Cy5.5	Peptide sequence	Glycoprotein IIb/IIIa	Platelet activation	Tung, CH. *et al.* 2005
Cy5.5	Peptide sequence	$\alpha_v\beta_3$ integrin	Angiogenesis	Chen, X. *et al*. 2004
Activatable				
Fluorescent Dye	**Unactivated molecule**	**Enzyme/analyte**	**Associated with**	**Reference**
Sulfonaphthofluorescein	SNAPF	Hypochlorous acid	Atherosclerosis	Shepherd, J. *et al*. 2007
Cy5.5	MMP-FITC-PLC-Cy5.5	Gelatinases MMP2 and MMP9	Myocardial Infarction	Chen, J. *et al.* 2005
Cy5.5	CatK-FITC-PGC-Cy5.5	Cathepsin K	Atherosclerosis	Jaffer F.A. *et al*. 2007
CyTE-777	CyPEG-1, -2, -3	Cathepsin S	Atherosclerosis	Galande, A. *et al*. 2006
Cy5.5, Cy7	PLL-MPEG-Cy5.5/-Cy7	Urokinase-type plasminogen activator	Angiogenesis	Law, B. *et al*. 2004
Tricarbocyanine	Diaminocyanines triazole	Nitric oxide	Vasodilatation	Sasaki, E. *et al*. 2005

VCAM-1: vascular cell adhesion molecule -1, VEGF: vascular endothelial growth factor, SNAPF: sulfonaphthoaminophenyl fluorescein, MMP: matrix metalloproteinase

1.5. Targeting endothelial cells

1.5.1. Endothelial cell structure and function

Endothelial cells form an important and specialized type of epithelium within the circulatory system. Structurally, the innermost layer of all blood vessels is comprised of a unicellular layer of endothelial cells, which forms the endothelium. Although classified as squamous epithelial tissue, the cell morphology is reflective of the direction of blood flow and flow pattern. In vessels where blood flow is laminar, the cells are aligned and elongated in the direction of blood flow whereas disturbed blood flow often causes the cells to appear polygonal (Chien 2008). The cytoplasm of the endothelial cells is similar to other animal cells in that it contains a small Golgi apparatus, mitochondria, free ribosomes, rough endoplasmic reticulum and a nucleus that often bulges into the lumen of blood vessels. In addition to these standard organelles, specialized cytoplasmic tubules called Weibel-Palade bodies have been described in the endothelial cells of small arteries. Weibel-Palade bodies contain von Willebrand factor, which is a protein released into the blood plasma following a vascular injury and aids in platelet adhesion (Valentijn *et al.* 2011).

Endothelial cells are functionally diverse according to the vessel that they line. At the most basic, endothelial cells mediate exchanges between blood plasma and interstitial fluid. These exchanges can involve small dissolvable molecules such as oxygen and carbon dioxide as well as large objects such as macrophages. Endothelial cells are also the target of many signal molecules and are responsible for the secretion of many important autocrine and paracrine substances, which in turn signal other cell types (Di Francescomarino *et al.* 2009). In specialized capillaries of the kidney, endothelial cells

form permanent gaps, which give rise to fenestrated capillaries that allow for more rapid exchange of macromolecules (Maul 1971). At the extreme, discontinuous capillaries also called sinusoids exist in organs such as the liver and allow for free molecule and cellular exchange (Poste *et al.* 1982).

Figure 1-4: Schematic diagram showing the different layers that form the walls of A) larger arteries and veins and B) capillaries. Not that the internal elastic lamina is only present in arteries and not veins.

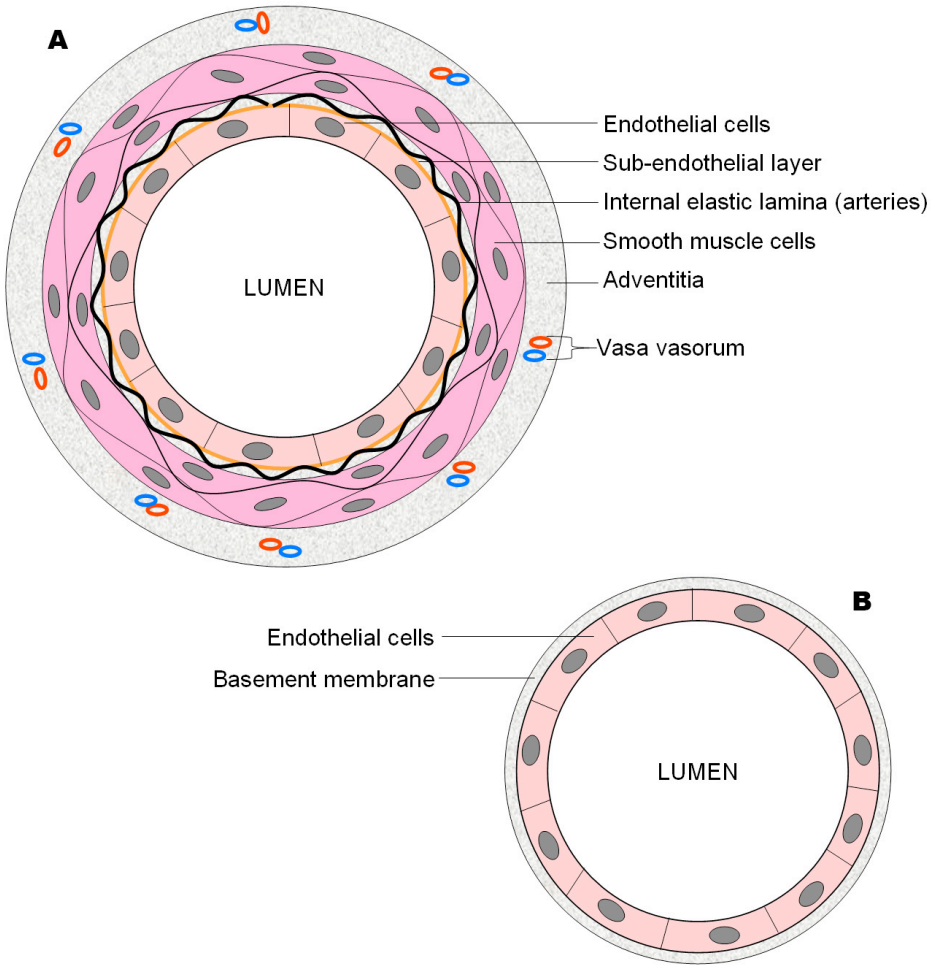

Endothelial cells, especially those in arteries are important in determining and maintaining proper vascular tone. Vascular tone, defined as the state of contraction of the smooth muscle surrounding the vessel, is an important component of the vascular system

as it is related to the maintenance of homeostasis in the body. Nowhere in the vascular system is this more evident than in the microvasculature of various organs. The micro-vascular system includes all small blood vessels such as: arterioles, metarterioles, capillaries and post-capillary venules. The architectural structure of the micro-vascular system allows arterioles and metarterioles to have partial control of blood flow and distribution into the surrounding capillary beds (Baez 1977). Blood flow into a capillary bed can increase when precapillary sphincters relax thereby increasing the diameter of the blood vessel, which allows for an increase in blood flow. For example, in thermoregulation, blood vessels, especially those near the surface of the skin must have the ability to dilate, which allows for increased blood flow to the surface of the skin at once in order to cool the body via radiation, convection and conduction (Campbell and Reece 2005). Vascular tone is also reflective of the workload on the cardiovascular system. Studies have shown that the blood flow throughout the myocardium is heterogeneous and is dynamic due to increased perfusion with increased workloads caused by stressors such as physical exercise (Austin *et al.* 1990). Increased workloads require more energy in the form of ATP, which is produced by oxidative phosphorylation therefore oxygen supply by the blood must increase under increased workload. This relationship highlights the importance of vascular tone when studying dynamics of the vascular system.

Although the physical action of constricting and dilating blood vessels is caused by the contraction and relaxation of smooth muscle, endothelial cells are responsible for the chemical trigger that causes these actions. An early study in endothelial research showed that the removal of the endothelium caused an imbalance in vaso-constriction and

dilation (Furchgott and Zawadzki 1980). It was later found that nitric oxide, produced by endothelial cells is the major vaso-dilating factor (Palmer *et al.* 1988). Since then, the main signal transduction pathway by which endothelial nitric oxide causes relaxation of smooth muscle cells has been elucidated (Figure 1-5). The pathway can be chemically initiated by the binding of acetylcholine to receptors on the luminal surface of the endothelial cell, which causes an increase in Ca^{2+} concentration within the cytoplasm of the cell (Triggle *et al.* 2003). This increase activates nitric oxide synthase, which converts L-arginine to nitric oxide. Two key endothelial acetylcholine receptors involved in NO production are: nicotinic acetylcholine receptors and muscarinic acetylcholine receptors (Cooke and Ghebremariam 2008). It is important to note that muscarinic acetylcholine receptors are also found on smooth muscle cells however, binding of acetylcholine to smooth muscle elicits the opposite result. This is because acetylcholine, released by parasympathetic nerves, initiates membrane depolarization in muscle cells, which causes calcium release into the cytoplasm resulting in muscle contraction (Ding *et al.* 2009). Other molecules that have been shown to activate endothelial nitric oxide synthase by increasing cytoplasmic Ca^{2+} are thrombin, bradykinin, vascular endothelial growth factor (VEGF), tumour necrosis factor-α, histamine, and insulin (da Silva *et al.* 2009; Fleming 2010; Thors *et al.* 2011). Physical exercise leading to increase in blood flow and shear stress has also been found to be capable of activating nitric oxide synthase (Wang *et al.* 1993). This mechanotransduction is extremely sensitive as shear stress within blood vessels is measured at approximately 10 to 20 dynes/cm^2 (Giles *et al.* 2012). Nitric oxide is capable of diffusing across the cell membrane and into adjacent smooth muscle cells where it activates guanylyl cyclase. Guanylyl cyclase synthesizes cyclic

guanine monophosphate (cGMP), a second messenger that leads to a phosphorylation cascade that ends with the relaxation of the smooth muscle cell. Vaso-dilating factors that are not directly involved with the NO system include endothelial-derived hyperpolarizing factors such as potassium ions, arachidonic acid metabolites, hydrogen peroxide, carbon monoxide, hydrogen sulphide and C-natriuretic peptide (Giles *et al.* 2012).

Figure 1-5: Signalling pathway for endothelial nitric oxide relaxation of smooth muscle cells. 1) Acetylcholine binds to specific receptor which triggers 2) influx of calcium ions through a calcium channel. 3) Nitric oxide synthase is activated, which converts arginine into nitric oxide. 4) Nitric oxide diffuses across the cell membrane into nearby smooth muscle cells. 5) Nitric oxide activates guanylyl cyclase in smooth muscle cells, which 5) converts GTP to cGMP and 6) causes smooth muscle cell relaxation. Ach: Acetylcholine, NOS: Nitric oxide synthase, Arg: Arginine, NO: Nitric oxide, GC: guanylyl cyclase, GTP: Guanine triphosphate, cGMP: Cyclic guanine monophosphate.

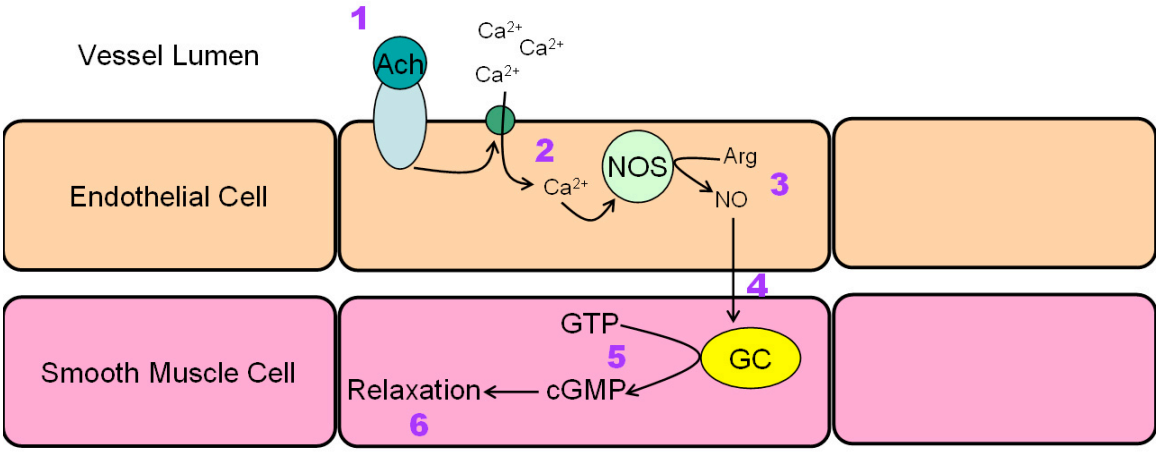

Endothelial involvement does not end at the relaxation of smooth muscle. Endothelial cells also produce a vaso-constriction factor called endothelin (Yanagisawa *et al.* 1988). Factors that promote synthesis of endothelin include but are not limited to thrombin, insulin, hypoxia and vascular shear stress (Kawanabe and Nauli 2011). Humans have 3 different isoforms of endothelin called endothelin-1, endothelin-2 and endothelin-3 (Gray and Webb 1996). Both the synthesis and signal transduction pathway for endothelin-1 have been characterized in vascular endothelial cells (Figure 1-6). In general, endothelin-converting enzyme cleaves a precursor for endothelin in the cytoplasm. Endothelin is exported out of the endothelial cell and binds to neighbouring smooth muscle cells at endothelin receptors A or B. This leads to an increase in cytoplasmic Ca^{2+} in the smooth muscle cell causing contraction of the cell. The nitric oxide and endothelin pathways are connected because nitric oxide inhibits endothelin production; endothelin production stimulates nitric oxide synthesis by binding to endothelin receptor B located on endothelial cells (Gray and Webb 1996). The balance between endothelin and nitric oxide production maintains a healthy vascular tone.

Figure 1-6: Endothelin signalling pathway. 1) An endothelin precursor is cleaved by endothelin-converting enzymes (ECE) into endothelin-1 (ET-1), which 2) can be exported out of the endothelial cell where it binds to endothelin receptors A or B (ET_A, ET_B). 3) This binding leads to an influx of calcium ions from the intracellular space into the smooth muscle cell causing calcium-induced calcium release from the sarcoplasmic reticulum. 4) High amounts of cytoplasmic calcium ions result in contraction of the muscle cell. 5) ET_B is also present on endothelial cells where, once activated by ET-1, it 6) activates nitric oxide synthase (NOS). 7) NOS then converts arginine (Arg) into nitric oxide (NO) which then diffuses through the cell and into neighbouring smooth muscle cells and causes 8) relaxation.

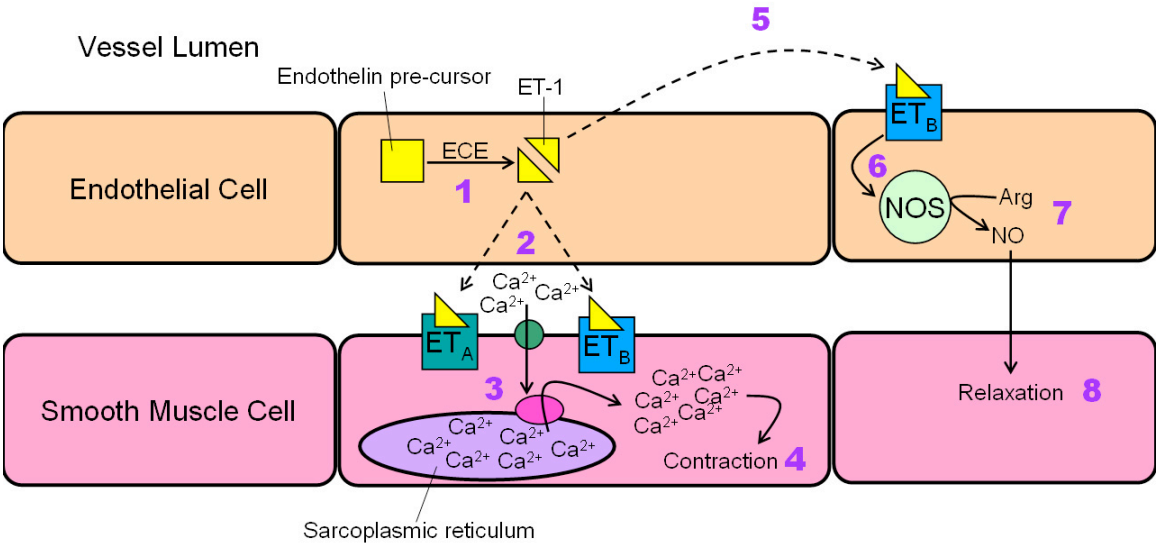

1.5.2. Associated diseases

Because endothelial cells play such a critical role in the cardiovascular system, endothelial dysfunction often leads to vascular complications. Diabetes mellitus, hypertension, atherosclerosis and more recently, obesity have all been associated with endothelial dysfunction (Bagi *et al.* 2004; Hoenig *et al.* 2008; Okon *et al.* 2005; Romero-Corral *et al.* 2010; Ross 1999; Sitia *et al.* 2010). Diabetes mellitus is often characterized

by an increase in blood glucose levels or hyperglycemia that has been shown, in animals, to interfere with the acetylcholine-triggered vasodilatation pathway as illustrated previously in Figure 1-3 (Kersten *et al.* 1995; Tesfamariam *et al.* 1990; Tesfamariam *et al.* 1991). Normal endothelial cell function is further inhibited in diabetes mellitus due to the excessive generation of reactive oxygen species (ROS) through the "receptor for advanced glycation end-products" (RAGE) signalling pathway. Briefly, glucose by-product accumulation activates nicotinamide adenine dinucleotide phosphate (NADPH) oxidase, which produces ROS (Inoguchi *et al.* 2000). It is well known that ROS are highly damaging to the cell because it interferes with critical cellular components such as DNA. ROS react with nucleic acids such as guanine and converts it to an oxidized form (e.g. 8-oxo-7,8-dihydroguanine) that causes mutations such as base pair mismatch during DNA replication (Maynard *et al.*2009; Roberts and Sindhu 2009). Under diseased states, the high production of ROS overcomes natural DNA repair mechanisms such as base excision repair and nucleotide excision repair (Cooke *et al.* 2003). DNA damage can then lead to cellular death via the apoptosis pathway (Roos and Kaina 2006). The accumulation of glucose by-products also up-regulates the RAGE signalling pathway and leads to apoptosis via caspase activation (Wautier *et al.* 2001). Endothelial cell death destroys the integrity of the blood vessel and results in leaky vessels. These by-products also activate the diacylglycerol/protein kinase C (DAG/PKC) pathway, which inhibits production of nitric oxide and thus leads to abnormal vascular tone (Alp and Channon 2004). PKC has been shown to block the expression of the messenger RNA responsible for the formation of endothelial nitric oxide synthase (Kuboki *et al.* 2000). It has also been shown to inhibit the transport of L-arginine, a critical molecule in the production of

nitric oxide, into the cytoplasm (Chu and Bohlen 2004). For these reasons, diabetic patients often have poor circulation that in chronic conditions can lead to blindness, limb amputations and stroke.

Vascular diseases tend to be associated with each other. Atherosclerosis is characterized by the formation of plaques within a blood vessel, which narrows the diameter of the vessel causing an increase in blood pressure. For this reason, atherosclerosis and hypertension are often linked and in both cases leads to some form of endothelial dysfunction. The most common prerequisite for atherosclerosis is high amounts of low-density lipoprotein cholesterol in the blood plasma, also known as hypercholesterolemia. Studies have shown that hypercholesterolemia interferes with the endothelial nitric oxide production and, similar to diabetes mellitus, causes an increase in the production of ROS (Matsuura *et al.* 2008). Both hypercholesterolemia and an increase in plasma sodium have been associated with the production of asymmetric dimethyl-*L*-arginine, which is a competitive inhibitor for endothelial nitric oxide synthase (Li *et al.* 2009; Vladimirova-Kitova *et al.* 2008). Impaired vasodilatation eventually manifests as hypertension. These and other vascular diseases illustrate the importance of understanding endothelial network structure and function.

1.5.3. *Lycopersicon esculentum* lectin

Lectins are a heterogeneous class of proteins and glycoproteins that are prevalent in plants (Sharon and Lis 1972). It is thought that lectins evolved as a defence mechanism for plants against bacteria since they cause cells to agglutinate (Chrispeels and Raikhel 1991). Lectin from the common tomato, *Lycopersicon esculentum* (LEA) has been used to identify group B streptococci grown in selective and non-selective

Todd-Hewitt broth because it causes observable agglutination (Slifkin and Cumbie 1987). Many natural lectins, such as those from the common bean, are also toxic to animals (Pusztai *et al.* 1981). All lectins share a chemical affinity to recognize and bind to specific carbohydrate groups found on the surface of target cells (Nachbar *et al.* 1980). *Lycopersicon esculentum* (LEA, tomato) lectin binds specifically to polylactosamine oligosaccharides (N-acetyl-D-glucosamine and N-acetyl-polylactosamine oligomers), which are abundant on the endothelial cell surface, thus making it an effective probe for endothelial cells (Debbage *et al.* 2000; Laitinen 1987; Mazzetti *et al.* 2009). Outside of the cardiovascular system, LEA lectin has been shown to also bind to the epithelium of the small intestine and type 1 alveolar epithelial cells (Tao *et al.* 2003; Bies *et al.* 2004). Binding to these other cells can be avoided in *in vivo* situations by injecting the labelled lectin directly into the blood vessels using techniques such as tail-vein injections. Early studies analyzing the amino acid composition of LEA lectin showed that this specific lectin has approximately 11 lysine residues and thus is able to react with the NHS-ester group to form a conjugate (Nachbar *et al.* 1980). LEA lectin has been shown to be relatively non-toxic in mammals, a characteristic that is crucial in the development of probes for *in vivo* imaging (Banchonglikitkul *et al.* 2002; Nachbar *et al.* 1980). LEA lectin does cause agglutination of human erythrocytes however the specific activity is very low (Kilpatrick 1980). It is interesting to note that LEA lectin is toxic to beetles such as weevils (Chrispeels and Raikhel 1991).

1.5.4. Cy5.5-lectin conjugate

The specificity of the binding of Cy5.5-lectin to endothelial cells opens up the possibility for use of the conjugate as a deposition flow tracer in different species as well as in

potential clinical applications for the purpose of visualizing microvascular networks (Prinzen and Bassingthwaighte 2000). Currently, most deposition flow tracers employed are too large (≥ 15 μm) to visualize flow through microvascular networks (e.g. microspheres) because although they are intravascular, their size may occlude microvessels (Arsos *et al.* 2009; Marshall *et al.* 2004; Munch *et al.* 2011). Comparatively, Cy5.5-lectin is a vascular micro-flow imaging probe that would reflect the micro-flow distribution more accurately and because of its ability to generate images through thicker tissues, Cy5.5-lectin could be used in physiological studies of microvascular endothelium function. For instance, endothelial staining can be used to analyze cardiac micro-vessel branching and filling under different workload conditions. Micro-vessel filling may change under conditions of higher workload and hypoxia, or in a disease that manifests itself as diffuse-type damage (e.g. diabetes, hypertension, inflammation associated microemboli etc.) as opposed to localized-type damage caused by occlusion of large coronary vessels, which is easily identified with current cardiac imaging techniques. Microemboli are frequently found in patients who die from sudden death and currently, this kind of myocardial damage is only confirmed in biopsies or by post-mortem histology (Heusch *et al.* 2004). In some conditions such as microembolization, the coronary flow reserve, which describes the increase in coronary blood flow above basal levels, is affected (Heusch *et al.* 2009). For these reasons, development of Cy5.5-lectin has important practical importance.

1.6. Objectives

The overall objective of this project is to develop a deposition flow tracer targeted to endothelial cells for the purpose of imaging microvascular perfusion in mouse hearts at

the near-infrared wavelength. It is hypothesized that if Cy5.5-lectin conjugate binding is limited to endothelial cells and is dependent on flow then the fluorescence signal captured will be reflective of the local micro-perfusion within the heart tissue. More specific objectives include 1) synthesis of the Cy5.5-lectin conjugate 2) infusion of conjugate into mouse hearts via *ex vivo* and *in vivo* methods 3) assessing specificity of Cy5.5-lectin binding to endothelial cells and 4) real-time monitoring of the distribution of the conjugate within normally and abnormally perfused mouse hearts.

Chapter 2 – Materials and Methods

All procedures in this study conform with the "Guide to the Care and Use of Experimental Animals" published by the Canadian Council on Animal Care (Ottawa, Canada, 1993).

2.1. Reagents

The following materials were acquired: Monofunctional and bisfunctional Cy5.5 N-hydroxysuccinimide (NHS)–ester reactive dyes (GE Healthcare Ltd., Buckinghamshire, UK); *Lycopersicon esculentum* (LEA) lectin, fluorescein isothiocyanate (FITC)–lectin conjugate and L-lysine monohydrochloride (Sigma, St. Louis, MO); Bovine serum albumin (BSA) (Lifeblood Medical, Inc, Freehold, NJ); 10% neutral buffered formalin (EMD Chemicals Inc, Gibbstown, NJ); Fluoro-Gel aqueous mounting medium (Electron Microscopy Sciences, Hatfield, PA); Pharmingen Anti-Rat Ig HRP Detection Kit and rat anti-mouse intercellular adhesion molecule 2 (ICAM2) antibodies (BD Sciences, San Diego, CA). All other chemicals used were of analytical grade. Buffer recipes not described in this chapter can be found in Appendix 3.

2.2. Synthesis

2.2.1. Synthesis of Cy5.5-lectin conjugate

Cy5.5-lectin conjugates were synthesized by reacting 3.4×10^{-4} M of FluoroLink Cy5.5 monofunctional or bisfunctional NHS–ester reactive dye with 6 mg of LEA lectin, which was dissolved in 6 ml of 0.1 M sodium carbonate-bicarbonate buffer (pH 9.3). The initial dye-to-protein (D/P) ratio was approximately 20-25 moles of dye per mole of protein. The reaction mixture was allowed to react over a period of 4-6 hours at 25°C in

the dark with mixing. Afterwards, 4 rounds of dialysis were used to remove any remaining free dye. Spectra/Por 7 regenerated cellulose dialysis membrane (MWCO = 25 000, Spectrum Laboratories, Inc., Rancho Dominguez, CA) and the following dialysis buffers were used: the first two rounds used 0.15 M NaCl and the last two rounds used 0.01 M phosphate buffered saline (PBS) with 0.01% NaN_3. Dialysis was performed on ice with stirring for 4 hrs after which the dialysate was transferred into fresh buffer and dialysis was continued (4°C) overnight. Cy5.5-lectin conjugate was stored in the dark at 4°C until needed.

The quality of the conjugate was determined by estimating the final D/P ratio. Applying the Beer-Lambert law, the D/P ratio was calculated using the following equation:

$$D/P = \frac{A_{675} A_{280protein}}{\varepsilon_{conj} l_{conj} (A_{280} - 0.18 A_{675}) C_{protein}} \quad (2)$$

The absorbance of the conjugate was measured at 280 nm and 675 nm using a microplate reader (BioTek Instruments, Inc. Winooski, USA) and defined in Equation 1 as A_{280} and A_{675} respectively. The pathlength, l_{conj}, was experimentally derived by measuring the absorbance of the conjugate solution at 900 nm and 977 nm. This is because water has a small absorbance peak at 977 nm, which in a standard 1 cm^3 cuvette at room temperature has an absorbance value of 0.18. By comparing this standard value to the values obtained at 977 nm, using 900 nm as a blank, the pathlength in centimetres can be calculated as shown in equation 3.

$$lconj = \frac{A_{977} - A_{900}}{0.18} \quad (3)$$

The extinction coefficient of Cy5.5-NHS ester, defined as ε_{conj}, is 250 000 M^{-1} cm^{-1} (GE Healthcare, manufacturer manual). Since the extinction coefficient of lectin was unknown, the absorbance and concentration of a solution of un-reacted protein was used and defined here as $A_{280protein}$ and $C_{protein}$. The factor of 0.18 accounts for the absorption of the dye at 280 nm, which is approximately 18% of the maximum dye absorbance at 675 nm. Comparisons were also made between the binding efficiency of monofunctional Cy5.5 and bisfunctional Cy5.5 to LEA lectin, as both were readily available. Smaller scaled reactions were also performed initially in order to test the methods described.

2.2.2. Synthesis of Cy5.5-BSA and Cy5.5-lysine conjugates

Synthesis of Cy5.5-BSA was performed under the same conditions as described for Cy5.5-lectin. No modification to the conjugation reaction procedure was necessary. Cy5.5-BSA was then used as a control for heart perfusion experiments.

Synthesis of Cy5.5-lysine was also performed under the same conditions as described for Cy5.5-lectin however modifications were made for the Cy5.5-lysine reaction in order to ensure complete blockage of the Cy5.5-lectin conjugation reaction. The amount of lysine added was 100-fold the amount of lectin in moles. Cy5.5-lysine was created for two purposes: 1) Cy5.5-lysine was used to test the ability of dialysis as a method to remove free dye and 2) to use Cy5.5-lysine as a negative control in the experiments involving heart perfusion. For the first purpose, Cy5.5-NHS ester was combined with 1 mg of lectin and lysine (100-fold the amount of lectin in moles). Dialysis was performed in a similar fashion to normal Cy5.5-lectin reactions. Samples of the dialysis buffer were taken in order to estimate the amount of Cy5.5-lysine lost during

the dialysis. The absorbance of the final product post-dialysis was also measured to determine if any Cy5.5-lysine was present.

For the Cy5.5-lysine reactions used as a negative control in the heart perfusion and injection experiments, purification steps involving dialysis were omitted due to the small size of lysine (MW = 146.19 Da) and the limitations of the dialysis membrane. These reactions did not involve lectin.

2.2.3. Measuring Cy5.5 fluorescence in solutions

In the dark, a 650 nm laser diode (3 mW, NVG Inc., Georgia USA) was placed against the quartz cuvette containing a solution of Cy5.5 or Cy5.5-lectin, causing excitation of the chromophores. Emitted fluorescence was detected at 90° using a fibre optic cable connected to a spectrometer (Control Development, Inc., South Bend, IN). Single-read fluorescence spectra between 480-1100 nm with a $\Delta\lambda = 1$ nm were acquired. The program CDI Spec32 (Control Development, Inc., South Bend, IN) was used for data collection and processing. A dilution series of Cy5.5 in known concentrations was also used to aid in the determination of Cy5.5 concentration in solution.

Figure 2-1: The fluorescence at 695 nm for Cy5.5-NHS ester (excited at 650 nm) at 0.001 µM, 0.002 µM, 0.004 µM, 0.008 µM, 0.016 µM, 0.032 µM, 0.064 µM, 0.129 µM, 0.258 µM, 0.516 µM and 1.031 µM, forming the standard curve on which the unknown concentration of the dye can be estimated.

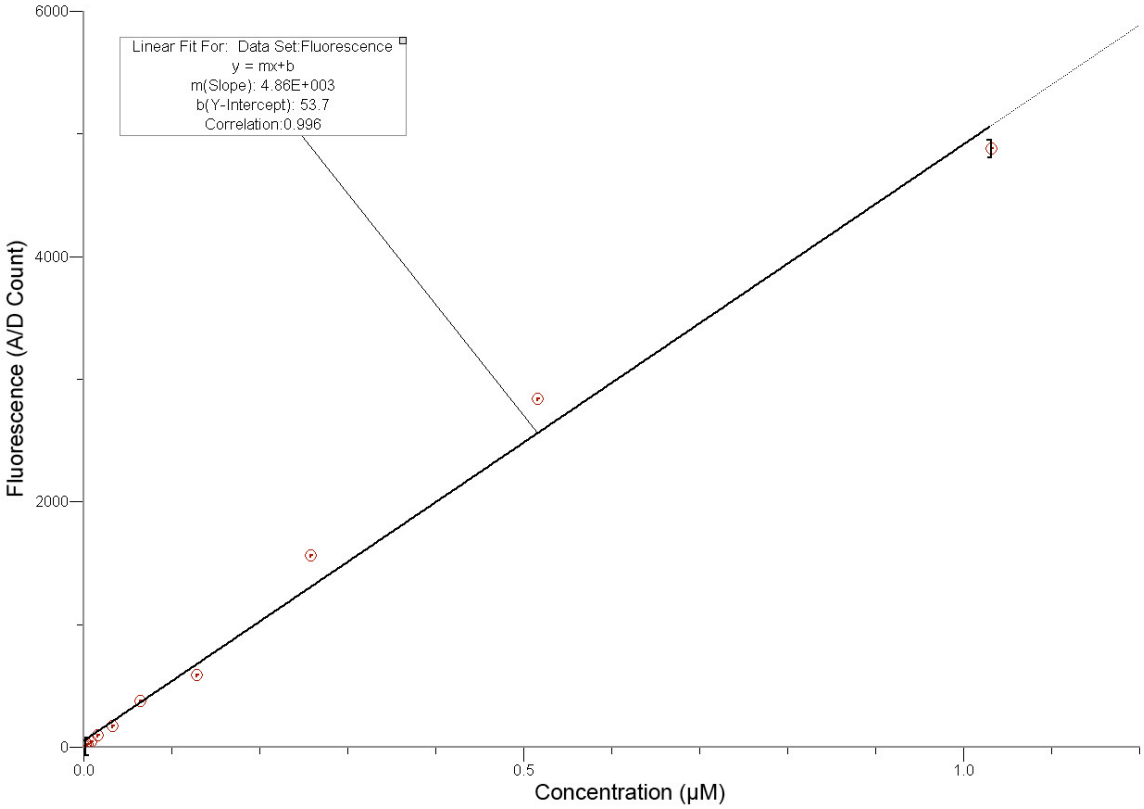

2.3. Mouse heart isolation and perfusion (*ex vivo* dye loading)

Male and female C57BL6 mice (body weight = 33.0 ± 5.8 g, heart weight = 0.19 ± 0.04 g, n = 31), bred at the Institute for Biodiagnostics animal facility, were anaesthetized with 0.25 ml of a pentobarbital solution (65 mg/ml) as described by Jilkina *et al* (Jilkina *et al.* 2005). The hearts were quickly removed and perfused in a Langendorff mode with Krebs-Henseleit buffer (KHB) as described by Jilkina *et al* (Jilkina *et al.* 2006). The KHB solution consisted of (in mM): 118 NaCl, 4.7 KCl, 1.2 $MgSO_4$, 2.5 $CaCl_2$, 0.5 EDTA, 11 Glucose, 25 $NaHCO_3$ and 1.5 Na-pyruvate, which was aerated with a mixture

of 95% O_2 and 5% CO_2 at 36°C. The coronary flow rate provided by a peristaltic pump was 3 ml/min. The conjugates were mixed with KHB upon entering the hearts using a calibrated syringe pump set to an infusion rate of 3 ml/hr. Infusion time was either 10 or 20 minutes depending on the concentration of the injected probe. The concentration of the Cy5.5-lectin, Cy5.5-BSA and FITC-lectin conjugates within the syringe were 100 μg/ml for the 10 min injection and the 50 μg/ml for the 20 min injection. FITC-lectin, Cy5.5-BSA, and Cy5.5-lysine conjugates were used as positive and negative controls respectively. The mechanical function of the heart was measured by introducing a water-filled balloon into the left-ventricle (LV) of the heart. The balloon was connected to a pressure transducer interfaced to a Digi-Med Model- 210 heart performance analyzer (Micro-Med, Louisville, KY) to monitor heart rate, LV systolic pressure, LV end-diastolic pressure, and perfusion pressure. These variables were used to calculate the pressure rate product (PRP) defined as:

$$PRP = (LVSP-LVEDP)(HR) \quad (4)$$

…where the left ventricular end diastolic pressure (LVEDP) is subtracted from the left ventricular systolic pressure (LVSP) and the resulting value is then multiplied by the heart rate (HR). Effluent produced during the perfusion period with the probe was collected in order to estimate the amount of the conjugate that was retained by the heart.

Figure 2-2: Schematic diagram of the Langendorff perfusion system used to infuse conjugates into mouse hearts. Krebs-Henseleit buffer is pumped from the lower reservoir into the upper reservoir where it is aerated with a gas mixture. From there a second pump moves the buffer towards the heart and is used to control the flow rate. The syringe pump injects the conjugate at a predetermined rate into the line immediately before the cannula. Heart function is monitored and recorded by the left-ventricle (LV) pressure, heart rate analyzer.

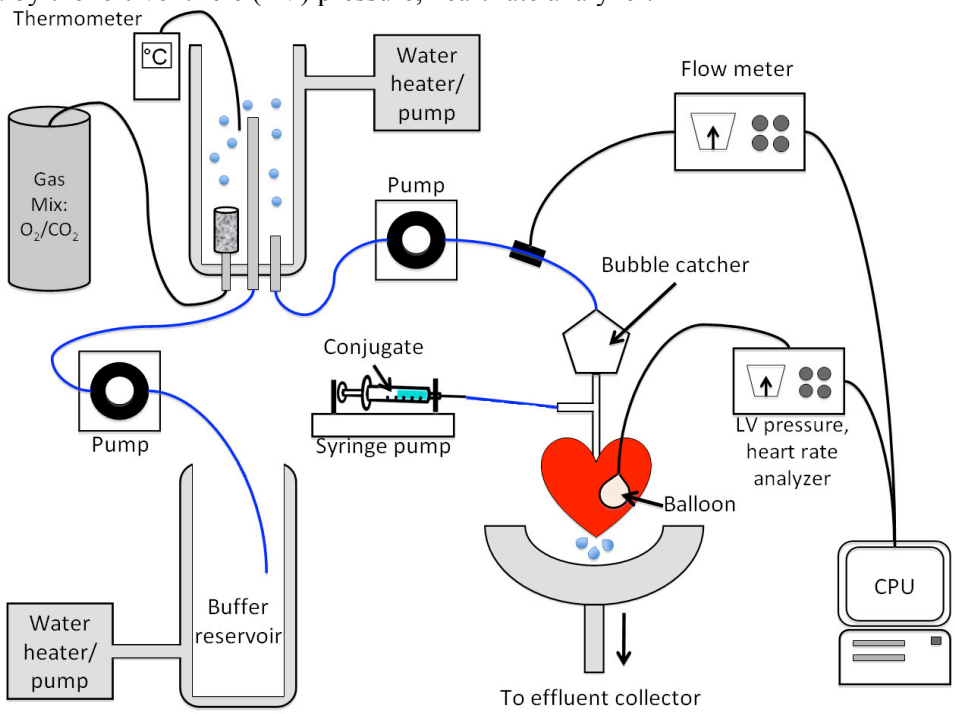

It is important to note that Langendorff perfusion differs from *in vivo* heart perfusion because the heart is perfused in a retrograde direction. This means that perfusion begins at the aorta and the subsequent pressure from the perfusate closes the aortic valve, which forces the solution to travel through the ostia and into the coronary arteries (Bell *et al.* 2011). A drainage hole is placed at the bottom tip of the left ventricle by the introduction and removal of a cannula to account for Thebesian flow. Unfortunately there are limitations to this method because firstly, the heart is isolated therefore normal humoral and neural influences are absent and secondly, heart tissue is

easily damaged during the cannulation and subsequent steps (Skrzypiec-Spring *et al.* 2007). For this reason, once the heart is properly attached to the perfusion apparatus, a 10 minute baseline reading of heart function is performed prior to the start of infusion. Hearts that do not meet minimum functional requirements are rejected. The simplicity of the method and the ability to control factors such as pressure or flow and the perfusion time outweigh the limitations mentioned.

Figure 2-3: Direction of heart perfusion in Langendorff mode. Normally, blood and plasma exit the heart at the aorta but in Langendorff mode the perfusion cannula is inserted into the aorta forcing the buffer into the aorta. Pressure from this causes the aortic valve to remain closed and buffer to redirect into the right and left coronary artery (RCA and LCA respectively). From there myocardial vasculature is perfused and eventually drains into the coronary veins which empties into the coronary sinus located in the right atrium. Fluid can freely drain out of the right atrium via the vena cava or can travel into the right ventricle where it can drain via the pulmonary arteries. A drainage cannula pierces a hole into the bottom tip of the left ventricle to account for Thebesian flow (indicated by the red dot). The schematic image of the heart is based on a human heart. Mouse hearts have an additional fourth branch that extends off the LCA and proceeds dorsally as well as a branch from the RCA called the septal artery (Icardo and Colvee 2001). CircA = Circumflex artery.

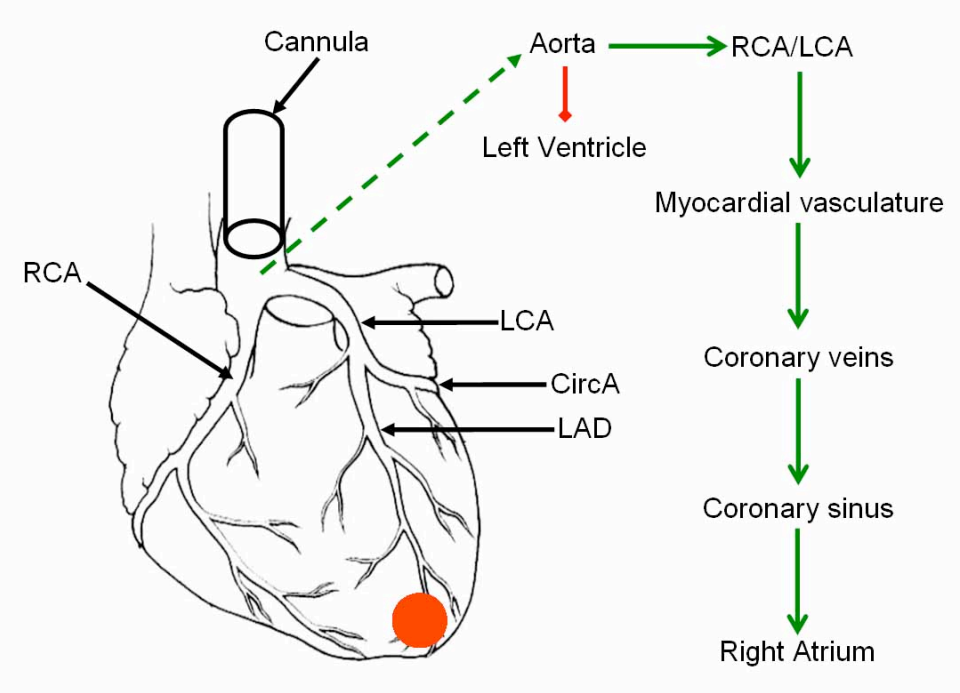

2.3.1. Optical point spectroscopy of perfused mouse hearts

During Langendorff perfusion the pseudo-absorbance spectra of the heart were captured using the fibre optic illuminator Oriel model 77501 (Stratford, CT) in conjunction with a spectrometer (model PDA-512, Control Developments Inc., South Bend, IN) (Jilkina *et al.* 2011). Spectra within the 400-1100 nm range were acquired with a 0.1 s integration time, a sample average of 120 and a delay of 48 s, which resulted in approximately one spectrum per minute. Pseudo-optical density (POD) was calculated according to the formula (Kupriyanov *et al.* 2004):

$$POD = -\log(I_s / I_0) \quad (5)$$

The variables I_s and I_0 represent the intensity of light diffusely reflected back by the sample and the light reflected by the Spectralon® standard respectively. The presence of oxy-myoglobin peaks at 545 and 581 nm was an indicator for adequate oxygenation of the myocardial tissue (Millar *et al.* 1996). POD spectra were not recorded during the infusion of Cy5.5-lectin into arrested hearts in real-time imaging experiments as the light source from the POD probe would have interfered with imaging. POD spectra however were taken prior to imaging session in these arrested hearts to confirm that the hearts, although arrested, were adequately perfused and/or correctly ligated in the LAD-ligation experiments.

2.3.2. Left anterior descending (LAD) artery ligation

In randomly selected hearts, the LAD artery was ligated with a 4-O silk surgical suture (Ethicon, Inc. Somerville, NJ). Optical point spectroscopy was used to determine quality of the ligation and degree of perfusion restriction. Areas unaffected by the ligation continued to have a normal oxygenation profile compared to the poorly

oxygenated ligated area downstream of the LAD ligation point. Infusion of the dye to the perfusion buffer proceeded as normal.

2.4. Real-time Imaging

Methods as described by Jilkina *et al*. for use in rats were modified for mice (Munch *et al.* 2011). Briefly, mouse hearts were excised and perfused in a Langendorf mode as described in 2.3. To avoid motion artefacts during imaging sessions, high potassium KHB (24 mM KCl) was used to arrest the hearts in place of regular KHB, which has a potassium concentration of 4 mM. The high potassium KHB causes depolarisation of the cellular membrane of cardiomyocytes and therefore stops membrane potential propagation. However, cardiac arrest in this cardioplegic solution is cardio-protective and preserves cardiac structure, oxygenation and energetics. High potassium KHB was used for both normal and ligated hearts for real-time imaging sessions. For ligated hearts, high potassium KHB was used to stop the heart before the ligation was performed.

The method and equipment used for the imaging sessions was previously described by Gussakovsky *et al* (Gussakovsky *et al.* 2011). Briefly, the heart was illuminated using six 635 nm 5 mW laser diodes and images were captured using an infrared-sensitive CCD camera (RS Roper Scientific NTE/CCD-512-EBTF.GR-1, Tucson, AZ), with a Nikon Micro AF60 lens at f/8 and a Schott RG 695 nm glass cut-off filter, which eliminated excitation light reflection and registered only fluorescence above 695 nm. The camera has a native pixel resolution of 1024 x 768 pixels. The camera was placed approximately 5 cm away from the heart. Images captured every 30 s with an

exposure time of 2500 ms for 70 minutes (20 min. baseline, 30 min. infusion, 20 min. washout) were then processed using Matlab (The MathWorks, Natick, MA).

In Matlab, 4 similar sized ROIs were selected. For LAD-ligated hearts, this meant that 2 regions were in the well perfused area and 2 regions were in the area below the ligation point (restricted perfusion). The average pixel intensity within the ROIs was calculated through a MatLab macro developed by Dr. Gussakovsky and plotted against time using Graphical Analysis 3.0 (Vernier Software & Technology, Canada).

Figure 2-4: Real-time imaging system set-up using six 635 nm 5 mW laser diodes. The laser diodes are mounted on a moveable plastic and metal support system, which is attached to the plastic rim around the filter. The combined unit is attached to the lens which is attached to the camera. The lasers are powered by a battery pack containing 2 DD batteries and the camera is powered via the USB connection.

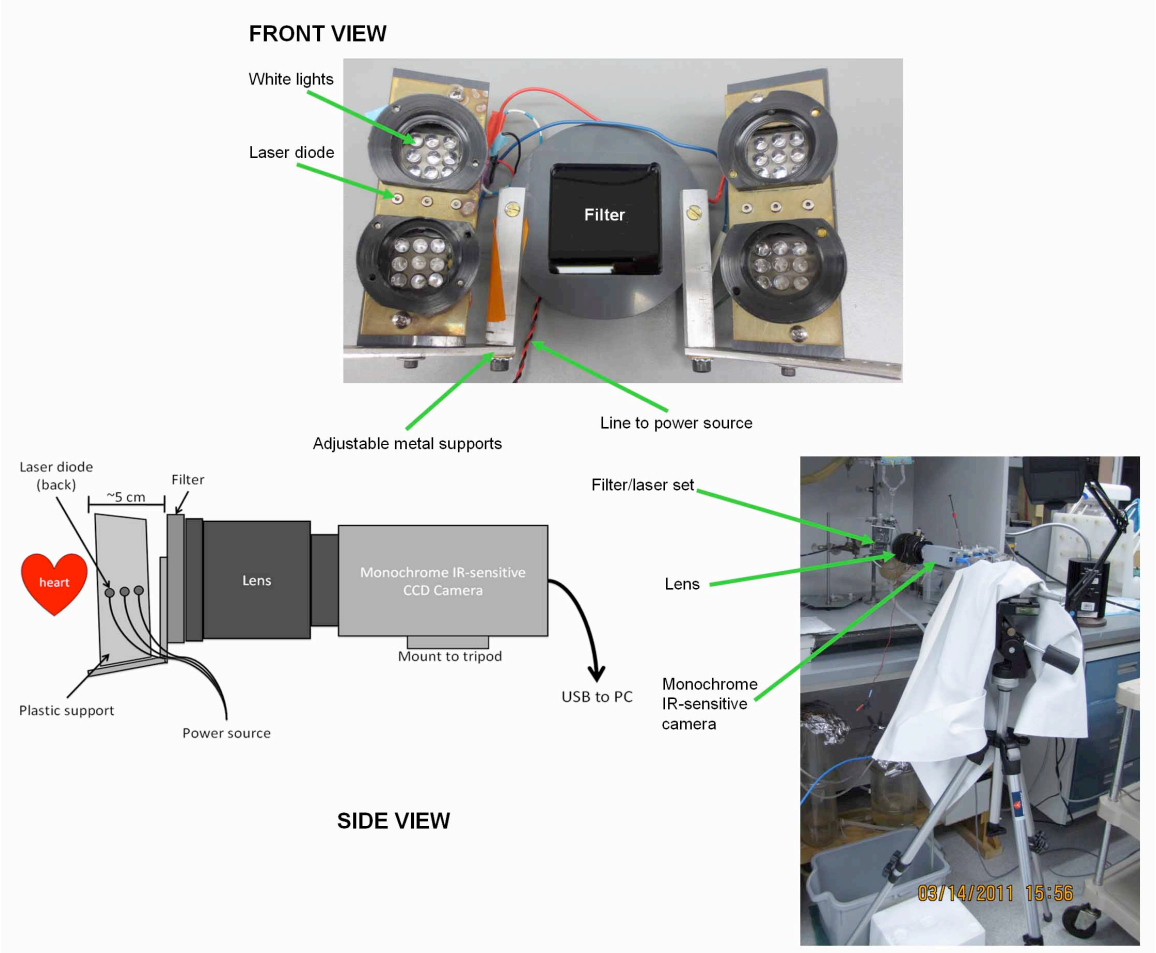

2.5. Tail-vein injection (*in vivo* dye loading)

Mice were anaesthetized with isofluorane (3-4% induction, 1.5-2% maintenance) in 100% oxygen at 0.6 l/min (Donovan and Brown 2001). Injection protocol was based on that described by McDonald *et al* (Thurston *et al.* 1996). Briefly, the anaesthetized mouse was rested on a flat bed with its tail soaked in some warm water to aid in the visibility of the vessel. Heat lamps were used to ensure adequate body temperature. The lateral tail-vein was located and injected with approximately 200 µl of the selected conjugate at concentrations between 0.5 mg/ml to 2.0 mg/ml. The injected solution was allowed to re-circulate up to 5 min. The mouse was then given an intraperitoneal injection of 0.25 ml pentobarbital solution (65 mg/ml), and removed from gas anaesthesia pending a midline thoracotomy and harvest of the heart and other tissues.

2.6. Histology

Harvested tissue samples were frozen into blocks by using labelled standard TissueTek cryomolds (Sakura Finetek USA, Inc., Torrance, CA) filled with Shandon Cryomatrix (Thermo Fisher Scientific, Cheshire, UK), and floated in liquid nitrogen. To ensure similar anatomical slices during sectioning, organs were always frozen into blocks oriented as follows:

Table 2-1: Tissue orientation when freezing into cryomolds.

Organ	Orientation
Heart	aorta down, apex up
Spleen	horizontal
Liver	cut in half vertically and laid horizontal
Kidney	horizontal

Blocks were wrapped in foil and stored at -80°C until sectioning.

2.6.1. Fluorescent slides

Frozen sections at 10 to 100 μm thickness were collected with minimum lighting on Fisher Plus Gold slides using a Leica CM3050S cryostat (Nussloch, Germany). The sections were fixed in 10% neutral buffered formalin for 10 minutes and then rinsed with filtered water. Sections were coverslipped using Fluoro-Gel aqueous mounting medium and were sealed at the edges with nail polish to prevent drying. Slides were allowed to dry briefly before they were stored in the dark at 4°C.

2.6.2. Hematoxylin and Eosin (H and E) staining

Hematoxylin and eosin staining provides basic structural information with hematoxylin staining structures such as cell nuclei blue and eosin staining cytoplasmic structures and proteins red. H and E staining methods were based on standard protocols provided by the chemical manufacturer. Briefly, frozen sections were collected for H and E staining at a thickness of 6 μm on charged Fisher Plus Gold slides and then fixed in 95% ethanol for 10 minutes followed by air drying. Sections were hydrated in running

tap water for 3 minutes, stained in Lillie's modified Mayer hematoxylin for 8 minutes, rinsed in tap water, the exposed in ammonia water and again rinsed in tap water to sharpen the blue colouring. Slides were dipped in 95% ethanol and stained in eosin for 30 seconds. The slides were dehydrated through graded alcohols and cleared in changes of xylene. They were then covered with a coverslip using entellan mounting medium.

2.6.3. Immunohistochemistry with intercellular adhesion molecule 2 (ICAM2) staining

Immunohistochemistry staining with ICAM2 was used as a comparison to labelling patterns of endothelial cells by Cy5.5-lectin. Immunohistochemistry methods were based on the standard procedure provided by BD Biosciences (San Diego, CA). Cryo-sections were also collected for immunohistochemical staining at a thickness of 6 μm on charged slides. Sections were collected in sequential order to keep anatomical structures similar from slide to slide. Slides were fixed in ice-cold acetone at -20°C for 10 minutes and air-dried. Slides were rinsed in 0.1M PBS and blocked for tissue endogenous peroxidase activity by incubating with 3% hydrogen peroxide diluted in methanol. After 0.1M PBS rinses, the sections were blocked against non-specific binding of the primary antibody by incubating with 10% goat serum in 0.1M PBS for 30 minutes at room temperature. Slides were incubated overnight at 4°C with the primary antibody, rat anti-mouse CD102, at dilutions of 1/25 and 1/50. The next day, slides were rinsed in 1% Triton X-100 in 0.1M PBS and incubated at room temperature for 1 hour with the secondary antibody, biotinylated goat anti-rat immunoglobulin, at dilutions of 1/25 and 1/50. The slides were rinsed again in 1% Triton in 0.1M PBS and incubated for 30 minutes at room temperature with streptavidin-horseradish peroxidase. Again, the slides

were rinsed in 1% Triton X-100 in 0.1M PBS and then incubated for 5 minutes in the dark with prepared diaminobenzidine (DAB). Finally, the slides were rinsed twice in tap water for 3 minutes each and counterstained with Lillie's modified Mayer hematoxylin for 1 minute. After dehydration in graded alcohols and clearing with xylene, the slides were mounted with entellan.

2.7. Microscopy

Both bright field and fluorescent microscopy were performed using a Zeiss Observer.Z1 non-confocal system (Carl Zeiss Canada Ltd, Toronto). The objective lenses used were: EC "Plan-neofluar" 10×/0.3 DICI (1.11 μm optical resolution) and "N-Achroplan" 40×/0.65 (0.51 μm optical resolution). Two excitation modes were used unless indicated otherwise in the text. For sections labeled with FITC-lectin, the Colibri LED-Module 470 nm with filter set 62 HE B/G/HR R was used (manufacturer preset). For sections labeled with Cy5.5-lectin, the Colibri LED-Module neutral white with filter set 32 AF 680 (excitation BP 665/45, emission 725/50, beam splitter FT 695) was used. Images were captured using Zeiss AxioCam MR Rev3 (1388 x 1040 standard mono resolution, digital gain factor of 2 with an index of 1) and ZeissAxioCamICc3 (2080 x 1540 8-bit RGB colour resolution, digital gain factor of 2 with an index of 1).

2.8. Intensity correlation analysis

Images were processed and analyzed using AxioVision v.4.7.2.0 and ImageJ v.1.44. Using ImageJ with the Intensity Correlation Analysis ImageJ plug-in described and developed by Li *et al.* (Li *et al.* 2004), pixel intensities for fluorescent images were

measured over a selected region of interest (ROI). The resulting plot profile was then used to determine signal to background noise.

2.9. Statistics

Unpaired student T-test was used for data comparison calculations. Differences were considered statistically significant when $P \leq 0.05$. Data are presented as means ± standard deviation.

Chapter 3 – Results

3.1. Synthesis of Cy5.5-lectin conjugates

Preliminary experiments involving both versions of the Cy5.5-NHS ester indicated a difference in the binding efficiency between monofunctional Cy5.5 dyes compared to bisfunctional Cy5.5 dyes (Nguyen *et al.* 2012). Further testing indicated that there was a statistically significant difference in the binding efficiency of the two dyes. Three sets of reactions were carried out to accurately compare the binding efficiency of the monofunctional Cy5.5 dye to the bisfunctional Cy5.5 dye. When using the same initial D/P ratio, the bisfunctional Cy5.5-NHS ester out performed the monofunctional Cy5.5-NHS ester by binding on average 10% more to lectin and thus resulting in a final dye to protein (D/P) ratio that is also higher (Table 4). The overall amount of dye that was lost however remained in the 80-90% range for both types of the Cy5.5-NHS ester.

Table 3-1: Comparison of binding efficiency of monofunctional and bisfunctional Cy5.5 dyes to lectin. Average before and after dialysis values determined spectrophotometrically using the absorbance values at 675 nm comparing monofunctional dye to bisfunctional dye. P-values were determined using paired T-tests.

	Monofunctional Dye n = 3	**Bisfunctional Dye n = 3**	
Average amount of dye before dialysis (moles)	$1.64 \times 10^{-8} \pm 1.24 \times 10^{-10}$	$1.64 \times 10^{-8} \pm 1.64 \times 10^{-10}$	P=0.423
Average amount of dye after dialysis (moles)	$1.15 \times 10^{-9} \pm 4.63 \times 10^{-10}$	$2.72 \times 10^{-9} \pm 9.74 \times 10^{-10}$	P=0.0360
% of dye lost	92.9 ± 2.56	83.6 ± 5.87	
Estimated amount of bound lectin (moles)	$4.71 \times 10^{-9} \pm 1.72 \times 10^{-9}$	$6.75 \times 10^{-9} \pm 1.46 \times 10^{-9}$	
Estimated dye to protein ratio	0.261 ± 0.100	0.400 ± 0.0850	

When these reactions were increased to full-scale (5 times the size of the preliminary reactions) reaction efficacy increased however, the differences between monofunctional and bisfunctional Cy5.5-NHS ester disappeared (Nguyen *et al.* 2012). Large-scale conjugation of both types of Cy5.5-NHS ester to lectin resulted in a Cy5.5-labelled product that had an average D/P ratio of 2.90 ± 1.54 (n = 6). The average amount of dye lost in these full-scale reactions was 82% ± 6% (n = 6).

To demonstrate the effectiveness of the reaction between Cy5.5-NHS ester and LEA lectin as well as the effectiveness of dialysis as a means to remove excess dye, Cy5.5-lectin conjugation reactions were conducted in the absence or presence of 100-fold excess of lysine over lectin. Figure 3-1 shows the absorbance spectra of post-dialysis Cy5.5-lectin conjugate (Ai) as well as the post-dialysis product of Cy5.5-NHS ester conjugation reaction blocked with lysine (Aii). The absorbance spectra acquired from the lysine-blocked reaction showed no peak at 675 nm, indicating removal of the small Cy5.5-lysine conjugate through the dialysis membrane. The protein peak at 280 nm due to lectin is present in both post-dialysis reactions. The fluorescence spectra (Figure 3-1B) showed similar results with the Cy5.5-lectin conjugate reaction showing a strong peak at 694 nm compared to the almost complete lack of peak in the lysine-blocked reaction.

Figure 3-1: Cy5.5-lectin conjugation reaction in the presence and absence of free lysine. **Ai)** Absorbance spectra of Cy5.5-lectin conjugate measured as described in "Materials and Methods" section 2.2.1. **Aii)** Absorbance spectra of Cy5.5-NHS ester reacted with lectin in the presence of free lysine (in 100-fold excess). **B)** Fluorescence spectra, acquired as described in "Materials and Methods" section 2.2.3., of the products after dialysis with the black spectrum representing the reaction product between activated dye and LEA lectin (corresponds to the absorbance spectra Ai) and the red spectrum representing the reaction product blocked by excess lysine (corresponds to the absorbance spectra Aii). The small peak at around 650 nm is due to scatter of the laser light.

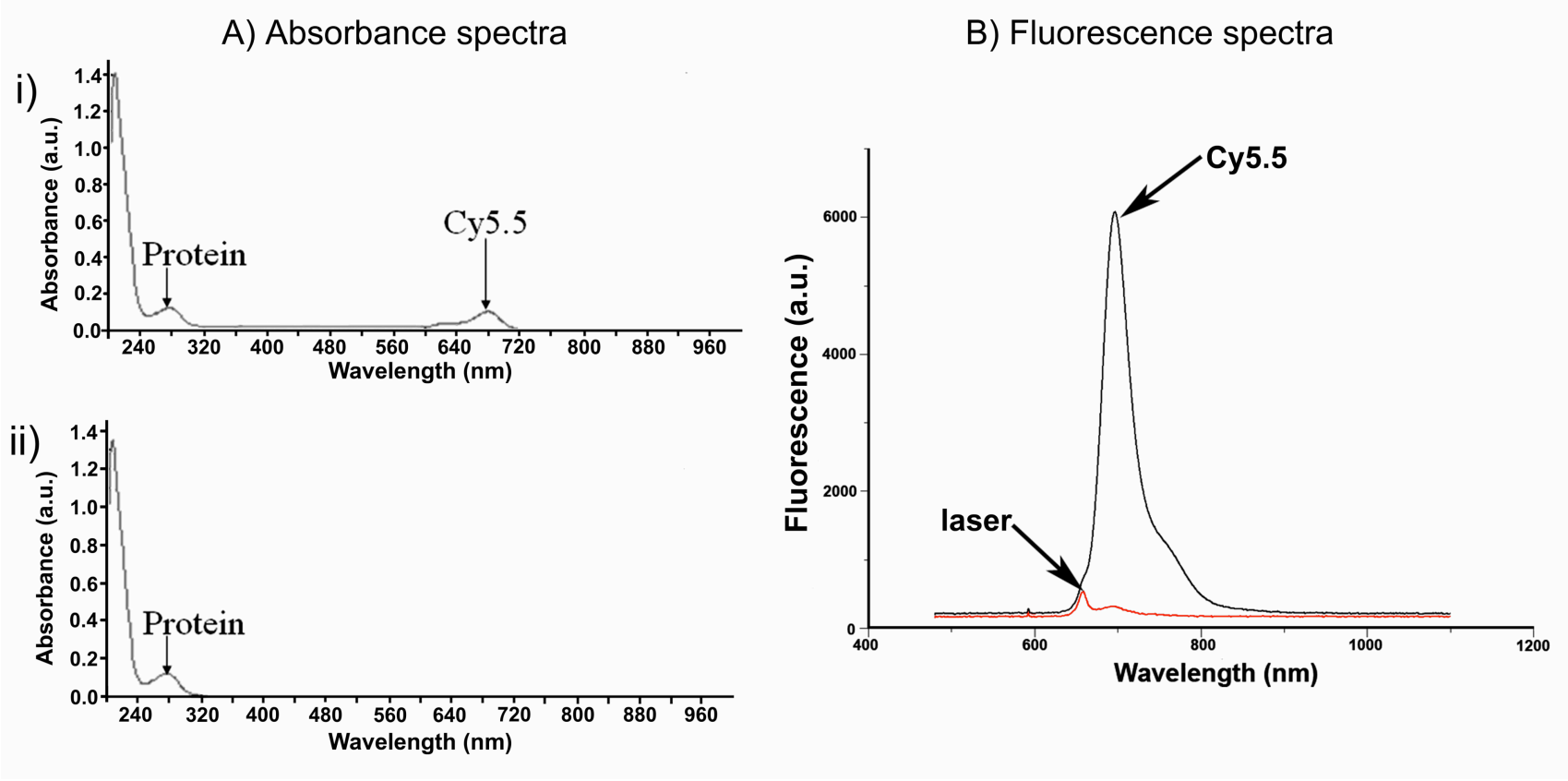

3.2. Binding of Cy5.5-lectin to endothelial cells in mouse hearts (Langendorff mode)

3.2.1. Visible-NIR point spectroscopy of Cy5.5-lectin perfused mouse hearts

Endothelial cells in intact live hearts, perfused in a Langendorff mode with KHB containing Cy5.5-lectin (3.3×10-8 mol/g wet tissue), were successfully labelled and uncompromised by the procedure. Cardiac functional data revealed that infusion of Cy5.5-lectin did not adversely affect the heart function, which is illustrated by the pressure rate product (PRP) (Jilkina *et al.* 2010). Following Cy5.5-lectin infusion, no change in the pressure rate product was observed: 6116.2 ± 3033.7 beats/min×mmHg versus 5013.0 ± 2603.1 at baseline (n=7) (Nguyen *et al.* 2012). The oxygenation of the heart, evaluated spectrophotometrically and seen in the oxygenation profile of a myocardial optical absorbance spectra (Figure 3-2) was adequate as demonstrated by the presence of two oxy-myoglobin peaks at 545 and 581 nm before, during and post-injection. Myocardial POD spectra acquired during Cy5.5-lectin conjugate infusion showed the steadily increasing POD peak at 680 nm due to accumulation of Cy5.5-lectin in the hearts (Figure 3-2B).

Figure 3-2: Pseudo-optical density (POD) spectra of a representative normal mouse heart perfused with Krebs-Henseleit buffer and Cy5.5-lectin as previously described. Spectra were taken prior to infusion as a baseline (thick line) and after the 20-min (dashed line) and 30-min (thin line) mark during the infusion period. For clarity of the presentation, spectra were offset to zero at 725nm. Oxy-myoglobin, Cy5.5 and water peaks are indicated with arrows.

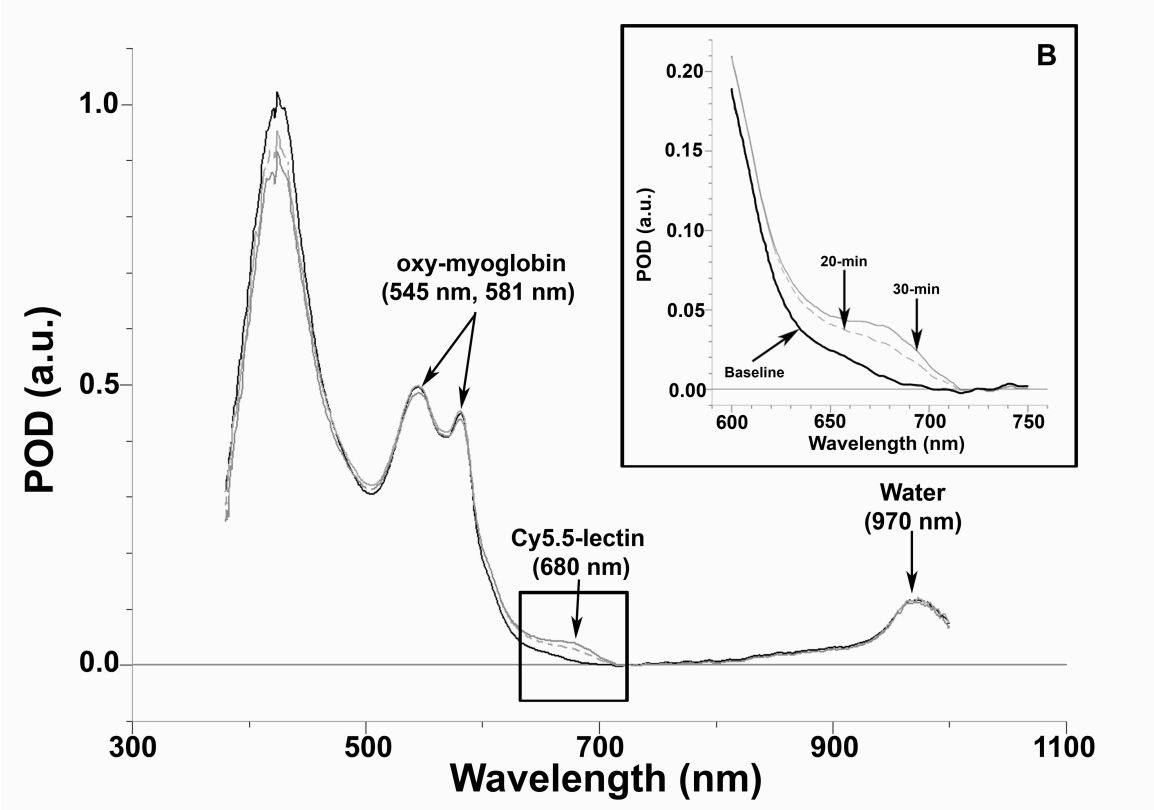

3.2.2. Histology of Cy5.5-lectin *ex vivo* perfused mouse hearts

A control experiment was carried out with Cy5.5-lysine as a substitute for Cy5.5-lectin in the Langendorff perfusion mode. Here, the deactivated dye did not bind to any structure and images of the heart post-infusion lacked fluorescence signal (Figure 3-3).

Figure 3-3: Control image of a 10 µm cross-section through a mouse heart perfused and infused with Cy5.5-lysine using the methods described in "Materials and Methods" section 2.3. No visible fluorescence is seen exposure times of 7773 ms.

Co-localization analysis of histological images captured from the hearts infused with both Cy5.5-lectin and FITC-lectin showed that the staining patterns from the two conjugates superimposed (Figure 3-4A). The same structures appeared to be stained by both conjugates pixel for pixel (Figure 3-4B). Due to the type of objective lens used, automatic sequential imaging at the two wavelengths was limited because chromatic aberration occurred. Manual correction post-imaging was performed so that the images more closely overlapped and quantitative analysis could be performed (Figure 3-4B). Specificity of Cy5.5-lectin binding to endothelial cells was demonstrated by replacing Cy5.5-lectin with Cy5.5-BSA. BSA did not bind any structures in the hearts and subsequently, images of the mouse heart post-infusion with Cy5.5-BSA showed a lack of fluorescence signal (Figure 3-4C). As a non-fluorescent control, endothelial cells were also identified via immunohistochemistry staining using ICAM2 antibodies. ICAM2 is a constitutively expressed protein in endothelial cells therefore ICAM2 antibodies have been used as a standard in immunohistochemistry to identify endothelial cells (Shimizu *et*

al. 1992; Gerwin *et al.* 1999). The brown stain indicated the location of the endothelial cells to be along the walls of larger vessels (Figure 3-4D). Smaller capillaries were also visible as small brown spots. Complete networks of capillaries that normally measure 5-10 μm in diameter were invisible due to the thickness of the sections (6 μm). Overall, staining pattern from cardiac tissue labelled with Cy5.5-lectin, FITC-lectin or ICAM2 antibodies were similar thus demonstrating specific binding of LEA lectin to the same structures, namely vascular endothelial cells. Hematoxylin and eosin stained sections were also acquired in order to determine the baseline anatomical structures (Figure3- 4E).

(Next page)►

Figure 3-4: Co-localization of Cy5.5-lectin labelling with FITC-lectin and ICAM2 labelling for endothelial cells. **A)** Images of a 10 μm cross-section through a mouse heart stained with both FITC-lectin ($\lambda_{excitation}$ at 494 nm, $\lambda_{emission}$ at 518 nm) and Cy5.5-lectin ($\lambda_{excitation}$ at 675 nm, $\lambda_{emission}$ at 694 nm) conjugates. Images are shown at 100x magnification and then focused on a large vessel at 400x magnification. All images were acquired in black and white and then pseudo-colored. FITC was excited at 470 nm and Cy5.5 was excited at 680 nm (See "Materials and Methods" section 2.7 for complete imaging parameters). Each image was captured in separate channels and then layered to show regions of overlapping signals, seen here as orange. The white dashed line indicated the ROI selected for the co-localization analysis. **B)** The graph shows a similar profile for both the FITC-lectin signal as well as the Cy5.5-lectin signal with intensities peaking at the similar pixels over a total distance of 1800 pixels. **C)** Control image obtained from a 10 μm cross-section through a mouse heart perfused and infused with Cy5.5-BSA under the conditions described in "A". Exposure time was 7773 ms. Note the lack of fluorescence signal. **D)** i) An example of stained vessels from a mouse heart section labelled with ICAM2 antibodies at 100x total magnification and ii) at 400x total magnification. A negative control section from the same heart was only stained with hematoxylin (viewed at 400x total magnification). **E)** Section of mouse heart tissue stained with H and E at 400x total magnification. The dark blue dots are nuclei and the magenta-red areas indicate cytoplasm and extracellular matrix.

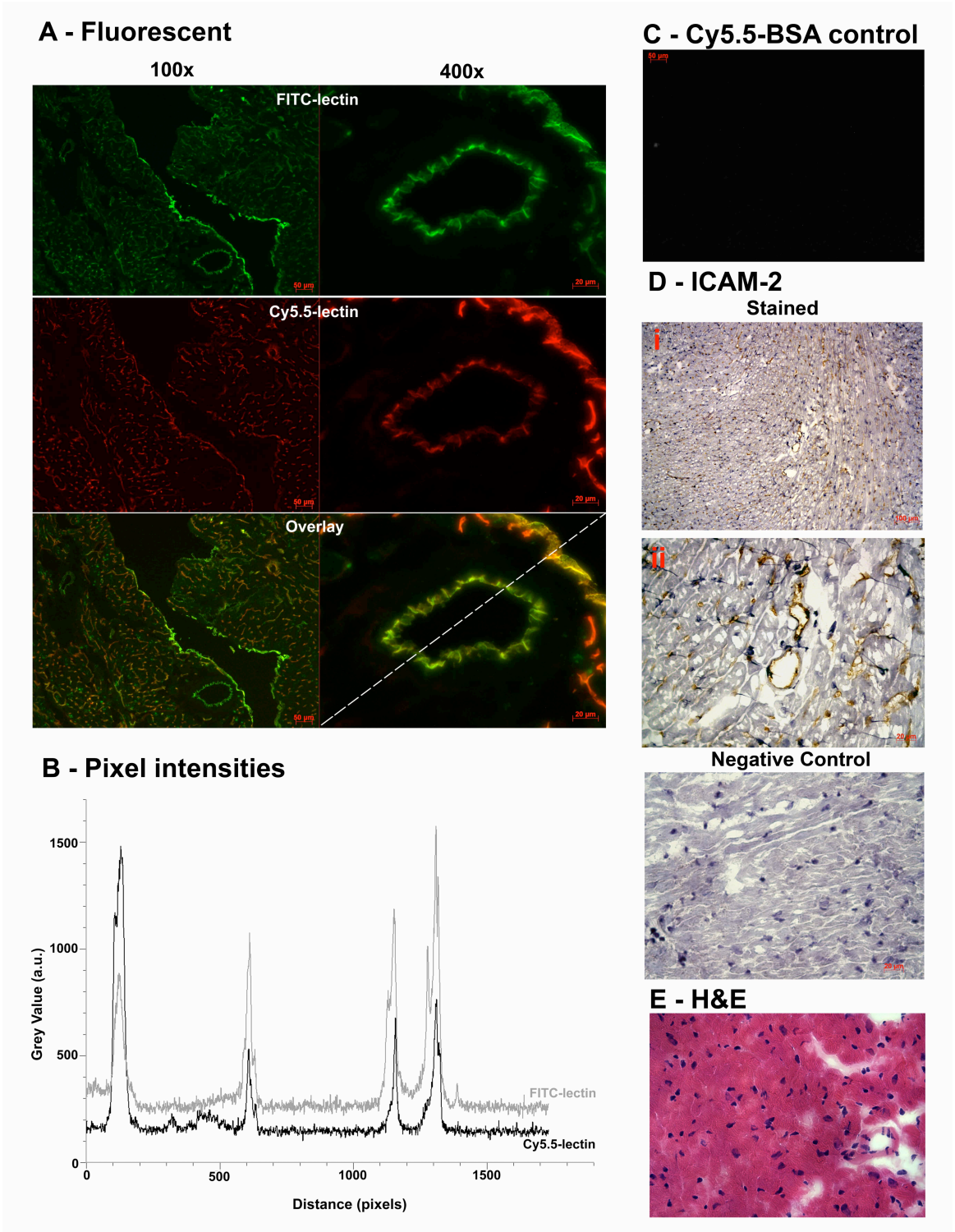
A - Fluorescent
100x
400x
FITC-lectin
Cy5.5-lectin
Overlay
B - Pixel intensities
Grey Value (a.u.)
Distance (pixels)
FITC-lectin
Cy5.5-lectin
C - Cy5.5-BSA control
D - ICAM-2
Stained
Negative Control
E - H&E

Background noise due mainly to autofluorescence at the 470 nm range was noticeably more prominent than that at 680 nm (Nguyen *et al.* 2012). To demonstrate the reduction of background fluorescence in the NIR spectral range, hearts infused with Cy5.5-lectin and FITC-lectin and prepared for fluorescence microscopy were excited at 470 nm, 590 nm and 680 nm (Figure 3-5). At 470 nm and 590 nm, autofluorescence for 10 μm sections was prominent and is mainly caused by NAD(P)H ($\lambda_{excitation}$: ~340 nm; $\lambda_{emission}$: 450 nm) and riboflavins ($\lambda_{excitation}$: ~450 nm; $\lambda_{emission}$: 530 nm). Although the fluorescence signal from FITC-lectin is very strong and structures can be clearly identified at 10 μm, autoflourescence can still be seen and would become prominent in thicker sections therefore limiting the usage of FITC-lectin to only thin sections. At 590 nm, autofluorescence again would impede imaging of thicker sections. At 680 nm, autofluorescence in comparison to the signal from Cy5.5-lectin was minimal thus allowing for experimentation with thicker tissue sections.

Increasing section thickness provided depth to the images at 680 nm (Figure 3-6). In thin 10 μm sections, capillaries appeared as spots and speckles in the image while at 35 μm these spots appeared as a visible network (Nguyen *et al.* 2012). Increasing the section thickness to 70 μm resulted in images where the capillary network was still clearly visible. At 100 μm however, the multiple stacked layers of capillary networks made it difficult to identify and trace individual capillaries beyond those directly at the surface of the tissue block. Comparatively, in the thicker sections imaged at 470 nm, stronger background noise significantly decreased the visibility of individual capillaries. Exposure times for the images captured at 680 nm also decreased from 7773 ms to 2525 ms as section thicknesses increased.

Figure 3-5: Reduction of autofluorescence within the NIR spectral range. At 590 nm excitation, images of cross-sections through mouse hearts were captured using the Colibri LED-Module 590 nm excitation laser with filter set 62 HE B/G/HR R preset for HcRed by Zeiss. At 470 nm and 680 nm, images were captured as described in section 2.6. The camera exposure time for the autofluorescence only image at 470 nm was 1086.6 ms. Comparatively, the FITC-lectin image was exposed for 200 ms and the Cy5.5-lectin image at both 590 nm and 680 nm was exposed for 7773 ms. All images are at 100x magnification. Note the difference in background signal even though the pattern of staining remains the same.

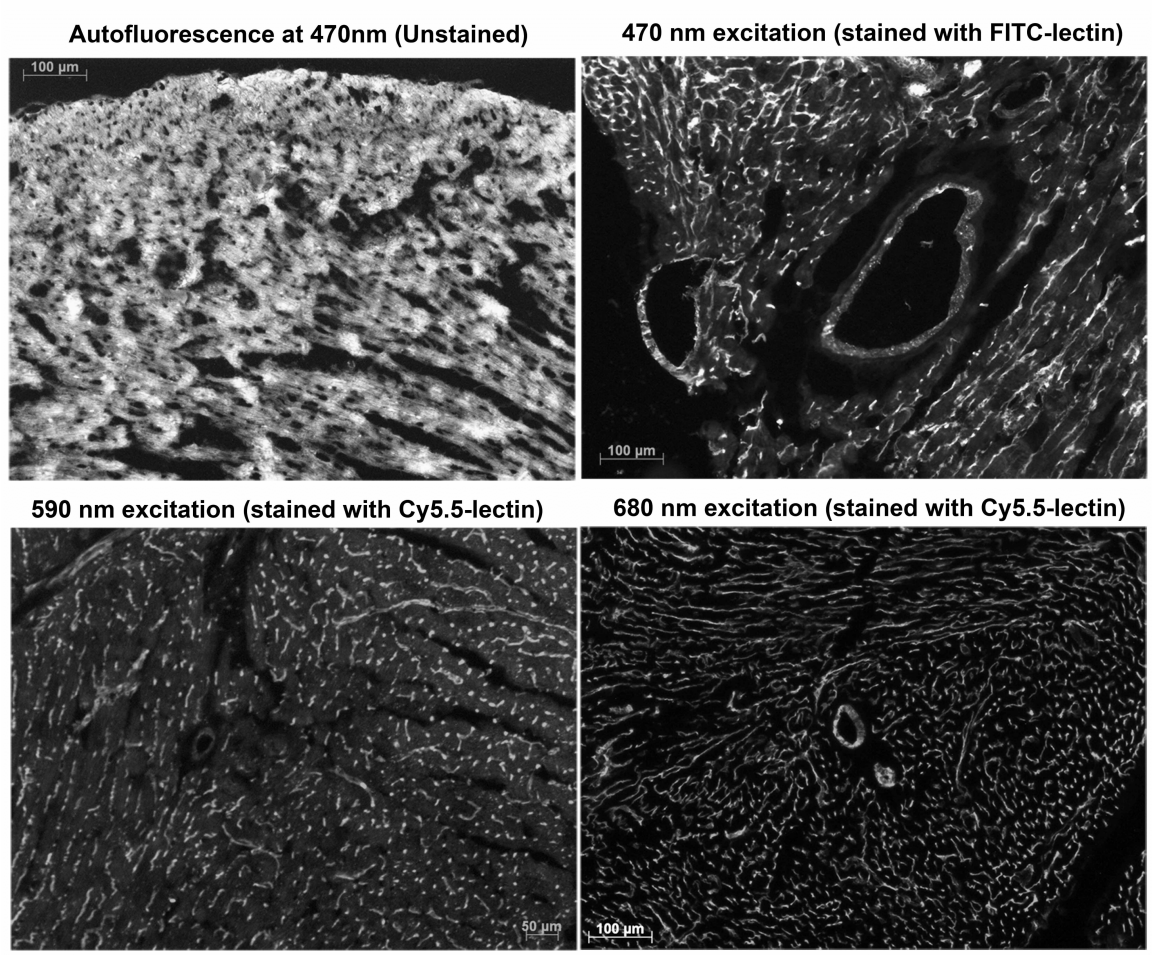

Figure 3-6: Cross-sections through a mouse heart infused with Cy5.5-lectin conjugate at 100x magnification and excited at 680 nm. Section thicknesses were set at 10 (a), 35 (b), 70 (c) and 100 µm (d). Exposure times also decreased accordingly from 7773 ms, to 5922 ms, to 2712 ms, to 2525 ms. Note the larger vessels that can be seen in the thicker sections.

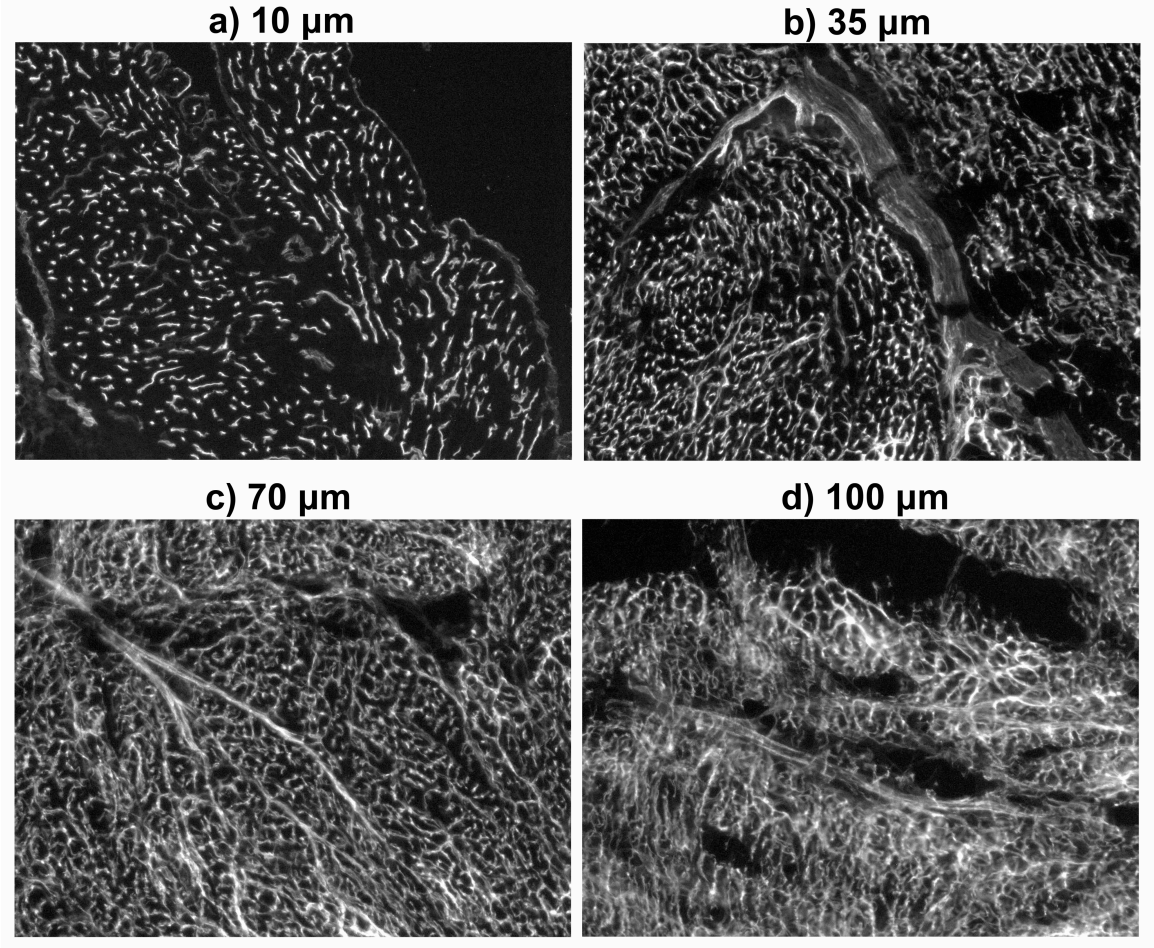

3.3. Real-time Fluorescence Imaging

Imaging of Cy5.5-lectin accumulation in intact hearts was successfully performed during infusion of Cy5.5-lectin conjugates into mouse hearts perfused in a Langendorff mode (Figures 3-7 and 3-8). To eliminate movement artefacts, the hearts were arrested with high-potassium KHB cardioplegic solution. High potassium cardioplegic arrest

preserved cardiac energetics and structure (Jilkina *et al.* 2003). Control hearts showed fairly uniformed staining with a linear increase in fluorescence during the infusion period of 30 minutes. Videos of both control and ligated hearts can be viewed under the supporting information section at <http://dx.doi.org/10.1002/jbio.201100119> (Nguyen *et al.* 2012). Average peak intensity of fluorescence was 150 a.u. (n=8). A kinetic curve was generated by comparing the pixel intensity from the same ROIs within approximately 140 images (1 image per 30 s) that were captured during the infusion (Figure 3-8). A linear fit of the slopes during the infusion period resulted in R^2 or correlation values close to 1 (0.992 ± 0.004, $n = 4$). Images captured during the washout period indicated that no significant loss of conjugate occurred during the 20 minutes because there was little or no change in fluorescence intensity (slope of linear fit was near 0) (Figure 3-8). This demonstrates that the binding between endothelial cells and Cy5.5-lectin is stable. To compare staining of endothelium in the perfused versus non-perfused areas of mouse hearts, surface images of normal and LAD-ligated hearts were acquired. LAD ligation was confirmed by optical point spectroscopy. Post-ligation, the area normally perfused by the LAD showed a POD spectrum lacking the two oxy-myoglobin peaks at 545 and 581 nm (as previously shown in Figure 3-2). Instead, a deoxy-myoglobin peak at 552 nm was seen (Figure 3-9). In captured images, these areas showed very little increase in fluorescence intensity from the baseline readings. Average peak intensity of fluorescence was 35 a.u. (n=6).

Figure 3-7: Images captured from real-time imaging of infusion of Cy5.5-lectin into arrested mouse hearts under normal Langendorff perfusion (A) and LAD-ligation conditions (B) as described in "Materials and Method" section 2.3. Under normal conditions, the fluorescence image shows a fairly uniform signal. In the ligated heart, a dark region below the ligation point area shows little fluorescence. Non-cardiac objects are also seen such as the cannula and water-filled balloon portion of the function probe (small black arrows). Post-infusion 40 μm cross-sections images were also captured using a microscope (C and D, normal and LAD-ligated respectively). Images are a mosaic of images captured sequentially at 100x magnification and then stitched together. The dashed line on the normal heart under white light indicates the approximate location from which the short-axis tissue section was taken and imaged. Boxes shown in the post-infusion image for the LAD ligated heart indicates the regions of interest (ROIs) used to calculate the kinetic curves in Figure 3-8. ROIs are numbered 1-4 starting at the top left and moving counter-clockwise.

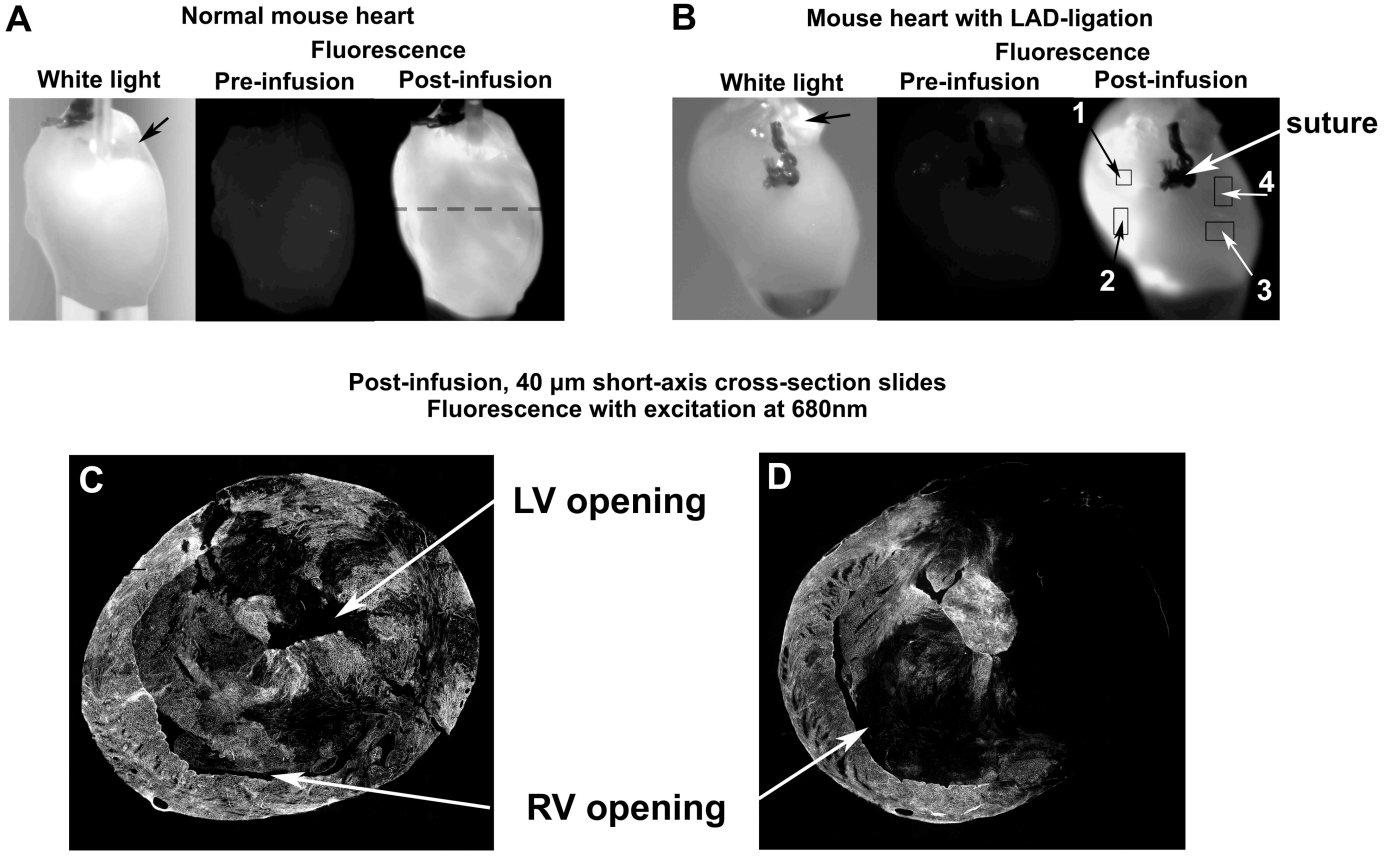

Figure 3-8: A representative kinetics graph showing Cy5.5-lectin binding in a LAD-ligated mouse heart based on data shown in Figure 3-6. ROI 1 and ROI 2 are from the well-perfused region of the heart whereas ROI 3 and ROI 4 are from the region of poor perfusion due to the ligation. The fluorescence intensity is a mean of pixel intensities collected from the ROI selected in the set of images captured real-time. A negligible amount of Cy5.5-lectin is lost in the washout since fluorescence intensity only slightly drops (slope≈0) after the end of the infusion period.

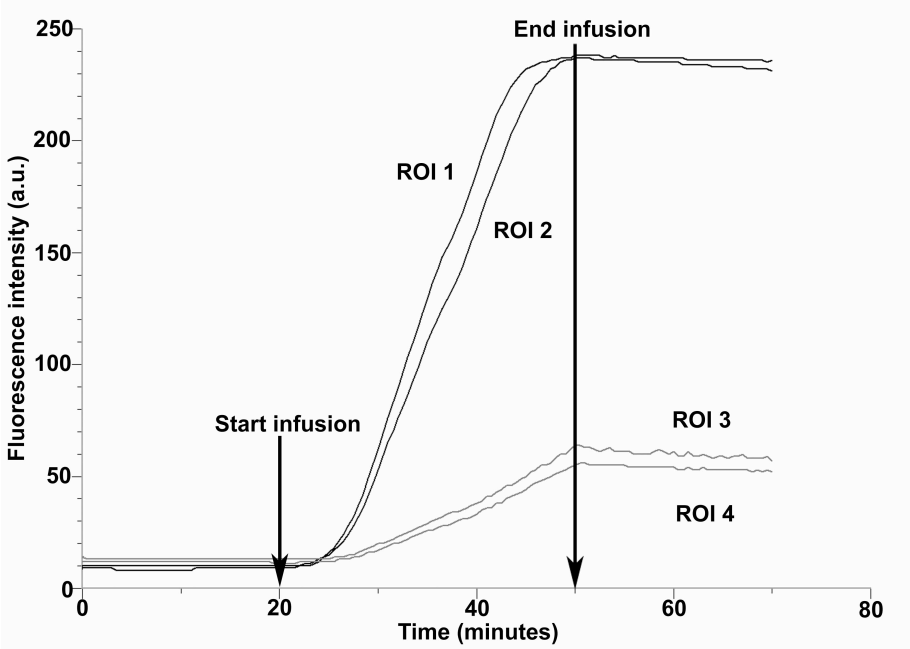

Figure 3-9: Pseudo-optical density (POD) spectra of a representative of an area below the LAD ligation point of a post-ligated mouse heart perfused with high potassium Krebs-Henseleit buffer. For clarity of the presentation, spectra were offset to zero at 706 nm. Deoxy-myoglobin and water peaks are indicated with arrows. The inset figure B depicts the region of interest from which the data on the graph was collected.

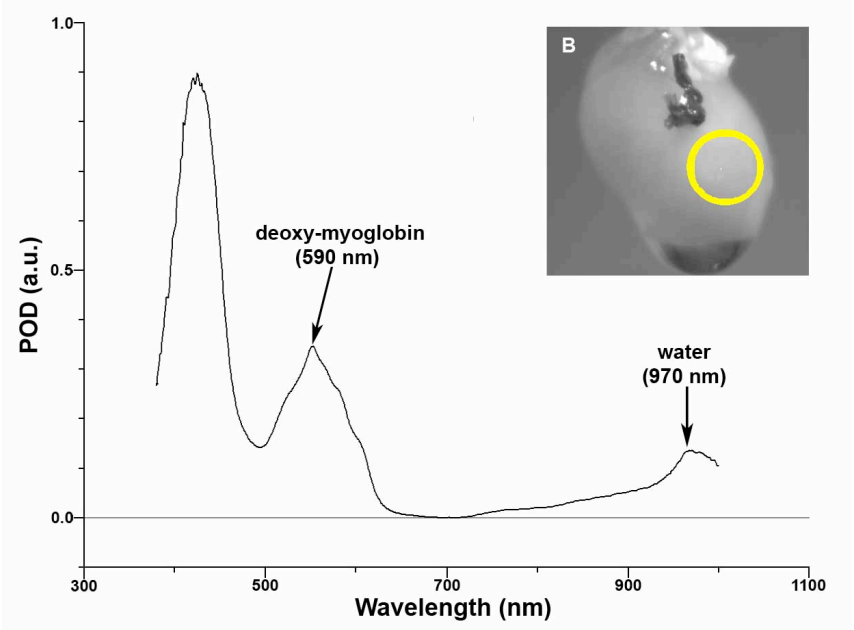

3.4. Histology and Imaging of *in vivo* Staining

Images collected from mouse hearts stained using *in vivo* methods showed staining patterns similar to those found when using the *ex vivo* injection of the conjugate (Figure 3-10). Exposure times for images excited at 670 nm were approximately 14 s for 10 µm heart slices, which was higher than the average of 7 s for 10 µm sections from hearts stained using *ex vivo* methods. Weaker signal *in vivo* is attributed to decreased Cy5.5-lectin per gram of tissue (1.8×10^{-10} moles of Cy5.5-lectin/g of tissue) as compared to the 3.3×10^{-8} mol/g achieved with the Langendorff mode.

Figure 3-10: A 30 µm cross-section through mouse cardiac tissue infused with Cy5.5-lectin using the *in vivo* tail-vein injection as described in "Materials and Methods" section 2.5. The exposure time was 13 seconds. Note the similar staining pattern between this image and the images from *ex vivo* staining (Figure 3-6). The 30 µm cross-sections through liver and kidney tissue was labeled and prepared in a similar fashion to the heart. The image of the spleen was acquired from a 50 µm section. The exposure time for the liver, kidney, and spleen images were 24 seconds. All images were acquired at 100x total magnification. BV: blood vessel, MZS: marginal zone sinuses, WP: white pulp, CV: central vein, S: sinusoids, RC: renal corpuscles.

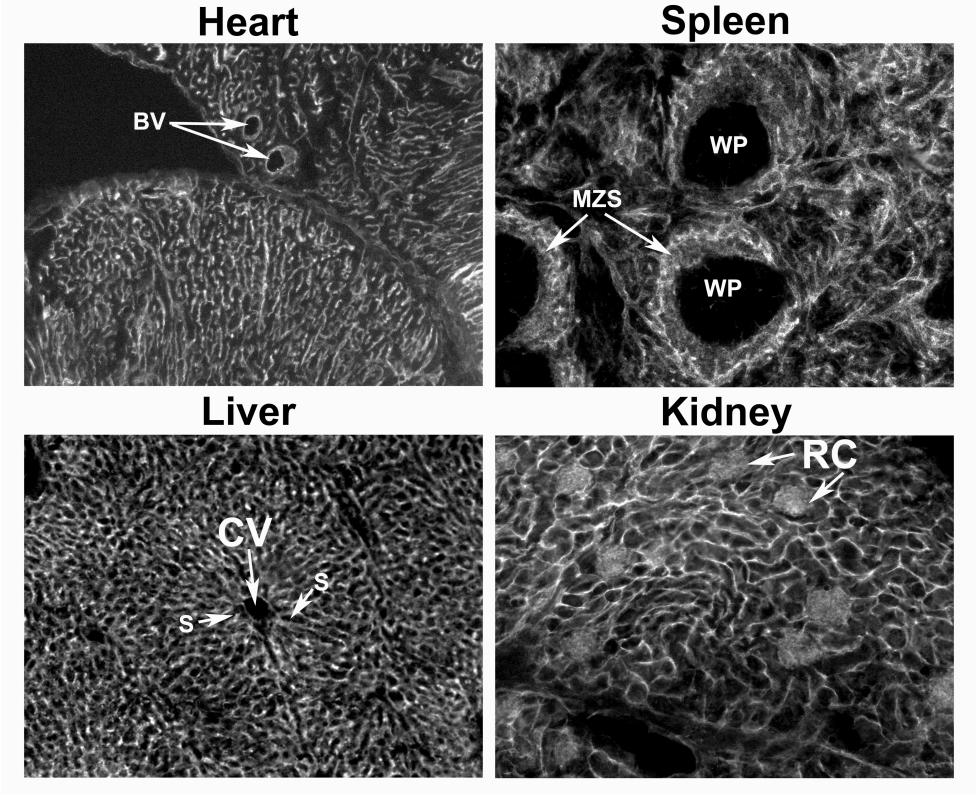

Chapter 4 – Discussion

4.1. Specificity of Cy5.5-lectin binding

Binding of Cy5.5-lectin is directed by the *Lycopersicon esculentum* (LEA) lectin component of the conjugate (MW ~ 71 kDa) as shown by the lack of binding in the experiments with Cy5.5-lysine (Figure 3-3) and Cy5.5-BSA (Figure 3-4C). BSA is a serum protein (MW ~ 68 kDa) that does not specifically bind to endothelial cells and Cy5.5-BSA has been shown to remain briefly in circulation before being cleared by metabolic organs (Hama *et al.* 2007). Cy5.5-lysine, which represents the dye in a non-reactive but still fluorescent state, perhaps is small enough to enter into the interstitial spaces between cells and leave the vascular system. However due to lack of binding the dye is washed out and no non-specific binding is seen. This shows that binding of Cy5.5-lectin is not directed by the dye groups. With Cy5.5-lectin injected into circulation, binding is limited to vascular endothelial cells. Qualitatively and quantitatively, staining patterns seen with Cy5.5-lectin match the staining pattern of a proven probe for endothelial cells such as FITC-lectin (Figure 3-4A and 3-4B). Other cells such as red blood cells were not labelled with Cy5.5-lectin since no signal was seen in blood samples collected from tail-vein experiments post-injection. Also, in LAD-ligation experiments, binding of Cy5.5-lectin conjugate was limited to areas of the heart that were perfused. This was seen in the lack of fluorescence signal from the area below the ligation point in LAD ligated hearts and is best demonstrated by the histological slides in Figure 3-7.

4.2. Synthesis

The D/P ratio achieved for the reaction, 2.90 ± 1.54 (n = 6), was within the 2-6 moles of dye per mole of LEA lectin range that commercial products such as FITC-lectin tend to have (Nguyen *et al.* 2012). By choosing to use the monofunctional Cy5.5-NHS ester instead of the bisfunctional form of the dye, oligomer formation was prevented which guaranteed a clean end-product post-dialysis and decreased chances of self-quenching due to dye-dye interactions (Ogawa *et al.* 2009). Although dialysis is a simple and basic purification method, it was proven to be sufficient for this purpose through experimentations with lysine-blocked reactions. The current scale of the synthesis is suitable for mouse experiments as one reaction produces enough product for 10-15 experiments (*in vivo* and/or *ex vivo*). For future purposes, even larger scale reactions are possible.

4.3. Cy5.5-lectin conjugate as a deposition flow tracer

The minimal amount of background interference within the NIR-range allowed for imaging of thicker sections of upward to 100 μm and even imaging of the whole heart as shown (Figure 3-7), which is impossible with non-NIR dye-conjugates. Non-NIR dye-conjugates are greatly affected by background fluorescence as tissue sections increase in thickness. Images captured from real-time *ex vivo* cardiac imaging sessions were limited by the camera resolution, which was approximately 76.8 pixels/mm. Even so, the images can still clearly indicate differences in perfusion (Nguyen *et al.* 2012). In the control heart, normal microvascular perfusion heterogeneity that is known to exist in healthy hearts was observed (Matsumoto and Kajiya 2001). The heterogeneity displayed by normal heart perfusion is a reflection of local oxygen consumption, which is based on the

heart rate, contractility and wall tension of the vessels involved (Bourdarias 1995). Other studies have shown that these areas of lower oxygen consumption are the result of the shunting of blood through short arteriole-venous pathways, which bypasses local capillary beds (Pries and Secomb 2009). Since distribution and binding of Cy5.5-lectin is based on flow, areas with lower flow will produce a lower signal, resulting in images that show heterogeneity in perfusion. In order to see this distribution, images must be captured before the tissue saturation point and at the dilutions and amount used in both *ex vivo* and *in vivo* experiments; this saturation point was not reached and therefore did not affect the imaging results. Further evidence showed that Cy5.5-lectin is flow dependent. In the LAD-ligation models, areas downstream of the ligation point had restricted perfusion which was reflected by the distinctly lower fluorescence signal (Nguyen *et al.* 2012). The fluorescence captured in the poorly perfused area of the heart post-ligation is largely due to light scatter and tissue transparency in the NIR range. Indeed, NIR light can penetrate cardiac tissue for up to 4 mm, which is almost the full thickness of the mouse heart (Nighswander-Rempel *et al.* 2005).

From the evidence gathered, Cy5.5-lectin can be characterized as a deposition flow tracer as opposed to a first-pass flow tracer. First-pass flow tracers (e.g., indocyanine green, ICG) transiently pass through the organ (e.g., heart) and the tracer's distribution and/or clearance kinetics is determined during this time and used to evaluate the perfusion (Kupriyanov *et al.* 2004). For this type of tracer, clearance kinetics is very important. First-pass flow tracers are also commonly used in MRI (e.g. gadolinium) (Bartholoma *et al.* 2010). In contrast, a deposition flow tracer (e.g., microspheres) is retained by the tissue; it can be later detected in the tissue and quantitated (Prinzen and

Bassingthwaighte 2000). Distribution and/or clearance kinetics is not a factor for deposition flow tracers. Deposition flow tracers, however, must satisfy a different set of criteria that has been described in detail by Prizen and Bassigthwaighte in regards to microspheres, which are the most widely used type of deposition flow tracer in animal experiments (Prinzen and Bassingthwaighte 2000). The first criterion is that in systemic studies, the tracer must be able to properly mix in the central circulatory system. In *in vivo* experiments, both the left and right kidneys appeared to be equally labelled by Cy5.5-lectin therefore Cy5.5-lectin satisfies this criterion. Deposition flow tracers should be of an appropriate size where the tracer will not block blood flow through the vessel (Prinzen and Bassingthwaighte 2000). The overall size of the Cy5.5-lectin molecule is approximately 75 kDa, which will not likely hinder blood flow through capillaries since average capillary diameter in mice is approximately 8 μm (Thurston *et al.* 1999). This is one of the advantages of using Cy5.5-lectin over microsphere for the purpose of visualizing microvascular systems. While other tracers, such as radioactive desmethylimipramine, may not block vessels, they cannot be used for real-time *in vivo* imaging (Little and Bassingthwaighte 1983). Binding of a deposition flow tracer should be stable (Prinzen and Bassingthwaighte 2000). From Figure 3-8, the binding of Cy5.5-lectin was very stable (over 30 min *ex vivo*); therefore, redistribution or diffusion into the non-perfused areas was unlikely thus allowing Cy5.5-lectin conjugate to be used as a deposition microperfusion tracer. For fluorescent deposition tracers, fluorescence imaging has been previously shown to be capable of evaluating heart perfusion (Gussakovsky *et al.* 2011). Deposition flow tracers should also be detectable. Results from both *in vivo* and *ex vivo* experiments show that the fluorescence signal from Cy5.5-

lectin is detectable and clearly reflects perfused areas of the heart. The only criterion that does not apply to Cy5.5-lectin is extractability. This is important for microspheres because in order to quantify the amount of spheres trapped in the tissue, the organ (i.e. heart) has to be extracted and processed, an option often not available in clinical settings. Cy5.5-lectin binding can be quantified by measuring absorbance or fluorescence signal in optical spectroscopy or imaging experiments (Gussakovsky *et al.* 2011). Using the criteria illustrated Prizen and Bassigthwaighte, Cy5.5-lectin can be classified as a classic deposition flow tracer.

Potential applications for Cy5.5-lectin as a flow tracer are numerous. Since the binding of Cy5.5-lectin is reflective of the local blood flow through different areas of the heart, the probe could be used to visualize perfusion when it is manipulated thorough changes in workload caused by physical stressors such as exercise or the use of chemicals such as adrenergic β-blockers. Cy5.5-lectin could be also used to visualize blood in situations where the coronary reserve is impaired. Also, vasodilatation and constriction are controlled at the cellular level by endothelial cells and in certain disease cases such as diabetes and hypercholesterolemia, there is an imbalance between dilatation and constriction which results in poor perfusion in the areas affected (Inoguchi *et al.* 2000; Matsuura *et al.* 2008). Cy5.5-lectin could be used to monitor perfusion changes in these abnormal situations at the microvascular level. These applications are not limited to the heart. Perfusion heterogeneity has been described in other tissues including mesenteric and skeletal muscle (Kuschinsky and Paulson 1992; Pries and Secomb 2009).

Although there was a difference in signal intensity between *in vivo* and *ex vivo* infusion methods, mostly due to a difference in dye content per gram of tissue, the overall

quality of the signal produced is sufficient for the detection methods used. Once the tissue is processed into slides, the fluorescent signal remains stable for several days with proper storage. However, decay of the signal could be accelerated by the imaging process, which sometimes required repeated excitation of the dye thus causing photobleaching. Variations in signal intensity could be due to various effects such as quenching. Based on absorbance spectra there is some minimal self-quenching that occurs for Cy5.5-lectin (determined by the increased shoulder peak at approximately 630 nm post-conjugation in Figure 3-1). The appearance of this shoulder peak is caused by the H-type aggregate that is of higher energy (An *et al.* 2002). Although the fluorescence intensity is not optimal due to the self-quenching, it is still strong enough for the *ex vivo* and *in vivo* imaging used. It is possible that *in vivo* protease activity could cause the cleavage of the LEA lectin molecule and recover the fluorescence lost due to self-quenching however; binding of the probe would then be compromised.

4.4. Comparison to other cardiac imaging modalities

NIR imaging using Cy5.5-lectin is capable of providing both physiological and structural data. Physiological data provided by NIR imaging using Cy5.5-lectin, although not quantitative, is reflective of local oxygen consumption, blood flow, and metabolism, which are all interconnected (Pries and Secomb 2009). The structural data provided by NIR imaging using Cy5.5-lectin is a map of the microvascular organization because the target of Cy5.5-lectin, endothelial cells, lines every blood vessel. Due to the small size of Cy5.5-lectin, even the smallest capillaries (~8 μm) are labelled. Comparatively, some current cardiac imaging modalities, such as NIR absorbance imaging, are only capable of functional imaging, while others such as echocardiography are better at structural

imaging but lacks accuracy in terms of function measurements (Gardner *et al.* 2009). The spatial resolution achieved in the real-time *ex vivo* set-up (76.8 pixels/mm), although currently captured only in 2 dimensions, is comparable to the standard spatial resolutions achieved by real-time 3 dimensional echocardiography (~ $1mm^3$) as well as MRI (~ $1mm^3$). Future development in camera technology and camera design will likely allow for 3 dimensional NIR imaging at which point, Cy5.5-lectin will still be a viable probe because the signal it produces is not limited to 2 dimensions. One of the benefits of using NIR fluorescence imaging is that the image acquisition time is very short and very little post-imaging processing is required. For *ex vivo* real-time imaging the exposure time per image was only 2500 ms, which is very short compared to single image acquisition times for MRI, CT, and PET scans (a few minutes) that rely heavily on computer reconstruction (Rudin and Weissleder 2003). Cy5.5-lectin used as a probe in NIR imaging has the added benefit of being non-radioactive, which means that radiation dose during imaging sessions are comparable to echocardiography, MRI scans and natural background radiation (Fazel *et al.* 2009). Studies have shown that exposure to high levels of radiation from CT scans may lead to the development of cancer (Sodickson *et al.* 2009). For practical uses, NIR-imaging with Cy5.5-lectin is comparable to echocardiography because the physical imaging apparatus is very portable and Cy5.5-lectin can be made and stored for long periods of time (months) prior to usage, unlike the radio-opaque contrast agents used in CT and PET scans which must be used immediately. However, imaging with Cy5.5-lectin does have a few limitations. Current NIR imaging cannot occur through thick layers of tissue including bones and fat therefore cardiac imaging

must occur in open chest settings or via catheters as described by Funovics and Zhu (Funovics *et al.* 2003; Zhu *et al.* 2005).

4.4.1. Multichannel imaging

One advantage NIR fluorescence imaging has over other *in vivo* imaging modalities is the ability to use multiple imaging channels. At the microscopic level, multichannel imaging has been used to visualize multiple targets and probes simultaneously (i.e. Cy5.5-lectin used in conjunction with FITC-lectin). At the macroscopic level, it is possible to use different NIR-probes, which have excitation and emission wavelengths that are separable, to achieve multichannel imaging. Cy5.5-lectin, which is excited at 675 nm and has a maximum emission wavelength at 694 nm, could be used in conjunction with a IRDye800CW conjugate, which has an excitation (783 nm) and emission (801 nm) wavelength much farther red than Cy5.5-lectin (Table 1-2). Recently, multichannel NIR imaging with five different NIR probes (Cy5, Alexa660, Alexa680, Alexa700 and Alexa750) attached to dendrimers has been used to visualize lymph nodes in mice (Kobayashi *et al.* 2007).

4.4.2. Multimodal imaging

Most current cardiac imaging modalities cannot be easily integrated with each other however, NIR fluorescence imaging with Cy5.5-lectin can be combined with the previously described cardiac imaging modalities. In a recent study, NIR fluorescence imaging was successfully integrated with CT scans through Cy5.5-labelled antibodies used in conjunction with an iodine-based contrast agent that both probed for mammary carcinomas (Dullin *et al.* 2009).

4.5. Future applications based on *in vivo* imaging

Currently, *in vivo* imaging is limited to open chest situations where imaging must be gated to respiration and heart beat in order to avoid motion artifacts. Future applications of Cy5.5-lectin for *in vivo* cardiac imaging could be greatly expanded by use of imaging catheters, a technology that is currently being developed and would eliminate the invasiveness caused by open-chest imaging (Zhu *et al.* 2005).

Use of the conjugate is not limited to the heart as we observed staining of the microvascular endothelium in the liver, kidney, and spleen during *in vivo* experiments (Figure 3-10). The non-toxic nature of the Cy5.5-lectin conjugate allows it to have potential uses in *in vivo* imaging that could also expand beyond the mouse to other animal models. Other LEA lectin conjugates have been used in rat, guinea pig and bovine studies (Mazzetti *et al.* 2009; Porter *et al.* 1990; Schnitzer *et al.* 1994). Larger animals however, will require more Cy5.5-lectin but larger scale synthesis of Cy5.5-lectin is feasible.

4.6. Conclusion

Cy5.5-lectin conjugate can be easily synthesized and is comparable to other lectin conjugates. The advantages of this conjugate are: 1) it fluoresces in the NIR range, which eliminates background interference from endogenous chromophores 2) non-specific binding is limited 3) binding is mostly limited to endothelial cells and is stable for at least 30 minutes 4) Cy5.5-lectin can be used both *in vivo* and *ex vivo* 5) can be used as a deposition flow tracer 6) Cy5.5-lectin can be used systemically as well as in other specific organs and 7) real-time imaging of intact live hearts can be performed. One of the disadvantages of using Cy5.5-lectin is the lack of easily available detection tools and

current imaging techniques are limited to open-chest models or vascular catheters. Many of the well known dye-conjugates have detection tools that are optimized for that specific wavelength. Many of the detection tools used for Cy5.5-lectin had to be customized. NIR imaging is still a fairly new imaging modality therefore as the technique becomes more popular, detection tools should become more readily available. Presently, Cy5.5-lectin has been proven to be a unique endothelial imaging tool in histological and functional cardiac studies.

Appendix 1 – Supplemental Images

Supplemental images extracted from real-time videos of Cy5.5-lectin infusion into arrested mouse hearts.

Normal mouse heart

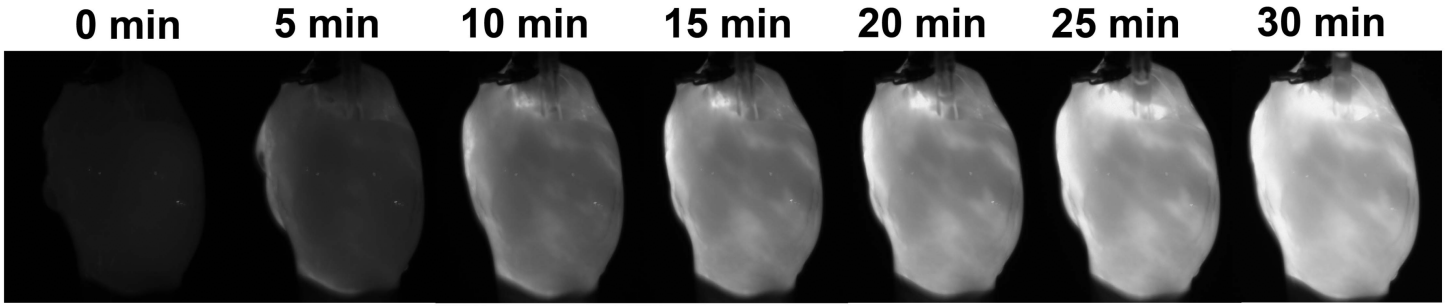

Mouse heart with LAD-ligation

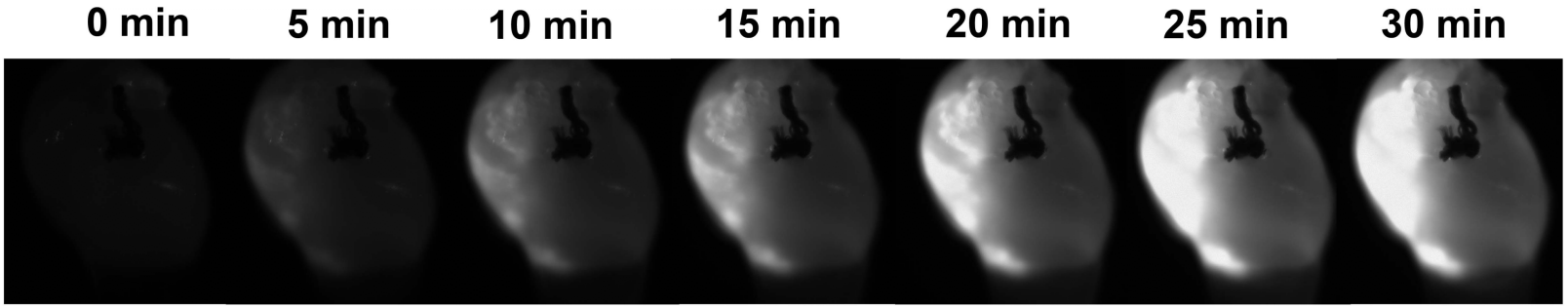

Appendix 2 - Abstracts

Proceedings of XX World Congress of the International Society for Heart Research, p. 237, Kyoto, Japan, May 2010:

Near-infrared (NIR) molecular imaging of myocardial microvascular endothelium using lectin-Cy5.5 conjugate

Olga Jilkina[1,2], Cecilia Nguyen[3], Saro Bascaramurty[1], Bozena Kuzio[1], Valery Kupriyanov[1,2]

Institute for Biodiagnostics, NRC Canada[1], University of Manitoba[2], University of Winnipeg[3], Winnipeg Canada

Background: Existing endothelial cell staining techniques are restricted to the visible range chromophores. However, extension of the spectral range to the NIR region would allow not only increasing the depth of tissue penetration, but also performing dynamic studies by sequentially using several different fluorescent labels in the same heart. It is known that *Lycopersicon esculentum* (tomato) lectin specifically binds to the endothelial cells. A fluorescent anionic dye, Cy5.5, has NIR excitation and emission maxima: λexc=675 nm and λem=694 nm, respectively. Therefore, Cy5.5-lectin conjugate should bind to endothelial cells and its' fluorescence will not interfere with the endogenous fluorescent chromophores (cytochromes and flavoproteins). **Results:** Bis-Succynylimidil ester Cy5.5-(SE)2, was covalently linked to the tomato lectin. C56BL6 mouse hearts were perfused in a retrograde mode with Cy5.5-lectin in the presence or absence of a commercially available visible range FITC-lectin conjugate (λexc=494 nm, λem=518 nm). Fluorescent microscopy confirmed co-localization of Cy5.5- and FITC-lectin to the lining of the microvessels and capillaries (40× magnification). Immunohistochemistry using ICAM-2 antibody was performed as a control to identify microvascular endothelium. **Conclusions:** lectin-Cy5.5 conjugate can be used to visualize myocardial microvasculature with the spatial resolution of 5 μm and assess microvessel density at the depth of several mm, in the absence of the background fluorescence.

As submitted to the Canadian Student Health Research Forum 2012:

Near-infrared Fluorescence Imaging of Mouse Myocardial Microvascular Endothelium Using Cy5.5-Lectin Conjugate

Cecilia Nguyen[1], Saro Bascaramurty[2], Bozena Kuzio[2], Lori Gregorash[2], Valery Kupriyanov[3], and Olga Jilkina[2]

[1]Department of Oral Biology, University of Manitoba, Winnipeg MB, [2]Institute for Biodiagnostics, National Research Council of Canada, [3]Retired, Former affiliation: Institute for Biodiagnostics, National Research Council of Canada.

In cardiovascular research, near-infrared (NIR) fluorescence imaging has emerged as a new imaging modality. There are many advantages to imaging within the NIR spectral range (700 - 900 nm) which include minimal interference from endogenous chromophores and low tissue absorption by haemoglobin and myoglobin. These characteristics are desirable in the imaging of endothelial cells and the endothelial network within intact organs. Endothelial cells are of interest because many cardiovascular diseases, such as diabetes mellitus, hypertension and atherosclerosis are associated with endothelial dysfunction. Development of a tool that can visualize the normal and disease conditions within the cardiovascular system would improve the ability to understand, monitor and diagnose various cardiovascular conditions. In this study, endothelial cell-specific fluorescent conjugate using tomato lectin and Cy5.5-NHS ester was synthesized. The binding of the conjugate to endothelial cells in mouse models using both *in vivo* and *ex vivo* infusion methods was evaluated. With mouse *in vivo* tail-vein injections, other organs such as the liver, spleen and kidney were also stained. ICAM-2 and FITC-lectin staining patterns were compared to Cy5.5-lectin labelling patterns and showed co-localization. This was very promising as there is currently no readily available optical probe capable of imaging endothelial cells in the NIR range under *in vivo* conditions. Finally, it was shown that Cy5.5-lectin conjugate, used as a deposition flow tracer, could aid in real-time imaging of normal and abnormal heart perfusion. The promising results of this research can be applied to many different scenarios involving simulated cardiovascular disease conditions and perhaps used in different animal models.

Appendix 3 - Recipes

0.1M Sodium carbonate-bicarbonate buffer, pH 9.3

1) Make 250 ml 0.5 M Na_2CO_3 and 500 ml 0.5 M $NaHCO_3$ stock solutions.

    a. Na_2CO_3 = 105.9884 g/mol (Anhydrous)
        i. Dissolve 13.24855 g in 250 ml of filtered de-ionized water.

    b. $NaHCO_3$ = 84.0066 g/mol
        i. Dissolve 21.0016 g in 500 ml of filtered de-ionized water.

2) Add 10 ml of 0.5 M Na_2CO_3 to 40 ml of 0.5 M $NaHCO_3$ (pH 9.4 at 20°C). Stir.

3) Slowly add either 0.5 M Na_2CO_3 or 0.5 M $NaHCO_3$ drop by drop to adjust the pH to 9.3. Use a pH meter and stir constantly. Record the temperature.

4) Measure the final volume.

5) Dilute the solution 5 times in filtered de-ionized water to achieve a 0.1 M solution.

Store at 4°C. This makes approximately 250 ml of buffer.

0.15M Sodium chloride

1) Make a 4 M NaCl (mw = 58.44) stock solution by dissolving 23.38 g of NaCl in 100 ml of filtered de-ionized water.

2) Dilute 75 ml of 4M NaCl in 1925 ml of filtered de-ionized water.

Store at 4°C. Makes 2L of buffer.

0.1M Phosphate buffered saline (PBS), pH 7.4

1) Make 500 ml 0.5 M NaH_2PO_4 and 500 ml 0.5 M Na_2HPO_4 stock solutions.

    a. 0.5 M NaH_2PO_4
        i. 30.00 g NaH_2PO_4; filtered de-ionized water to 500 ml
        ii. 34.50 g $NaH_2PO_4 \bullet H_2O$; filtered de-ionized water to 500 ml
        iii. 39.00 g $NaH_2PO_4 \bullet 2H_2O$; filtered de-ionized water to 500 ml

    b. 0.5 M Na_2HPO_4 (Gentle heating may be required to completely dissolve solids. If so, allow the solution to return to room temperature before further usage. Store at room temperature)
        i. 35.5 g Na_2HPO_4; filtered de-ionized water to 500 ml
        ii. 44.5 g $Na_2HPO_4 \bullet 2H_2O$; filtered de-ionized water to 500 ml
        iii. 67.03 g $Na_2HPO_4 \bullet 7H_2O$; filtered de-ionized water to 500 ml
        iv. 89.52 g $Na_2HPO_4 \bullet 12H_2O$; filtered de-ionized water to 500 ml

2) Add 3.4 ml of 0.5 M NaH_2PO_4 to 16.6 ml of 0.5 M Na_2HPO_4 (pH 7.4). Stir.

3) Slowly add 0.5 M NaH_2PO_4 drop-by-drop to adjust the pH to 7.4. Use a pH meter and stir constantly. Record the temperature.

4) Measure the final volume (y).

5) Determine from the final volume the amount of NaCl to be added.

$$\frac{\text{9 g of NaCl}}{\text{200 ml of phosphate buffer}} = \frac{\text{x}}{\text{y ml of phosphate buffer}}$$

6) Dilute the final solution 5 times in filtered de-ionized water to achieve a 0.1M solution.

Makes approximately 150 ml.

0.01 M Phosphate buffered saline (PBS), pH 7.4, 0.01% Sodium azide

1) Using 100mL of the previous buffer, add filtered de-ionized water to make 1L. This makes a 0.01 M solution.

0.01% Sodium azide means 0.01g of sodium azide per 100ml therefore add 0.1g of sodium azide to 1L of our solution to make a 0.01% solution.

References

Aldana J, Wang YA, Peng X. 2001. Photochemical instability of CdSe nanocrystals coated by hydrophilic thiols. J Am Chem Soc 123(36):8844-50.

Alivisatos AP, Gu W, Larabell C. 2005. Quantum dots as celluar probes. Annu Rev Biomed Eng 7(1):55-76.

Alp NJ and Channon KM. 2004. Regulation of endothelial nitric oxide synthase by tetrahydrobiopterin in vascular disease. Arteriosclerosis, Thrombosis, and Vascular Biology 24(3):413-20.

An B, Kwon S, Jung S, Park SY. 2002. Enhanced emission and its switching in fluorescent organic nanoparticles. J Am Chem Soc 124(48):14410-5.

Arakaki LSL, Ciesielski WA, Thackray BD, Feigl EO, Schenkman KA. 2010. Simultaneous optical spectroscopic measurement of hemoglobin and myoglobin saturations and cytochrome aa3 oxidation in vivo. Appl Spectrosc 64(9):973-9.

Arsos G, Kyparos A, Moralidis E, Kyparos D, Georga S, Sotiriadou S, Matziari C, Karakatsanis C. 2009. (99m) tc-sestamibi uptake in rat skeletal muscle and heart: Physiological determinants and correlations. Physiol Res 58(1):21-28.

Austin RE, Aldea GS, Coggins DL, Flynn AE, Hoffman JI. 1990. Profound spatial heterogeneity of coronary reserve. discordance between patterns of resting and maximal myocardial blood flow. Circulation Research 67(2):319-31.

Baez S. 1977. Microcirculation. Annu Rev Physiol 39(1):391-415.

Bagi Z, Koller A, Kaley G. 2004. PPARγ activation, by reducing oxidative stress, increases NO bioavailability in coronary arterioles of mice with type 2 diabetes. American Journal of Physiology - Heart and Circulatory Physiology 286(2):H742-8.

Banchonglikitkul C, Smart JD, Gibbs RV, Donovan SJ, Cook DJ. 2002. An in-vitro evaluation of lectin cytotoxicity using cell lines derived from the ocular surface. J Drug Target 10(8):601-6.

Bandettini WP and Arai AE. 2008. Advances in clinical applications of cardiovascular magnetic resonance imaging. Heart 94(11):1485-95.

Bartholoma MD, Louie AS, Valliant JF, Zubieta J. 2010. Technetium and gallium derived radiopharmaceuticals: Comparing and contrasting the chemistry of two important radiometals for the molecular imaging era. Chem Rev 110(5):2903-20.

Bell RM, Mocanu MM, Yellon DM. 2011. Retrograde heart perfusion: The langendorff technique of isolated heart perfusion. J Mol Cell Cardiol 50(6):940-50.

Blankenberg FG and Strauss HW. 2002. Nuclear medicine applications in molecular imaging. Journal of Magnetic Resonance Imaging 16(4):352-61.

Boeneman K, Delehanty JB, Susumu K, Stewart MH, Deschamps JR, Medintz IL. 2012. Quantum dots and fluorescent protein FRET-based biosensors. Adv Exp Med Biol 733:63-74.

Bogdanov A, Lin C, Kang HW. 2007. Optical imaging of the adoptive transfer of human endothelial cells in mice using anti-human CD31 monoclonal antibody. Pharm Res 24(6):1186-92.

Bourdarias JP. 1995. Coronary reserve: Concept and physiological variations. European Heart Journal 16(suppl I):2-6.

Brutsaert DL. 1989. The endocardium. Annu Rev Physiol 51(1):263-73.

Burri MV, Gupta D, Kerber RE, Weiss RM. 2012. Review of novel clinical applications of advanced, real-time, 3-dimensional echocardiography. Translational Research 159(3):149-64.

Buzug TM. 2012. Springer Handbook of Medical Technology. "Computed tomography". Springer Berlin Heidelberg: Berlin, Germany. 311-42.

Cademartiri F, Luccichenti G, van Der Lugt A, Pavone P, Pattynama PM, de Feyter PJ, Krestin GP. 2004. Sixteen-row multislice computed tomography: Basic concepts, protocols, and enhanced clinical applications. Seminars in Ultrasound, CT, and MRI 25(1):2-16.

Cademartiri F, de Monye C, Pugliese F, Mollet NR, Runza G, van der Lugt A, Midiri M, de Feyter PJ, Lagalla R, Krestin GP. 2006. High iodine concentration contrast material for noninvasive multislice computed tomography coronary angiography: Iopromide 370 versus iomeprol 400. Invest Radiol 41(3).

Campbell NA and Reece JB. 2005. Biology. 7th ed. San Francisco, USA: Pearson Education, Inc.

Carvalho P, Chiu M, Kronauge J, Kawamura M, Jones A, Holman B, Piwnica-Worms D. 1992. Subcellular distribution and analysis of technetium-99m-MIBI in isolated perfused rat hearts. J Nucl Med 33(8):1516-22.

Chang K and Jaffer F. 2008. Advances in fluorescence imaging of the cardiovascular system. Journal of Nuclear Cardiology 15(3):417-28.

Chen J, Tung C, Allport JR, Chen S, Weissleder R, Huang PL. 2005. Near-infrared fluorescent imaging of matrix metalloproteinase activity after myocardial infarction. Circulation 111(14):1800-5.

Chen T, Zeng S, Zhou W, Luo Q. 2003. A quantitative theory model of a photobleaching mechanism. Chinese Physics Letters 20(11):1940.

Chen X, Conti PS, Moats RA. 2004. In vivo near-infrared fluorescence imaging of integrin αvβ3 in brain tumor xenografts. Cancer Research 64(21):8009-14.

Cherrick GR, Stein SW, Leevy CM, Davidson CS. 1960. Indocyanine green: Observations on its physical properties, plasma decay and hepatic extraction. J Clin Invest 39(4):592-600.

Chien S. 2008. Effects of disturbed flow on endothelial cells. Annals of Biomedical Engineering 36(4):554-62.

Chrispeels MJ and Raikhel NV. 1991. Lectins, lectin genes, and their role in plant defense. The Plant Cell Online 3(1):1-9.

Chu S and Bohlen HG. 2004. High concentration of glucose inhibits glomerular endothelial eNOS through a PKC mechanism. American Journal of Physiology - Renal Physiology 287(3):F384-92.

Citrin D, Lee AK, Scott T, Sproull M, Ménard C, Tofilon PJ, Camphausen K. 2004. In vivo tumor imaging in mice with near-infrared labeled endostatin. Molecular Cancer Therapeutics 3(4):481-8.

Clegg RM. 1995. Fluorescence resonance energy transfer. Curr Opin Biotechnol 6(1):103.

Cooke JP and Ghebremariam YT. 2008. Endothelial nicotinic acetylcholine receptors and angiogenesis. Trends Cardiovasc Med 18(7):247-53.

Cooke MS, Evans MD, Dizdaroglu M, Lunec J. 2003. Oxidative DNA damage: Mechanisms, mutation, and disease. The FASEB Journal 17(10):1195-214.

Croney JC, Jameson DM, Learmonth RP. 2001. Fluorescence spectroscopy in biochemistry: Teaching basic principles with visual demonstrations. Biochemistry and Molecular Biology Education 29(2):60-5.

da Silva CG, Specht A, Wegiel B, Ferran C, Kaczmarek E. 2009. Mechanism of purinergic activation of endothelial nitric oxide synthase in endothelial cells. Circulation 119(6):871-9.

Dayton PA and Ferrara KW. 2002. Targeted imaging using ultrasound. Journal of Magnetic Resonance Imaging 16(4):362-77.

Debbage PL, Seidl S, Kreczy A, Hutzler P, Pavelka M, Lukas P. 2000. Vascular permeability and hyperpermeability in a murine adenocarcinoma after fractionated radiotherapy: An ultrastructural tracer study. Histochemistry and Cell Biology 114(4):259-75.

DePuey E, Nichols K, Dobrinsky C. 1993. Left ventricular ejection fraction assessed from gated technetium-99m-sestamibi SPECT. J Nucl Med 34(11):1871-6.

Desmettre T, Devoisselle JM, Mordon S. 2000. Fluorescence properties and metabolic features of indocyanine green (ICG) as related to angiography. Surv Ophthalmol 45(1):15-27.

Di Francescomarino S, Sciartilli A, Di Valerio V, Di Baldassarre A, Gallina S. 2009. The effect of physical exercise on endothelial function. Sports Medicine 39(10):797-812.

Ding H, Ryder JW, Stull JT, Kamm KE. 2009. Signaling processes for initiating smooth muscle contraction upon neural stimulation. Journal of Biological Chemistry 284(23):15541-8.

Donovan J and Brown P. 2001. Anesthesia. Current Protocols in Immunology 27:1.4.1,1.4.5.

Dullin C, Zientkowska M, Napp J, Missbach-Guentner J, Krell H, Muller F, Grabbe E, Tietze L, Alves F. 2009. Semiautomatic landmark-based two-dimensional-three-dimensional image fusion in living mice : Correlation of near-infrared fluorescence imaging of Cy5.5-labeled antibodies with flat-panel volume computed tomography. .

Edelman RR. 2004. Contrast-enhanced MR imaging of the heart: Overview of the Literature. Radiology 232(3):653-68.

Faber DJ, Mik EG, Aalders MCG, van Leeuwen TG. 2003. Light absorption of (oxy-)hemoglobin assessed by spectroscopic optical coherence tomography. Opt Lett 28(16):1436-8.

Fazel R, Krumholz HM, Wang Y, Ross JS, Chen J, Ting HH, Shah ND, Nasir K, Einstein AJ, Nallamothu BK. 2009. Exposure to low-dose ionizing radiation from medical imaging procedures. N Engl J Med 361(9):849-57.

Fleming I. 2010. Molecular mechanisms underlying the activation of eNOS. Pflugers Archiv European Journal of Physiology 459(6):793-806.

Fletcher J, Clark MD, Sutton FA, Wellings R, Garas K. 1999. The cost of MRI: Changes in costs 1989-1996. British Journal of Radiology 72(857):432-7.

Funovics MA, Alencar H, Su HS, Khazaie K, Weissleder R, Mahmood U. 2003. Miniaturized multichannel near infrared endoscope for mouse imaging. Mol Imaging 2(4):350-7.

Furchgott RF and Zawadzki JV. 1980. The obligatory role of endothelial cells in the relaxation of arterial smooth muscle by acetylcholine. Nature 288(5789):373-6.

Galande AK, Hilderbrand SA, Weissleder R, Tung C. 2006. Enzyme-targeted fluorescent imaging probes on a multiple antigenic peptide core. J Med Chem 49(15):4715-20.

Gardner B, Bingham S, Allen M, Blatter D, Anderson J. 2009. Cardiac magnetic resonance versus transthoracic echocardiography for the assessment of cardiac volumes and regional function after myocardial infarction: An intrasubject comparison using simultaneous intrasubject recordings. Cardiovascular Ultrasound 7(38).

Gerwin N, Gonzalo J, Lloyd C, Coyle AJ, Reiss Y, Banu N, Wang B, Xu H, Avraham H, Englhardt B, Springer TA, Gutierrez-Ramos JC. 1999. Prolonged eosinophil accumulation in allergic lung interstitium of ICAM-2-deficcient mice results in extended hyperresponsiveness. Immunity 10(1):9-19.

Geuns RMv, Wielopolski PA, Bruin HGd, Rensing BJ, Ooijen PMAv, Hulshoff M, Oudkerk M, Feyter PJd. 1999. Basic principles of magnetic resonance imaging. Prog Cardiovasc Dis 42(2):149.

Giles TD, Sander GE, Nossaman BD, Kadowitz PJ. 2012. Impaired vasodilation in the pathogenesis of hypertension: Focus on nitric oxide, endothelial-derived hyperpolarizing factors, and prostaglandins. The Journal of Clinical Hypertension 14(4):198-205.

Gray GA and Webb DJ. 1996. The endothelin system and its potential as a therapeutic target in cardiovascular disease. Pharmacol Ther 72(2):109-48.

Gruszecki WI. 1991. Structural characterization of the aggregated forms of violaxanthin. J Biol Phys 18(2):99-109.

Gullberg GT, Reutter BW, Sitek A, Maltz JS, Budinger TF. 2010. Dynamic single photon emission computed tomography: basic principles and cardiac applications. Phys Med Biol 55(20):R111.

Gussakovsky E, Kuzio B, Yang Y, Kupriyanov V. 2011. Fluorescence imaging to quantify the fluorescent microspheres in cardiac tissue. Journal of Biophotonics 4(4):277-87.

Gussakovsky E and Kupriyanov V. 2008. Assessment of near-infrared path length in fibrous phantom and muscle tissue. Appl Spectrosc 62(6):671-6.

Gussakovsky E, Yang Y, Rendell J, Jilkina O, Kupriyanov V. 2012. NIR spectroscopic imaging to map hemoglobin + myoglobin oxygenation, their concentration and optical pathlength across a beating pig heart during surgery. Journal of Biophotonics 5(2):128-39.

Hama Y, Koyama Y, Choyke PL, Kobayashi H. 2007. Two-color *in vivo* dynamic contrast-enhanced pharmacokinetic imaging. J Biomed Opt 12(3):034016.

Hauff P, Reinhardt M, Foster S. 2008. Ultrasound basics. In: Molecular imaging I. Semmler W and Schwaiger M, editors. Springer Berlin Heidelberg. 91 p.

Haugland RP. 2002. Handbook of fluorescent probes and research products. 9th ed. USA: Molecular Probes, Inc.

Heusch G, Schulz R, Haude M, Erbel R. 2004. Coronary microembolization. J Mol Cell Cardiol 37(1):23-31.

Heusch G, Kleinbongard P, Böse D, Levkau B, Haude M, Schulz R, Erbel R. 2009. Coronary microembolization. Circulation 120(18):1822-36.

Hoenig MR, Bianchi C, Rosenzweig A, Sellke FW. 2008. The cardiac microvasculature in hypertension, cardiac hypertrophy and diastolic heart failure. Current Vascular Pharmacology 6(4):292-300.

Holly T, Abbott B, Al-Mallah M, Calnon D, Cohen M, DiFilippo F, Ficaro E, Freeman M, Hendel R, Jain D, et al. 2010. Single photon-emission computed tomography. Journal of Nuclear Cardiology 17(5):941-73.

Husmann L, Herzog BA, Gaemperli O, Tatsugami F, Burkhard N, Valenta I, Veit-Haibach P, Wyss CA, Landmesser U, Kaufmann PA. 2009. Diagnostic accuracy of computed tomography coronary angiography and evaluation of stress-only single-photon emission computed tomography/computed tomography hybrid imaging: Comparison of prospective electrocardiogram-triggering vs. retrospective gating. European Heart Journal 30(5):600-7.

Icardo JM and Colvee E. 2001. Origin and course of the coronary arteries in normal mice and in iv/iv mice. J Anat 199(4):473-82.

Inoguchi T, Li P, Umeda F, Yu HY, Kakimoto M, Imamura M, Aoki T, Etoh T, Hashimoto T, Naruse M, et al. 2000. High glucose level and free fatty acid stimulate reactive oxygen species production through protein kinase C--dependent activation of NAD(P)H oxidase in cultured vascular cells. Diabetes 49(11):1939-45.

Jaffer FA and Weissleder R. 2004. Seeing within: Molecular imaging of the cariovascular system
. Circulation Research 94(4):433-45.

Jaffer FA, Calfon MA, Rosenthal A, Mallas G, Razansky RN, Mauskapf A, Weissleder R, Libby P, Ntziachristos V. 2011. Two-dimensional intravascular near-infrared fluorescence molecular imaging of inflammation in atherosclerosis and stent-induced vascular injury. J Am Coll Cardiol 57(25):2516-26.

Jaffer FA, Kim D, Quinti L, Tung C, Aikawa E, Pande AN, Kohler RH, Shi G, Libby P, Weissleder R. 2007. Optical visualization of cathepsin K activity in

atherosclerosis with a novel, protease-activatable fluorescence sensor. Circulation 115(17):2292-8.

Jameson DM, Croney JC, Moens PDJ. 2003. Fluorescence: Basic concepts, practical aspects, and some anecdotes. In: Biophotonics, part A. Gerard Marriott IP, editor. Academic Press. 1 p.

Jilkina O, Kuzio B, Rendell J, Xiang B, Kupriyanov VV. 2006. K+ transport and energetics in Kir6.2−/− mouse hearts assessed by 87Rb and 31P magnetic resonance and optical spectroscopy. J Mol Cell Cardiol 41(5):893-901.

Jilkina O, Xiang B, Kuzio B, Rendell J, Kupriyanov VV. 2005. Potassium transport in langendorff-perfused mouse hearts assessed by 87Rb NMR spectroscopy. Magnetic Resonance in Medicine 53(5):1172-6.

Jilkina O, Glogowski M, Kuzio B, Zhilkin PA, Gussakovsky E, Kupriyanov VV. 2011. Defects in myoglobin oxygenation in KATP-deficient mouse hearts under normal and stress conditions characterized by near infrared spectroscopy and imaging. Int J Cardiol 149(3):315-22.

Jilkina O, Kuzio B, Grover GJ, Folmes CDL, Kong H, Kupriyanov VV. 2003. Sarcolemmal and mitochondrial effects of a KATP opener, P-1075, in “polarized” and “depolarized” langendorff-perfused rat hearts. Biochimica Et Biophysica Acta (BBA) - Biomembranes 1618(1):39-50.

Jilkina O, Kong H, Hwi L, Kuzio B, Xiang B, Manley D, Jackson M, Kupriyanov VV. 2006. Interaction of a mitochondrial membrane potential-sensitive dye, rhodamine 800, with rat mitochondria, cells, and perfused hearts. J Biomed Opt 11(1):014009.

Jilkina O, Nguyen C, Bascaramurty S, Kuzio B, Kupriyanov V. 2010. Near-infrared (NIR) molecular imaging of myocardial microvascular endothelium using lectin-Cy5.5 conjugate. Abstract # 51954. ISHR2010 Kyoto.

Kasha M. 1950. Characterization of electronic transitions in complex molecules. Discuss Faraday Soc 9:14-9.

Kawanabe Y and Nauli S. 2011. Endothelin. Cellular and Molecular Life Sciences 68(2):195-203.

Kelly KA, Allport JR, Tsourkas A, Shinde-Patil VR, Josephson L, Weissleder R. 2005. Detection of vascular adhesion molecule-1 expression using a novel multimodal nanoparticle. Circulation Research 96(3):327-36.

Kersten JR, Brooks LA, Dellsperger KC. 1995. Impaired microvascular response to graded coronary occlusion in diabetic and hyperglycemic dogs. American Journal of Physiology - Heart and Circulatory Physiology 268(4):H1667-74.

Kilpatrick D. 1980. Purification and some properties of a lectin from the fruit juice of the tomato (lycopersicon esculentum). Biochem J 185(1):269-72.

Ko YG and Ma PX. 2009. Surface-grafting of phosphates onto a polymer for potential biomimetic functionalization of biomaterials. J Colloid Interface Sci 330(1):77-83.

Kobayashi H, Koyama Y, Barrett T, Hama Y, Regino CAS, Shin IS, Jang B, Le N, Paik CH, Choyke PL, et al. 2007. Multimodal nanoprobes for radionuclide and five-color near-infrared optical lymphatic imaging. ACS Nano 1(4):258-64.

Kovar JL, Simpson MA, Schutz-Geschwender A, Olive DM. 2007. A systematic approach to the development of fluorescent contrast agents for optical imaging of mouse cancer models. Anal Biochem 367(1):1-12.

Kuboki K, Jiang ZY, Takahara N, Ha SW, Igarashi M, Yamauchi T, Feener EP, Herbert TP, Rhodes CJ, King GL. 2000. Regulation of endothelial constitutive nitric oxide synthase gene expression in endothelial cells and in vivo. Circulation 101(6):676-81.

Kupriyanov V, Manley D, Xiang B. 2008. Detection of moderate regional ischemia in pig hearts in vivo by near-infrared and thermal imaging: Effects of dipyridamole. The International Journal of Cardiovascular Imaging (Formerly Cardiac Imaging) 24(1):113-23.

Kupriyanov VV, Nighswander-Rempel S, Xiang B. 2004. Mapping regional oxygenation and flow in pig hearts in vivo using near-infrared spectroscopic imaging. J Mol Cell Cardiol 37(5):947-57.

Kuschinsky W and Paulson O. 1992. Capillary circulation in the brain. Cerebrovasc Brain Metab Rev 4(3):261-86.

Laitinen L. 1987. *Griffonia simplicifolia* lectins bind specifically to endothelial cells and some epithelial cells in mouse tissues. The Histochemical Journal 19(4):225-34.

Law B, Curino A, Bugge TH, Weissleder R, Tung C. 2004. Design, synthesis, and characterization of urokinase plasminogen-activator-sensitive near-infrared reporter. Chem Biol 11(1):99-106.

Lettinga MP, Zuilhof H, van Zandvoort MAMJ. 2000. Phosphorescence and fluorescence characterization of fluorescein derivatives immobilized in various polymer matrices. Phys.Chem.Chem.Phys. 2(16):3697-707.

Li J, White J, Guo L, Zhao X, Wang J, Smart EJ, Li X. March 2009. Salt inactivates endothelial nitric oxide synthase in endothelial cells. The Journal of Nutrition 139(3):447-51.

Li K, Buonaccorsi G, Thompson G, Cain JR, Watkins A, Russell D, Qureshi S, Evans DG, Lloyd SK, Zhu X, et al. 2011. An improved coverage and spatial resolutionâ€"using dual injection dynamic contrast-enhanced (ICE-DICE) MRI: A novel dynamic contrast-enhanced technique for cerebral tumors. Magnetic Resonance in Medicine :n/a,n/a.

Li Q, Lau A, Morris TJ, Guo L, Fordyce CB, Stanley EF. 2004. A syntaxin 1, gαo, and N-type calcium channel complex at a presynaptic nerve terminal: Analysis by quantitative immunocolocalization. The Journal of Neuroscience 24(16):4070-81.

Little SE and Bassingthwaighte JB. 1983. Plasma-soluble marker for intraorgan regional flows. American Journal of Physiology - Heart and Circulatory Physiology 245(4):H707-12.

Lu X, Nadvoretskiy V, Bu L, Stolpen A, Ayres N, Pignatelli RH, Kovalchin JP, Grenier M, Klas B, Ge S. 2008. Accuracy and reproducibility of real-time three-dimensional echocardiography for assessment of right ventricular volumes and ejection fraction in children. Journal of the American Society of Echocardiography 21(1):84.

Malin SF, Ruchti TL, Blank TB, Thennadil SN, Monfre SL. 1999. Noninvasive prediction of glucose by near-infrared diffuse reflectance spectroscopy. Clinical Chemistry 45(9):1651-8.

Marshall MV, Rasmussen JC, Tan I, Aldrich MB, Adams KE, Wang X, Fife CE, Maus EA, Smith LA, Sevick-Muraca EM. 2010. Near-infrared fluorescence imaging in humans with indocyanine green: A review and update. The Open Surgical Oncology Journal 2:12-25.

Marshall RC, Powers-Risius P, Reutter BW, O'Neil JP, La Belle M, Huesman RH, VanBrocklin HF. 2004. Kinetic analysis of 18F-fluorodihydrorotenone as a deposited myocardial flow tracer: Comparison to 201Tl. Journal of Nuclear Medicine 45(11):1950-9.

Matsumoto T and Kajiya F. 2001. Microheterogeneity of myocardial blood flow. Basic Research in Cardiology 96(6):547-52.

Matsuura E, Hughes GRV, Khamashta MA. 2008. Oxidation of LDL and its clinical implication. Autoimmunity Reviews 7(7):558-66.

Matter CM, Schuler PK, Alessi P, Meier P, Ricci R, Zhang D, Halin C, Castellani P, Zardi L, Hofer CK, et al. 2004. Molecular imaging of atherosclerotic plaques using a human antibody against the extra-domain B of fibronectin. Circulation Research 95(12):1225-33.

Mattoussi H, Mauro JM, Goldman ER, Green TM, Anderson GP, Sundar VC, Bawendi MG. 2001. Bioconjugation of highly luminescent colloidal CdSeâ€"ZnS quantum

dots with an engineered two-domain recombinant protein. Physica Status Solidi (b) 224(1):277-83.

Maul GG. 1971. Structure and formation of pores in fenestrated capillaries. J Ultrastruct Res 36(5–6):768-82.

Maynard S, Schurman SH, Harboe C, de Souza-Pinto NC, Bohr VA. 2009. Base excision repair of oxidative DNA damage and association with cancer and aging. Carcinogenesis 30(1):2-10.

Mazzetti S, Frigerio S, Gelati M, Salmaggi A, Vitellaro-Zuccarello L. 2009. Lycopersicon esculentum lectin: An effective and versatile endothelial marker of normal and tumoral blood vessels in the central nervous system. European Journal of Histochemistry; Vol 48, no 4 (2004) .

McCarthy JR, Patel P, Botnaru I, Haghayeghi P, Weissleder R, Jaffer FA. 2009. Multimodal nanoagents for the detection of intravascular thrombi. Bioconjugate Chem 20(6):1251-5.

McVeigh ER. 2006. Emerging imaging techniques. Circulation Research 98(7):879-86.

Millar SJ, Moss BW, Stevenson MH. 1996. Some observations on the absorption spectra of various myoglobin derivatives found in meat. Meat Sci 42(3):277-88.

Miller JC and Thrall JH. 2004. Clinical molecular imaging. Journal of the American College of Radiology 1(1, Supplement):4-23.

Mishra A, Behera RK, Behera PK, Mishra BK, Behera GB. 2000. Cyanines during the 1990s: A review. Chem Rev 100(6):1973-2012.

Miyazaki M and Akahane M. 2012. Non-contrast enhanced MR angiography: Established techniques. Journal of Magnetic Resonance Imaging 35(1):1-19.

Mojzych M and Henary M. 2008. Synthesis of cyanine dyes. Topics in Heterocyclic Chemistry 14:1-9.

Muehllehner G and Karp JS. 2006. Positron emission tomography. Phys Med Biol 51(13):R117.

Munch G, McKay S, Gussakovsky E, Kuzio B, Kupriyanov VV, Jilkina O. 2011. Rhodamine 800 as a near-infrared fluorescent deposition flow tracer in rodent hearts. J Biomed Opt 16(6):065001.

Nachbar M, Oppenheim J, Thomas J. 1980. Lectins in the U.S. diet. isolation and characterization of a lectin from the tomato (lycopersicon esculentum). J Biol Chem 255(5):2056-61.

Nguyen C, Bascaramurty S, Kuzio B, Kupriyanov V, Jilkina O. 2012. Near-infrared molecular imaging of myocardial microvascular endothelium using Cy5.5-lectin conjugate. Abstract. Health Research Forum (Winnipeg, MB).

Nguyen C, Bascaramurty S, Kuzio B, Gregorash L, Kupriyanov V, Jilkina O. 2012. Near-infrared fluorescence imaging of mouse myocardial microvascular endothelium using Cy5.5-lectin conjugate. Journal of Biophotonics (early view). <10.1002/jbio.201100119>.

Nighswander-Rempel SP, Kupriyanov VV, Shaw RA. 2005. Assessment of optical path length in tissue using neodymium and water absorptions for application to near-infrared spectroscopy. J Biomed Opt 10(2):024023.

Nighswander-Rempel SP, Anthony Shaw R, Mansfield JR, Hewko M, Kupriyanov VV, Mantsch HH. 2002. Regional variations in myocardial tissue oxygenation mapped by near-infrared spectroscopic imaging. J Mol Cell Cardiol 34(9):1195-203.

Ntziachristos V, Ripoll J, Wang LV, Weissleder R. 2005. Looking and listening to light: The evolution of whole-body photonic imaging. Nat Biotech 23(3):313-20.

Nuiachristos V. 2006. Fluorescence molecular imaging. Annu Rev Biomed Eng 8:1-33.

Ogawa M, Regino CAS, Choyke PL, Kobayashi H. 2009. In vivo target-specific activatable near-infrared optical labeling of humanized monoclonal antibodies. Molecular Cancer Therapeutics 8(1):232-9.

Okizaki A, Shuke N, Sato J, Sasaki T, Hasebe N, Kikuchi K, Aburano T. 2007. A compartment model analysis for investigation of myocardial fatty acid metabolism in patients with hypertrophic cardiomyopathy. Nucl Med Commun 28(9):726 - 735.

Okon EB, Chung AWY, Rauniyar P, Padilla E, Tejerina T, McManus BM, Luo H, van Breemen C. 2005. Compromised arterial function in human type 2 diabetic patients. Diabetes 54(8):2415-23.

Osborn J. 2002. A review of the suitability of CyDye fluors for use in high-throughput drug screening applications. Discovery Matters: .

Palmer RMJ, Ashton DS, Moncada S. 1988. Vascular endothelial cells synthesize nitric oxide from L-arginine. Nature 333(6174):664-6.

Parker CA and Rees WT. 1962. Fluorescence spectrometry. A review. Analyst 87(1031).

Petrella JR and Provenzale JM. 2000. MR perfusion imaging of the brain. American Journal of Roentgenology 175(1):207-19.

Porter G, Palade G, Milici A. 1990. Differential binding of the lectins griffonia simplicifolia I and lycopersicon esculentum to microvascular endothelium:

Organ-specific localization and partial glycoprotein characterization. Eur J Cell Biol 51(1):85-95.

Poste G, Bucana C, Raz A, Bugelski P, Kirsh R, Fidler IJ. 1982. Analysis of the fate of systemically administered liposomes and implications for their use in drug delivery. Cancer Research 42(4):1412-22.

Pries AR and Secomb TW. 2009. Origins of heterogeneity in tissue perfusion and metabolism. Cardiovascular Research 81(2):328-35.

Prinzen FW and Bassingthwaighte JB. 2000. Blood flow distributions by microsphere deposition methods. Cardiovascular Research 45(1):13-21.

Pusztai A, Clarke EMW, Grant G, King TP. 1981. The toxicity of phaseolus vulgaris lectins. nitrogen balance and immunochemical studies. J Sci Food Agric 32(10):1037-46.

Robert H. W. 2010. Anatomy of the heart. Medicine 38(7):333-5.

Roberts CK and Sindhu KK. 2009. Oxidative stress and metabolic syndrome. Life Sci 84(21–22):705-12.

Rodgers CT and Robson MD. 2011. Cardiovascular magnetic resonance: Physics and terminology. Progress in Cardiovascular Diseases 54(3):181-90.

Romero-Corral A, Sert-Kuniyoshi FH, Sierra-Johnson J, Orban M, Gami A, Davison D, Singh P, Pusalavidyasagar S, Huyber C, Votruba S, et al. 2010. Modest visceral fat gain causes endothelial dysfunction in healthy humans. J Am Coll Cardiol 56(8):662-6.

Roos WP and Kaina B. 2006. DNA damage-induced cell death by apoptosis. Trends Mol Med 12(9):440-50.

Ross R. 1999. Atherosclerosis-an inflammatory disease. N Engl J Med 340:115-26.

Rudin M and Weissleder R. 2003. Molecular imaging in drug discovery and development. Nat Rev Drug Discov 2(2):123-31.

Ruth T. 2009. Accelerating production of medical isotopes. Nature 457(7229):536-7.

Sasaki E, Kojima H, Nishimatsu H, Urano Y, Kikuchi K, Hirata Y, Nagano T. 2005. Highly sensitive near-infrared fluorescent probes for nitric oxide and their application to isolated organs. J Am Chem Soc 127(11):3684-5.

Schnitzer JE, Siflingerbirnboim A, Delvecchio PJ, Malik AB. 1994. Segmental differentiation of permeability, protein glycosylation, and morphology of cultured bovine lung vascular endothelium. Biochem Biophys Res Commun 199(1):11.

Schroeder S, Achenbach S, Bengel F, Burgstahler C, Cademartiri F, de Feyter P, George R, Kaufmann P, Kopp AF, Knuuti J, et al. 2008. Cardiac computed tomography: Indications, applications, limitations, and training requirements. European Heart Journal 29(4):531-56.

Selvin P. 2000. The renaissance of fluorescence resonance energy transfer. Nat Struct Biol 7(9):730-4.

Sharon N and Lis H. 1972. Lectins: Cell-agglutinating and sugar-specific proteins. Science 177(4053):949-59.

Shepherd J, Hilderbrand SA, Waterman P, Heinecke JW, Weissleder R, Libby P. 2007. A fluorescent probe for the detection of myeloperoxidase activity in atherosclerosis-associated macrophages. Chem Biol 14(11):1221-31.

Shimizu Y, Newman W, Tanaka Y, Shaw S. 1992. Lymphocyte interactions with endothelial cells. Immunol Today 13(3):106-12.

Simonetti OP, Kim RJ, Fieno DS, Hillenbrand HB, Wu E, Bundy JM, Finn JP, Judd RM. 2001. An improved MR imaging technique for the visualization of myocardial Infarction1. Radiology 218(1):215-23.

Sitia S, Tomasoni L, Atzeni F, Ambrosio G, Cordiano C, Catapano A, Tramontana S, Perticone F, Naccarato P, Camici P, et al. 2010. From endothelial dysfunction to atherosclerosis. Autoimmunity Reviews 9(12):830-4.

Skrzypiec-Spring M, Grotthus B, Szeląg A, Schulz R. 2007. Isolated heart perfusion according to Langendorff—Still viable in the new millennium. J Pharmacol Toxicol Methods 55(2):113-26.

Slifkin M and Cumbie R. 1987. Identification of group B streptococcal antigen with lectin-bound polystyrene particles. Journal of Clinical Microbiology 25(7):1172-5.

Sodickson A, Baeyens PF, Andriole KP, Prevedello LM, Nawfel RD, Hanson R, Khorasani R. April 2009. Recurrent CT, cumulative radiation exposure, and associated radiation-induced cancer risks from CT of Adults1. Radiology 251(1):175-84.

Steinberg HO, Chaker H, Leaming R, Johnson A, Brechtel G, Baron AD. 1996. Obesity/insulin resistance is associated with endothelial dysfunction. implications for the syndrome of insulin resistance. J Clin Invest 97(11):2601-10.

Stephens DJ and Allan VJ. 2003. Light microscopy techniques for live cell imaging. Science 300(5616):82-6.

Sugeng L, Shernan SK, Weinert L, Shook D, Raman J, Jeevanandam V, DuPont F, Fox J, Mor-Avi V, Lang RM. 2008. Real-time three-dimensional transesophageal

echocardiography in valve disease: Comparison with surgical findings and evaluation of prosthetic valves. Journal of the American Society of Echocardiography 21(12):1347-54.

Swinehart DF. 1962. The beer-lambert law. J Chem Educ 39(7):333.

Taggart DP, Choudhary B, Anastasiadis K, Abu-Omar Y, Balacumaraswami L, Pigott DW. 2003. Preliminary experience with a novel intraoperative fluorescence imaging technique to evaluate the patency of bypass grafts in total arterial revascularization. Ann Thorac Surg 75(3):870-3.

Takahashi M, Ishikawa T, Higashidani K, Katoh H. 2004. SPY™: An innovative intra-operative imaging system to evaluate graft patency during off-pump coronary artery bypass grafting. Interactive CardioVascular and Thoracic Surgery 3(3):479-83.

Terwisscha van Scheltinga AGT, van Dam GM, Nagengast WB, Ntziachristos V, Hollema H, Herek JL, Schröder CP, Kosterink JGW, Lub-de Hoog MN, de Vries EGE. 2011. Intraoperative near-infrared fluorescence tumor imaging with vascular endothelial growth factor and human epidermal growth factor receptor 2 targeting antibodies. Journal of Nuclear Medicine 52(11):1778-85.

Tesfamariam B, Brown ML, Cohen RA. 1991. Elevated glucose impairs endothelium-dependent relaxation by activating protein kinase C. J Clin Invest 87(5):1643-8.

Tesfamariam B, Brown ML, Deykin D, Cohen RA. 1990. Elevated glucose promotes generation of endothelium-derived vasoconstrictor prostanoids in rabbit aorta. J Clin Invest 85(3):929-32.

Thiberville L, Moreno-Swirc S, Vercauteren T, Peltier E, Cavé C, Bourg Heckly G. 2007. In vivo imaging of the bronchial wall microstructure using fibered confocal fluorescence microscopy. American Journal of Respiratory and Critical Care Medicine 175(1):22-31.

Thornell LE and Eriksson A. 1981. Filament systems in the purkinje fibers of the heart. American Journal of Physiology - Heart and Circulatory Physiology 241(3):H291-305.

Thorpe S, Salkovskis PM, Dittner A. 2008. Claustrophobia in MRI: The role of cognitions. Magn Reson Imaging 26(8):1081-8.

Thors B, Halldórsson H, Thorgeirsson G. 2011. eNOS activation mediated by AMPK after stimulation of endothelial cells with histamine or thrombin is dependent on LKB1. Biochimica Et Biophysica Acta (BBA) - Molecular Cell Research 1813(2):322-31.

Thurston G, Baluk P, Hirata A, McDonald DM. 1996. Permeability-related changes revealed at endothelial cell borders in inflamed venules by lectin binding. American Journal of Physiology - Heart and Circulatory Physiology 271(6):H2547-62.

Thurston G, Suri C, Smith K, McClain J, Sato TN, Yancopoulos GD, McDonald DM. 1999. Leakage-resistant blood vessels in mice transgenically overexpressing angiopoietin-1. Science 286(5449):2511-4.

Triggle C, Hollenberg M, Anderson T, Ding H, Jiang Y, Ceroni L, Wiehler W, Ng E, Ellis A, Andrews K, et al. 2003. The endothelium in health and disease--a target for therapeutic intervention. J Smooth Muscle Res 39(6):249-67.

Tung C, Gerszten RE, Jaffer FA, Weissleder R. 2002. A novel near-infrared fluorescence sensor for detection of thrombin activation in blood. ChemBioChem 3(2-3):207-11.

Tung C, Ho N, Zeng Q, Tang Y, Jaffer FA, Reed GL, Weissleder R. 2003. Novel factor XIII probes for blood coagulation imaging. ChemBioChem 4(9):897-9.

Tung C, Quinti L, Jaffer FA, Weissleder R. 2005. A branched fluorescent peptide probe for imaging of activated platelets. Mol Pharmaceutics 2(1):92-5.

Valentijn KM, Sadler JE, Valentijn JA, Voorberg J, Eikenboom J. 2011. Functional architecture of weibel-palade bodies. Blood 117(19):5033-43.

Van Der Laarse A, Vliegen HW, Van Der Nat KH, Hollaar L, Egas JM, Swier GPH, Van Den Broek AJCM. 1989. Comparison of myocardial changes between pressure induced hypertrophy and normal growth in the rat heart. Cardiovascular Research 23(4):308-14.

Vinegoni C, Razansky D, Hilderbrand SA, Shao F, Ntziachristos V, Weissleder R. 2009. Transillumination fluorescence imaging in mice using biocompatible upconverting nanoparticles. Opt Lett 34(17):2566-8.

Vishy M. 2008. Anatomy of the heart. Surgery (Oxford) 26(12):473-6.

Vladimirova-Kitova L, Deneva T, Angelova E, Nikolov F, Marinov B, Mateva N. 2008. Relationship of asymmetric dimethylarginine with flow-mediated dilatation in subjects with newly detected severe hypercholesterolemia. Clinical Physiology and Functional Imaging 28(6):417-25.

Wagenknecht PS and Ford PC. 2011. Metal centered ligand field excited states: Their roles in the design and performance of transition metal based photochemical molecular devices. Coord Chem Rev 255(5â€“6):591.

Walker JS. 2004. Physics. 2nd ed. New Jersey, USA: Pearson Education, Inc.

Wang J, Wolin M, Hintze T. 1993. Chronic exercise enhances endothelium-mediated dilation of epicardial coronary artery in conscious dogs. Circulation Research 73(5):829-38.

Wautier M, Chappey O, Corda S, Stern DM, Schmidt AM, Wautier J. 2001. Activation of NADPH oxidase by AGE links oxidant stress to altered gene expression via RAGE. American Journal of Physiology - Endocrinology and Metabolism 280(5):E685-94.

Weissleder R, Tung CH, Mahmood U, Bogdanov A. 1999. In vivo imaging of tumors with protease-activated near-infrared fluorescent probes. Nat Biotech 17(4):375-8.

Williams ATR, Winfield SA, Miller JN. 1983. Relative fluorescence quantum yields using a computer-controlled luminescence spectrometer. Analyst 108(1290):1067-71.

Wood RW. 1910. Photography by invisible rays. The Photographic Journal 50(10):329-338.

Yanagisawa M, Kurihara H, Kimura S, Tomobe Y, Kobayashi M, Mitsui Y, Yazaki Y, Goto K, Masaki T. 1988. A novel potent vasoconstrictor peptide produced by vascular endothelial cells. Nature 332(6163):411-5.

Zhu B, Jaffer FA, Ntziachristos V, Weissleder R. 2005. Development of a near infrared fluorescence catheter: Operating characteristics and feasibility for atherosclerotic plaque detection. J Phys D 38(15):2701.